UNIVERSITY OF OKLAHOMA

GRADUATE COLLEGE

INTERACTION OF METAL IONS WITH THE POLYANIONIC GRAM-POSITIVE CELL WALL AND THE EFFECT OF ANTIMICROBIAL CATIONIC BRANCHED POLYETHYLENEIMINE ON METAL BINDING

A DISSERTATION

SUBMITTED TO THE GRADUATE FACULTY

in partial fulfillment of the requirements for the

Degree of

DOCTOR OF PHILOSOPHY

By

KIETH JUANDEL THOMAS III
Norman, Oklahoma
2014

Downloaded from SHAREOK. Persistent Handle URL: https://hdl.handle.net/11244/13868

INTERACTION OF METAL IONS WITH THE POLYANIONIC GRAM-POSITIVE CELL WALL AND THE EFFECT OF ANTIMICROBIAL CATIONIC BRANCHED POLYETHYLENEIMINE ON METAL BINDING

A DISSERTATION APPROVED FOR THE
DEPARTMENT OF CHEMISTRY AND BIOCHEMISTRY

BY

_____
Dr. Charles V. Rice, Chair

_____
Dr. Robert L. White

_____
Dr. Zhibo Yang

_____
Dr. Wai tak Yip

_____
Dr. John Albert

© Copyright by KIETH JUANDEL THOMAS III 2014
All Rights Reserved

Acknowledgements

I would like to thank everyone who has helped me in pursuit of my degree. To give everyone the recognition and thanks that they deserve would require a separate chapter, but I will be brief. First and foremost, I want to thank my advisor, Dr. Rice, for his guidance, patience, and enthusiasm for research. He never had any qualms about giving me the independence in my projects, yet he provided much useful advice when my research didn't go as planned.

I was fortunate to obtain a wealth of experience while working in the Mass Spectrometry Facility at OU thanks to Dr. Foster. He was always accommodating with my work schedule and provided many useful tips on the topic of instrument maintenance and interpreting unusual spectra. For this, I am thankful. The skills that he taught me will be an asset in my job search.

I would like to express gratitude towards my fiancée, Clare, for her love and support during my final years in grad school. I appreciate all of her help and understanding when I had to work late or make trips to the lab on weekends to briefly collect data points. I could not have done this without her.

I would like to thank all members of my graduate advisory committee (Dr. White, Dr. Yip, Dr. Yang, and Dr. Albert) as well as past members (Dr. Blank and Dr. Taylor) who left after retirement. Thank you for taking time out of your schedules to make sure that I was on track and focused. I must also give special thanks to my out of departmental committee member, Dr. Albert, who had to take extra time from his schedule to drive from main campus to the

Stephenson Life Sciences Research Center for each meeting after the Chemistry Department moved to its new location.

I also want thank all of my fellow lab mates, past and present: Ravi Garimella Jeff Halye, Anthony Friedline, Kevin Pastoor, William Harrison, Malcolm Zachariah, Jessica Jensen, Amy Middaugh, and Erin Scull. Thank you for your friendship and fun times in the office. I wish all of you the best in your future endeavors.

Lastly, my acknowledgements cannot be complete without mentioning the vast support and encouragement of my parents, Kieth and Rose. They have always encouraged me to go the extra step.

Table of Contents

Acknowledgements iv

Table of Contents vi

List of Tables xi

List of Figures xiii

Abstract xix

Chapter 1: Background Information of Gram-Positive Cell Wall 1

Cell Wall of Gram-Positive Bacteria 3

Peptidoglycan 3

Teichoic Acids 5

Wall Teichoic Acid Deficient Bacterial Mutants 8

Role of Teichoic Acid in Pathogenesis 9

Role of Metals in Cell Viability and Pathogenesis 11

Metal Ion Homeostasis in Bacteria 12

Chapter 2: Experimental Procedures 13

Preparation of LB media 13

Cell Growth Protocol 13

Cell Wall Purification 14

Hydrolysis to Separate WTA from Peptidoglycan 15

Preparation of Metal Ion Standard Solutions 16

Fundamentals of Dialysis 17

Membrane Dialysis Procedure 18

General Principles of Flame AA 19

Dialysis Equilibration Optimization 23
Scatchard Plot Analysis 24
Hill Plot Analysis 25
Characterization of BPEI by Mass Spectrometry 27
Spectrophotometric Quantification of BPEI 29
Examination of Matrix Effects Due to PEI on Flame AA Response 32
Determination of Mg^{2+} in LB Growth Media 33
Quantity of Phosphate in WTA Sample 34
WTA Equilibrium dialysis 35
Growth Curves with Antibiotics and BPEI 36
Chapter 3: Mg^{2+} and Ca^{2+} Binding Characteristics of Gram-Positive Bacterial Cell Walls 37
Introduction 37
Importance of WTA 39
Experimental Procedures 40
Cell Growth Protocol 40
Cell Wall Purification 41
WTA Hydrolysis 42
Membrane Dialysis Procedure 42
Results 43
Discussion 50
Two Regions of Binding Behavior 50
Deprotonation of Binding Sites 56

Binding Stoichiometry 58
Chapter 4: Mg^{2+} Binding Characteristics with Wall Teichoic Acid 71
Introduction 71
Materials and Methods 73
Wall Teichoic Acid Purification 73
Membrane Dialysis Procedure 74
Phosphorus Concentration 75
Mg^{2+} Binding Capacity to WTA 75
Results 76
Positive Cooperativity of Mg^{2+} Binding to WTA 77
Binding Affinity of Mg^{2+} to WTA 81
Electrostatic Effects and Binding Capacity 84
Comparison of Metal Binding with RNA 85
Proposed Model of Facilitated Ion Movement to Membrane 86
Conclusion 89
Chapter 5: Antimicrobial Branched Polyethyleneimine Functions by Blocking Chelation of Essential Mg^{2+} Ions 91
Introduction 91
Experimental Procedures 94
Preparation and Characterization of Branched Polyethyleneimine 94
Spectrophotometric Quantification of BPEI 96
Effect on Growth Rate of B. subtilis by BPEI and Metal Ion Supplementation 96

Investigation of BPEI on Metal Binding 97
Cell Wall Purification 97
TCA hydrolysis 98
Binding of BPEI to Cell Wall 98
Displacement of Metal Ions on the Cell Wall by BPEI 99
Displacement of Metal Ions on Whole Cells by BPEI 99
Results 100
Effect on Growth Rate of *B. subtilis* by BPEI 100
BPEI Displaces Metal Ions on Whole Cells 102
BPEI Binds to the Cell Wall 103
BPEI Inhibits Metal Binding 104
BPEI Displaces Metal Ions on the Cell Wall 105
Discussion 106
Conclusion 110
Chapter 6: Antimicrobial Synergy of BPEI with Antibiotics and Morphological Changes Associated with BPEI Exposure 112
Introduction and Background 112
Synergetic Effect of PEI on Gram-Negative Bacteria 113
BPEI's Mode of Action toward Gram-Positive Bacteria 115
Experimental 116
Investigation of BPEI and Antibiotics on Growth Rate 116
Morphology Examination with Phase Contrast Microscopy 117
Morphology Examination with Scanning Electron Microscopy 117

Results 118
Synergy with Resistant Bacteria and Antibiotics 118
Morphology Changes in the Presence of BPEI 122
Scanning Electron Microscopy of Cells 129
Morphology Changes in Presence of EDTA and Supplemented Mg^{2+} 134
Discussion 136
Conclusion 139
References 140

List of Tables

Table 1.1 Functions of teichoic acids. 9

Table 2.1. Flame AA absorbance values of Mg^{2+} standard solutions with and without 0.1 g/L BPEI to examine matrix effects. 32

Table 2.2. Standard addition volumes and concentrations used to determine the Mg^{2+} content in fresh Lysogeny broth growth media shown in Figure 2.13..... 34

Table 3.1. Composite data table showing the metal binding properties for each cell wall sample..... 47

Table 3.2. Metal Binding Properties of *B. subtilis* (1A578) with Ca^{2+} at pH 5.65 and T=4°C 63

Table 3.3. Metal Binding Properties of *B. subtilis* (EB1451) with Ca^{2+} at pH 5.65 and T=4°C 64

Table 3.4. Metal Binding Properties of *B. subtilis* (1A578) purified peptidoglycan with Ca^{2+} at pH 5.65 and T=4°C 65

Table 3.5. Metal Binding Properties of *B. subtilis* (1A578) with Mg^{2+} at pH 5.65 and T=4°C 66

Table 3.6. Metal Binding Properties of *B. subtilis* (EB1451) with Mg^{2+} at pH 5.65 and T=4°C 67

Table 3.7. Metal Binding Properties of *B. subtilis* (1A578) purified peptidoglycan with Mg^{2+} at pH 5.65 and T=4°C..... 68

Table 3.8. Metal Binding Properties of *B. subtilis* (1A578) with Mg^{2+} at pH 7.25 in 0.001 M HEPES buffer and T=4°C 69

Table 3.9. Metal Binding Properties of *B. subtilis* (EB1451) with Mg^{2+} at pH 7.25 in 0.001 M HEPES buffer and T=4°C 70

Table 5.1. The growth of *B. subtilis* is delayed in the presence of ≥ 25 µg/mL BPEI. 101

Table 5.2. Metal ion supplementation causes lag phase to appear sooner depending on its concentration. 102

Table 5.3a. BPEI binding to the cell wall after soaking in 50 mL of 15 µg/mL BPEI for two days in Milli-Q H_2O at a buffered pH of 7.25 with 0.001 M HEPES (T=4ºC). 105

Table 5.3b. Both the binding affinity and binding capacity of Mg^{2+} ions decrease when measurements are taken after addition of 15 µg/mL BPEI (Table 3a). 105

Table 6.1. Mechanism of action of different antibiotic families. Adapted from Levy *et al*. 114

Table 6.2 Cell Thickness with and without BPEI. 130

List of Figures

Figure 1.1: The cell wall of Gram-positive bacteria is composed of thick 3-dimension mesh consisting of cross-linked peptidoglycan, teichoic acids, and various transmembrane and membrane associated proteins 3

Figure 1.2: The structure of a monomer of peptidoglycan which have various crosslinking with neighboring amino acids and diaminopimielic acid components of other monomers forming a three dimensional mesh consisting of various layers..... 5

Figure 1.3: Teichoic acids are named based on their location and how they are connected to the cell wall..... 6

Figure 1.4: The structure of all teichoic acids are based on a polyphosphate backbone. 7

Figure 1.5: Phase contrast images of two strains of *B. subtilis*..... 8

Figure 2.1: Results of the cell wall purification process and the WTA hydrolysis. 16

Figure 2.2: Structure of Cellulose. 18

Figure 2.3: Membrane dialysis of cell wall material involved having a known quantity of cell wall material on the inside of a closed dialysis bag with a pore size that lets metal ions flow freely in and out, while keeping the cell wall material trapped inside. 19

Figure 2.4: Flowchart of nebulization process leading to absorption of light energy emitted from the hollow cathode lamp. 21

Figure 2.5: The basic representation of a flame atomic absorption spectrophotomer..... 23
Figure 2.6: Length of time for Ca^{2+} ions to equilibrate inside and outside of the dialysis membrane..... 24
Figure 2.7: Characteristic Scatchard Plot. 25
Figure 2.8: Scatchard plot shapes and associated Hill plot in cooperative and non-cooperative systems..... 26
Figure 2.9: ESI(+) spectrum of the low molecular weight branched polyethyleneimine used in our experiments showing the molecular mass range of the polymer..... 28
Figure 2.10: An example of one structure of low molecular weight branched polyethyleneimine..... 29
Figure 2.11: The UV-Vis Spectrum for the BPEI and Cu2+ complex displaying two peaks at 285 nm and 630 nm..... 30
Figure 2.12: A linear relationship is obtained for concentrations of BPEI at 285 nm and 630 nm..... 31
Figure 2.13. Standard addition graph of Lysogeny broth growth media Mg^{2+} content using the parameters listed in Table 2.2. 34
Figure 3.1. Characteristic binding curve of metal binding to purified cell wall and the points corresponding to the two regions of binding affinity in Figure 3.2..... 44
Figure 3.2. Scatchard plot associated with the binding curve in Figure 3.1 showing two regions of binding affinity. 46

Figure 3.3. Phase contrast microscopy images of (A) *B. subtilis* 1A578 (B) and EB1451 cells grown in LB media (1000x magnification). 60

Figure 4.1: Polyglycerol backbone of wall teichoic acid. 72

Figure 4.2: The binding curve for WTA and Mg^{2+} during the early stages of metal binding. 77

Figure 4.3: The Scatchard plot formed from the initial data points of WTA and Mg^{2+} binding shown previously in Figure 4.2. 79

Figure 4.4: The binding curve formed from the second set of data points of WTA and Mg^{2+} that were taken 21 days later than the previous set shown previously (Figure 4.2). 81

Figure 4.5: The Scatchard plot of the metal binding data from Figure 4.4 showing the gradually decreasing affinity constant as more metal is added to the system. 82

Figure 4.6: WTA Binding Curve for all data points. 83

Figure 4.7. Potential binding modes between Mg^{2+} with WTA extending past the peptidoglycan layer and WTA inside the peptidoglycan layer. 86

Figure 5.1. ESI(+) mass spectrum of the mass distribution of the low molecular weight branched PEI that was used in experiments. 95

Figure 6.1: Growth curves for *B. subtilis* 1A578 with combinations of 10 µg/mL chloramphenicol with 0.12 and 0.14 g/L BPEI. 119

Figure 6.2: Growth curves for *B. subtilis* 1A578 with combinations of 10 ug/mL chloramphenicol with 0.16 and 0.18 g/L BPEI. 120

Figure 6.3: Growth curves showing a synergetic effect with combinations of 10 µg/mL erythromycin and varying concentrations of BPEI against an erythromycin resistant strain, WTA deficient mutant of *B. subtilis* (EB1451) 121

Figure 6.4: Growth of *B. subtilis* 1A578 with BPEI and chloramphenicol (extended time range)..... 122

Figure 6.5: Phase contrast images of *B. subtilis* 1A578 (No BPEI, OD_{600} = 0.174) 123

Figure 6.6: Phase contrast images of *B. subtilis* 1A578 (No BPEI, OD_{600} = 0.216) 124

Figure 6.7: Phase contrast images of *B. subtilis* 1A578 (No BPEI, OD_{600} = 0.270)……...125

Figure 6.8: Phase contrast images of *B. subtilis* 1A578 (No BPEI, OD_{600} = 0.488) 125

Figure 6.9: Phase contrast images of *B. subtilis* 1A578 (No BPEI, OD_{600} = 0.822)……...126

Figure 6.10: Phase contrast images of *B. subtilis* 1A578 (No BPEI, OD_{600} = 1.153) 126

Figure 6.11: Phase contrast images of *B. subtilis* 1A578 (150 µg/mL BPEI, OD_{600} = 0.091) 127

Figure 6.12: Phase contrast images of *B. subtilis* 1A578 (150 µg/mL BPEI, OD_{600} = 0.113) 127

Figure 6.13: Phase contrast images of *B. subtilis* 1A578 (150 µg/mL BPEI, OD_{600} = 0.164) 128
Figure 6.14: Phase contrast images of *B. subtilis* 1A578 (150 µg/mL BPEI, OD_{600} = 0.181)……128
Figure 6.15: Phase contrast images of *B. subtilis* 1A578 (150 µg/mL BPEI, OD_{600} = 0.243) 129
Figure 6.16: Phase contrast images of *B. subtilis* 1A578 (150 µg/mL BPEI, OD_{600} = 1.246) 129
Figure 6.17 SEM image, *B. subtilis* 1A578, No BPEI, OD_{600}=0.174, 1150x ... 131
Figure 6.18 SEM image, *B. subtilis* 1A578, 150 µg/mL BPEI, OD_{600}=0.212, 1150x..... 132
Figure 6.19 SEM image, *B. subtilis* 1A578, 150 µg/mL BPEI, OD_{600}=0.212, 4700x..... 132
Figure 6.20 SEM image, *B. subtilis* 1A578, 150 µg/mL BPEI, OD_{600}=0.187, 4700x..... 133
Figure 6.21 SEM image, *B. subtilis* 1A578, 150 µg/mL BPEI, OD_{600}=0.187, 4700x..... 133
Figure 6.22: Phase contrast images of *B. subtilis* 1A578 (0.0002 M EDTA, OD_{600} = 0.183) 134
Figure 6.23: Phase Contrast images of *B. subtilis* 1A578 (150 ug/mL BPEI and 0.01 M $MgCl_2$, OD_{600} = 0.066)..... 135
Figure 6.24: Phase Contrast images of *B. subtilis* 1A578 (150 µg/mL BPEI and 0.01 M $MgCl_2$, OD_{600} = 0.133) 135

Figure 6.25: The inhibition of growth by EDTA and rescue of growth by Mg^{2+} supplementation 135

Abstract

Metal binding is a known characteristic of the bacterial cell wall. Yet, the binding mechanisms and affinity constants are not fully understood. The cell wall of Gram-positive bacteria is characterized by a thick layer of peptidoglycan and anionic teichoic acids anchored in the cytoplasmic membrane (lipoteichoic acid) or covalently bound to the cell wall (wall teichoic acid). The polyphosphate groups contribute to metal binding, while previous studies have suggested that the carboxyl units of peptidoglycan are primarily responsible for the metal binding behavior of the cell wall. As a result, there are many contradictory theories that describe binding affinity and the binding mode of divalent metal cations.

Equilibrium association constants and total metal binding capacities for the interaction of calcium and magnesium ions with the bacterial cell wall will be reported in this dissertation. Cell wall fragments of a chloramphenicol resistant strain of *B. subtilis* 1A578 were able to bind approximately twice as much Ca^{2+} and Mg^{2+} than a mutant deficient of wall teichoic acid. However, association constants were similar for each sample with both metal ions. Curvature of Scatchard plots from the binding data and the resulting two regions of binding affinity suggest the presence of negative cooperative binding, meaning that the binding affinity decreases as more ions become bound to the sample. This contradicts the current paradigm of there being a single metal affinity value that is constant over a range of concentrations.

One of the many functions of teichoic acid involves obtaining and sequestering metal ions required for biochemical processes. These ions must traverse the thick layer of peptidoglycan and reach the cytoplasmic membrane where transmembrane proteins control transport into the cell. Delivery of metals is aided by anionic binding sites within the peptidoglycan and the along the phosphodiester polymer of teichoic acid. The interaction with metals is a delicate balance between the need for Coulombic attraction and ion diffusion to the membrane. Through the use of Flame AA and equilibrium dialysis, we are able to measure the metal binding capacity and metal binding affinity of wall teichoic acid and Mg^{2+}. The data show that Mg^{2+} binds to WTA with a 1:2 Mg^{2+} to phosphate ratio with a binding capacity of 1.27 μmol/mg. The affinity of Mg^{2+} to WTA was also found to be 41×10^3 M^{-1} at low salt concentrations and 1.3×10^3 M^{-1} at higher Mg^{2+} concentrations due to weakening electrostatic effects. These values are much lower than the values describing Mg^{2+} interactions with either peptidoglycan or peptidoglycan plus covalently bound WTA. Thus, we propose a model of facilitated ion transport to the inner cell wall surface by teichoic acids that permits increased structural integrity from metals binding to peptidoglycan.

Experiments to disrupt the metal binding behavior of the cell wall involved low molecular weight branched polyethyleneimine (BPEI). BPEI is reported to have an antimicrobial effect on bacteria. The killing mechanism of BPEI centers on its polycationic properties. Against Gram-negative bacteria, penetration into the cytoplasmic membrane leads to cell depolarization. The

mechanism of action against Gram-positive bacteria is less understood but work suggests that membrane depolarization also occurs. In this dissertation, a different explanation of cell death is reported. BPEI hinders the binding of essential metals to the cell wall by occupying anionic sites of peptidoglycan and teichoic acid. Through equilibrium dialysis experiments and spectrophotometric quantification methods for BPEI, our data indicate that BPEI becomes electrostatically bound to the cell. This interaction leads to a decrease in the cells wall's affinity and capacity towards Mg^{2+} cations. Additionally, BPEI also causes the release of Mg^{2+} ions from intact whole cells of *Bacillus subtilis.* The decrease in available metal binding sites also explains the ability of BPEI to a cause bacteriostatic effect on bacterial growth.

The in vitro synergistic effects of combinations of BPEI and antibiotics were examined between two resistant strains of *B. subtilis*. The emergence of multi-antibiotic resistant Gram-positive bacteria is becoming an increasing concern. Recent reports have shown PEI to have a synergetic effect with antibiotics on a clinical resistant strain of Gram-negative bacteria. Here we report that similar effects are observed with *B. subtilis*, a Gram-positive bacterium. Furthermore, morphological changes in response to BPEI exposure are reported through the use of both phase contrast microscopy and scanning electron microscopy. Thicker and random coiled bacterial cells that have a perturbed ability to form septa and separate are observed with these microscopy images. Lag phase was increased by up to two days when *B. subtilis* was exposed to sub-lethal concentrations. These cells eventually

reached exponential phase where they began to divide and exhibit traditional morphologies and cell widths.

Chapter 1: Background Information of Gram-Positive Cell Wall

The cell wall of Gram-positive bacteria is an elastic, amphoteric structure with anionic polymers containing charged groups. Metal binding is a known characteristic of the cell wall, although the binding mechanisms and affinity constants are not fully understood. The cell wall of Gram-positive bacteria is characterized by a thick layer of peptidoglycan that has carbohydrate based anionic polymers that, among other things, play a role in metal binding. In addition, there are teichoic acids that are either anchored in the cytoplasmic membrane (LTA) or covalently bound to the cell wall (WTA) that contain polyphosphate groups that additionally aid in metal binding. Previous studies have suggested that the carboxyl units of peptidoglycan are primarily responsible for the metal binding behavior of the cell. Although there have been studies of the metal binding behavior in the past, there are many contradictory results in response to binding affinity and binding modes of divalent metal ions.

The importance of calcium and magnesium ions for a cell's viability has been well documented. Calcium ions have shown to synergistically interact with enzymes that are responsible for anchoring surface proteins to the cell wall which then affect the bacterium's adhesion ability (1). Some pathogens also rely on Ca^{2+} for toxin activity (2). Magnesium ions have been shown to play a role in peptidoglycan synthesis, cell wall strength , and the prevention of cell lysis (3,4). Moreover, calcium and magnesium plays a role in various enzymatic processes. Calcium and magnesium ions are both important biologically active metal ions that are some of the most abundant divalent metal ions in nature.

Equilibrium association constants and total metal binding capacity of calcium and magnesium ions with purified cell walls were determined with *Bacillus subtilis* and a *B. subtilis* mutant deficient of wall teichoic acid. Wall teichoic acid, lipotechoic acid, and peptidoglycan are all major bacterial components for sequestering metal ions in solution. Titration experiments have shown that most Gram-positive cell walls of diverse strains of bacteria have similar functional groups that contribute to metal binding (5-8). This study focuses on the purified portions of peptidoglycan and covalently bound wall teichoic acid. A method of equilibrium dialysis with a concentration gradient of metal ions of a single sample were used experimentally determine binding stability constants and binding capacity using flame atomic absorption spectroscopy.

In the search of broad spectrum antibiotics to combat antibiotic resistance, the characteristics of a bacterium's need to sequester metal ions can be exploited. By inhibiting the uptake of metals we can inhibit cell growth. Polyethyleneimine, a cationic polymer, has been shown to exhibit antibacterial properties. These polymeric cationic antimicrobials supposedly interact with the negatively charged cell wall and do so without permeation through the cell's membrane. Branched polyethyleneimine's antibiotics properties will be reported in this dissertation along with results describing how sub-lethal concentrations of BPEI appear to inhibit metal binding of cell wall fragments. The effects of BPEI on a WTA deficient mutant (EB1451) of *B. subtilis* will be compared with that of *B. subtilis* 1A578.

Cell Wall of Gram-Positive Bacteria

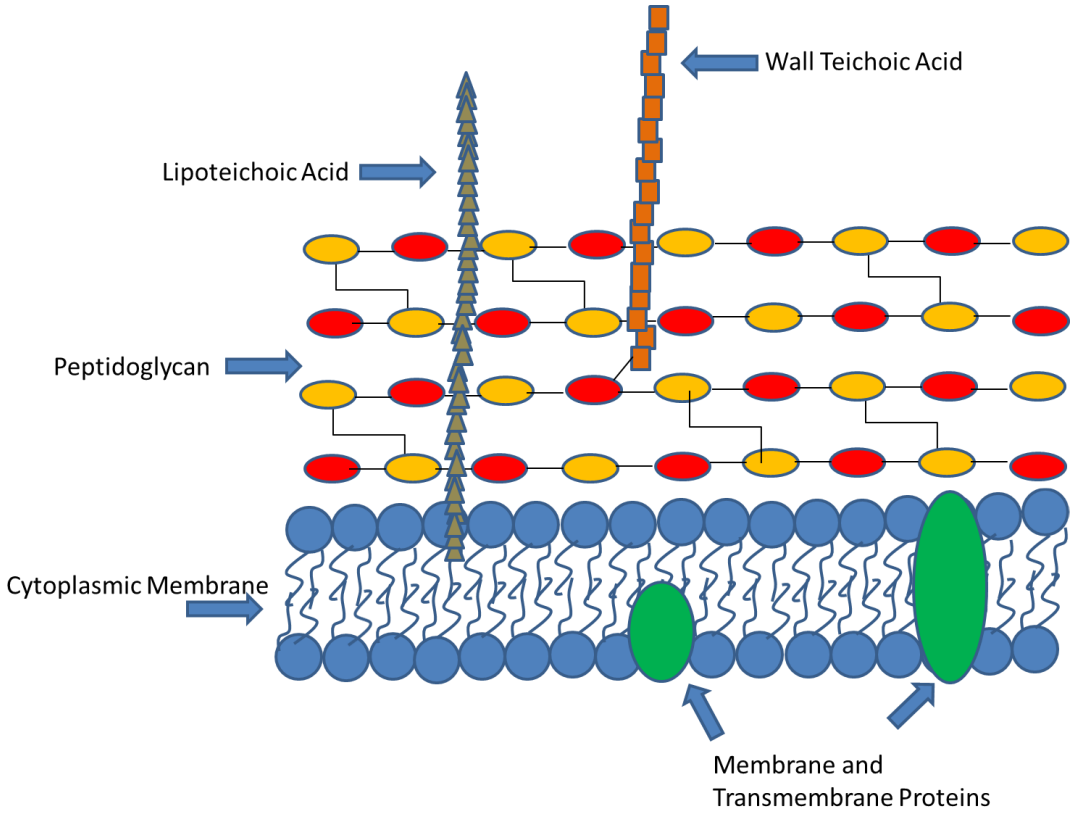


Figure 1.1: The cell wall of Gram-positive bacteria is composed of thick 3-dimension mesh consisting of cross-linked peptidoglycan, teichoic acids, and various transmembrane and membrane associated proteins (represented by green ovals). Adapted from Josset *et al.* (9)

Peptidoglycan

Peptidoglycan is a polymer consisting of a glycan (polysaccharide) backbone consisting of N-acetyl muramic acid and N-acety glucosamine with peptide side chains (amino acids and diaminopimelic acid) that are cross-linked through peptide bonds forming a three dimensional structure. The carboxyl groups on the peptide side chains are the anionic sites for metal binding. Peptidoglycan can have varying types of cross-links between different amino acid units (10,11). The degree of crosslinking can vary from bacterial strain. Cross-linking generally occurs between the amino group of the diaminopimelic

acid and the carboxyl group at position 4 on different peptide strands (11). This cross-linking is either direct or through a peptide bridge. For Gram-positive bacteria this crosslinking mostly occurs through an interpeptide bridge which can vary in length from one to seven amino acid residues. However, peptidoglycan has been reported to have a regular order and a three dimensional structure with 3-fold symmetry (12). The layer of peptidoglycan in Gram-positive bacteria is much thicker than in Gram-negative bacteria with a typical thickness of around 50 nm (13). This thick, 3D-mesh of peptidoglycan is able to withstand a turgor pressure of around 20 atm (13).

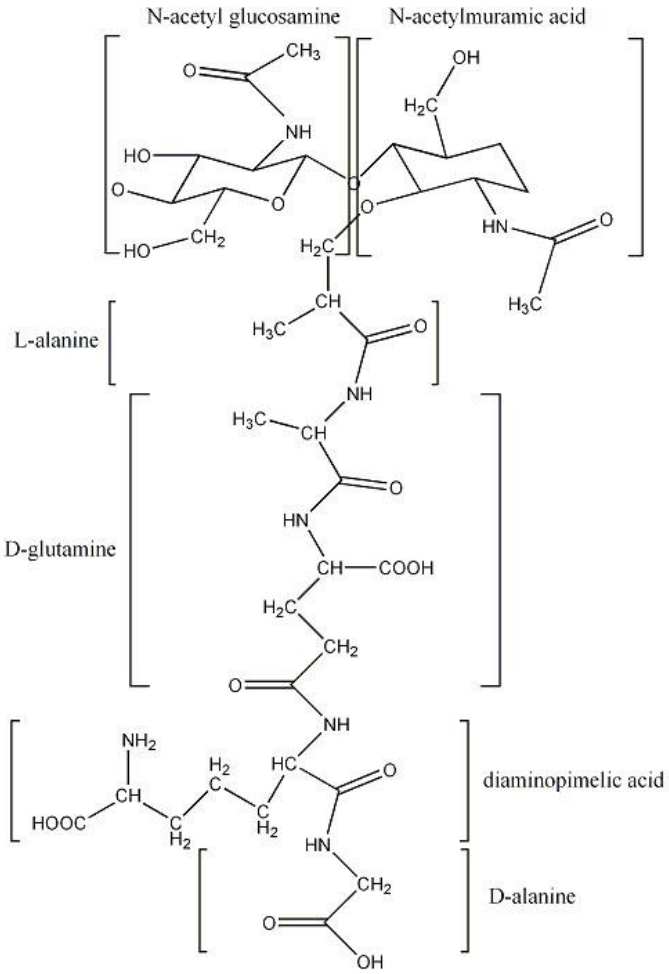


Figure 1.2: The structure of a monomer of peptidoglycan which have various crosslinking with neighboring amino acids and diaminopimielic acid components of other monomers forming a three dimensional mesh consisting of various layers.

Teichoic Acids

Teichoic acid is described based on its location on the cell. Lipoteichoic acid is anchored into the cytoplasmic membrane via a lipid tail, while wall teichoic acid is covalently bound via a linkage unit containing a disaccharide and one to three glycerol phosphate monomers (14). The *tar* and *tag* genes are respectively responsible for the production of these two forms of wall teichoic acid. Depending on the strain of bacteria, wall teichoic acid consists of either a poyl(glycerol phosphate) or a poly(ribitol phosphate) backbone*. B. subtilis* strain

W23 produces a poly(ribitol phosphate) while *B. subtilis* strain 168 produces a poly(glycerol phosphate). The phosphodiester linkages are the primary metal binding sites for teichoic acids.

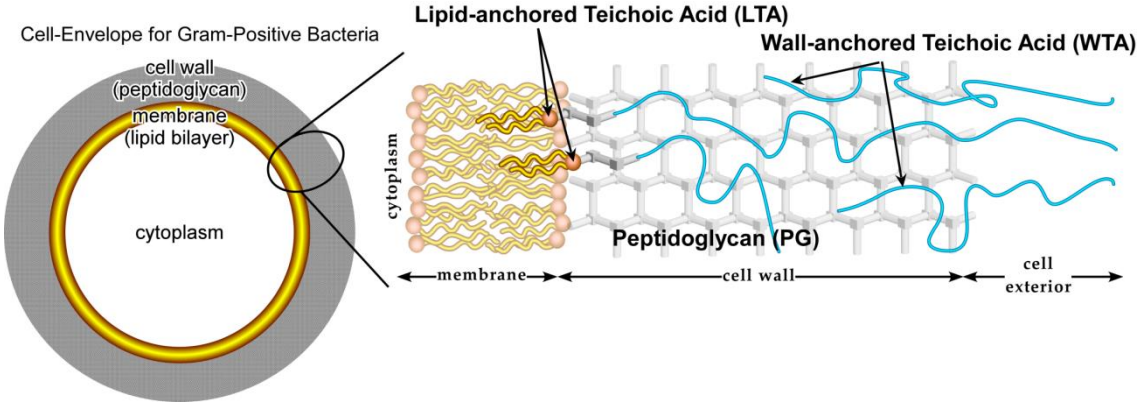


Figure 1.3: Teichoic acids are named based on their location and how they are connected to the cell wall. Liptoteichioc has a lipid tail anchored into the cytoplasmic membrane and wall teichoic acid is covalently bound to the cell wall peptidoglycan.

The D-alanylation of teichoic acids have been found to be affected by the pH of growth media, temperature of growth conditions, and NaCl content in the growth medium. As the pH of the growth media increased from 6.07 to 8.10 the D-alanine ester content of both WTA and LTA decreased. At 6.07, 7.05, and 8.10 the WTA D-alanine ester content in terms of moles of D-alanine per mole of phosphorus reported by MacArthur and Archibald were 0.65, 0.40, and 0.02 respectively (15). For LTA at the same pH values the D-alanine ester content was 0.75, 0.54, and 0.07. In addition, an increase in temperature has a negative effect on the amount of D-alanylation.

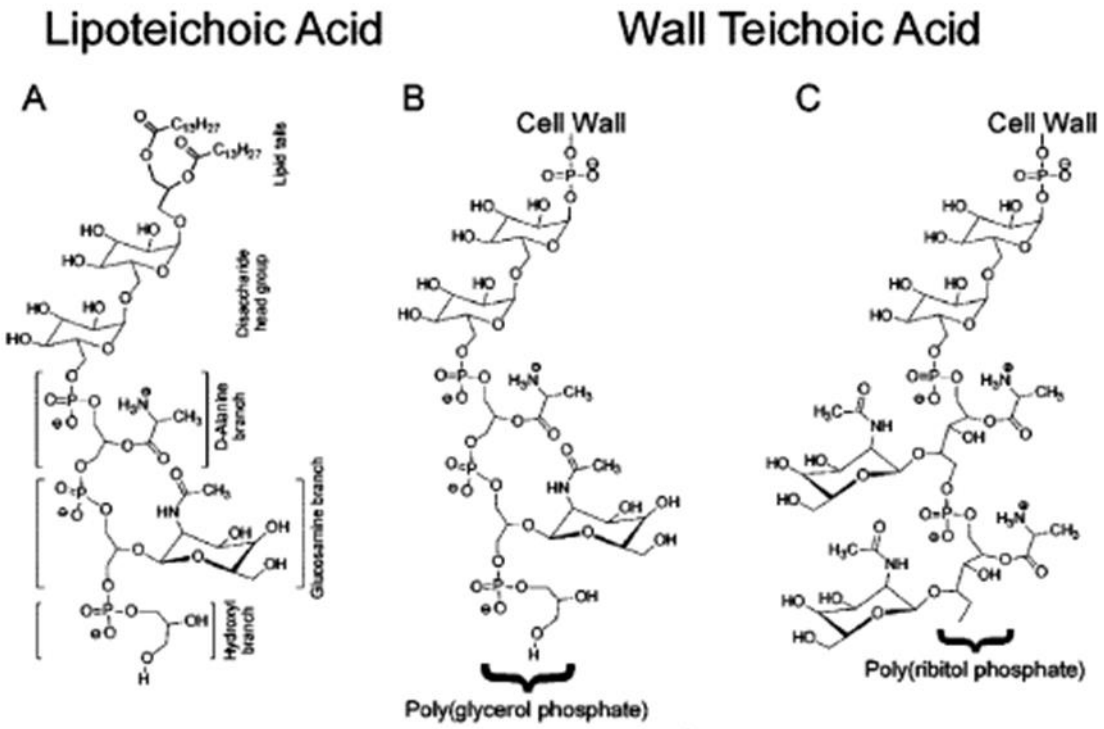


Figure 1.4: The structure of all teichoic acids are based on a polyphosphate backbone. Wall teichoic acids are strain dependent and either exist as a poly(glycerol phosphate) with 3 carbon atoms between each phosphorus or a poly(ribitol phosphate) with 5 carbon atoms between each phosphorus.

The D-alanine group is predicted to have a pK_a of 8.42, meaning that it is protonated around circumneutral pH and possesses a positive charge (16). Bacterial strains that don't possess D-alanylation because of a mutation on the *dlt* gene (which is responsible for synthesizing or attaching D-Ala ester to teichoic acids) have been shown to lose their ability to form biofilms on polystyrene or glass (17). The cause of their inability form biofilms on polystyrene or glass is reported to be because of its stronger negative charge.

The significance of the D-alanylation of teichoic lies in its ability to repel cationic antimicrobial peptides. A proposed property of the D-alanine to form a contact ion pair with near phosphate groups was originally thought to be the cause of the ability of D-alanine to repel CAMPs (Cationic Antimicrobial

Peptides), since the resulting net charge between the alanine and phosphate group would be zero. This proposed model would inhibit metal binding (18). Recent research with solid state NMR has shown that the nitrogen – phosphorus distance measurements are not in agreement with that model and that Mg^{2+} preferentially binds to the phosphate groups regardless of D-alanine present on teichoic acids (19).

Wall Teichoic Acid Deficient Bacterial Mutants

Teichoic acids are indispensable for cell viability. Deletion strains of bacteria either lacking LTA or WTA have been shown to be viable. These strains exhibit differences in morphology as shown in the WTA deficient mutant in Figure 1.5.



Figure 1.5: Phase contrast images of two strains of *B. subtilis*. Wall teichoic acid deficient *B. subtilis* mutants have drastically different morphologies at the cellular level. The *B. subtilis* WTA deficient mutant, EB1451 (right) exhibits swelling and clumping that uncharacteristic of the typical morphology of *B. subtilis*, 1A578 (left).

Additionally, mutant strains lacking either WTA or LTA have been shown to grow considerably slower than their parent strains. However, deletion of both

LTA and WTA stop cell growth completely. This evidence leads to the possibility that WTA and LTA have similar functions that can compensate for each other. Studies with bacterial mutants with altered teichoic acids have shown that they play a function in the following areas listed below in Table 1.1 (17,20-40). Most notably is the requirement of WTA for cell adhesion and biofilm production which are two aspects associated the bacteria's ability to infect hosts.

Function	**TA**	**References**
Protection against cell damage		
Resistance to antimicrobial peptides	D-ala of TA	(24,27,28,41)
Resistance to cationic antibiotics (e.g. vancomycin)	D-ala of TA	(42)
Resistance to lysozyme	WTA	(29)
Resistance to antimicrobial fatty acids	WTA	(22)
Resistance to heat stress	WTA, LTA	(23,25,30)
Resistance to low osmolarity	LTA	(23)
Controlling protein machines in the cell envelope		
Cell division site placement	LTA	(20,23)
Autolysin activity	WTA, LTA	(25,31,32)
Mediating interaction with receptors and biomaterials		
Adherence to epithelial and endothelial cells	WTA	(26,27,43)
Serving as a phage receptor	WTA	(39,40)
Mediation attachment to biomaterials and biofilm formation	LTA, WTA	(17,25,32)

Table 1.1 Functions of teichoic acids. (adapted from Xia *et al.* (44))

Role of Teichoic Acid in Pathogenesis

Cell wall teichoic acids are essential for the virulence of Gram-positive pathogens. The *tagO* mutant of *S. aureus* has been investigated in the past and such research has demonstrated that WTA is plays a major role in cell adhesion, biofilm production, host infection, and the binding of metal ions

(17,25,45). Studies with the *tagO* mutant of *S. aureus* have shown that WTA is needed to cause intranasal infections in experiments utilizing a rat model. Furthermore, WTA has been shown to be important for bacterial skin colonization and protects *S. aureus* against antimicrobial fatty acids present on skin as presented by Kohler *et al.* (22).

The use of genetic mutation studies using the *tagO* mutant of *Staphylococcus aureus* has found that WTA is essential for nasal colonization and infection. Utilizing a cotton rate model which have nares with histological properties similar to humans, Weidenmaier *et al.* infected the animals with equal numbers of either wild-type bacteria or WTA deficient bacteria with the *tagO* mutation (26). The results of this study showed that colonization of the *tagO* mutant group was present one and two days after instillation of rats at amounts of 90.7 ± 1.4% and 98.3 ± 0.3 when compared to the wild-type group. At 7 days, the *tagO* mutant group exhibited no colonization, while the wild-type group showed CFU (colony forming unit) values with a mean and media of 6011 and 6207 respectively. However, another mutant, the *dltA* mutant that lacks the DNA modification in teichoic acids showed colonization in 4 out the 10 rates in the group with very low CFU mean and median values of 30 and 33. D-alanylation of teichoic acids have been shown to be a mechanism in which Gram- positive bacteria defend themselves from cationic antimicrobial peptides. It has also been indicated that D-alanylation produces conformational changes of LTA which in return increase the cell wall density (46).

Due to the nature of WTA's role in causing infections, it has been proposed as a target for future antibiotics. A potential antibiotic is being investigated by others that inhibits a late step in wall teichoic acid biosynthesis (47). This antibiotic targets a transmembrane component that leads to the transports WTA to the cell's surface.

Role of Metals in Cell Viability and Pathogenesis

The importance of calcium and magnesium ions for a cell's viability has been well documented in the past. Calcium ions have been shown to synergistically interact with enzymes that are responsible for anchoring surface proteins to the cell wall which then affect the bacterium's adhesion ability. Magnesium ions have been shown to play a role in peptidoglycan synthesis, cell wall strength, and the prevention of cell lysis.

Calcium ions play a role in biofilm production. Dental plaque has been found to have a high calcium ion content and data from experiments performed by Rose *et al.* have found that in streptococci, calcium binding mostly occurs within the teichoic acid phosphate groups (48). This study found a wide array of calcium binding capacities for streptococcus ranging from 0.129-1.52 μmol/mg using a labeled calcium chloride with radioactive assays. In addition, the amount each functional group contributes to metal ion binding is dependent on the strain of bacteria being analyzed.

In addition, calcium ions have been said to synergistically interact with enzymes that are responsible for anchoring proteins that aid in the adhesion of bacteria. Sortase, a protein responsible for bacterial adhesion, is a proposed

target for anti-infective therapy. Calcium ions have been found to increase the activity of *Staphylococcus aureus* by 8-fold (49).

Metal Ion Homeostasis in Bacteria

Mg^{2+} and Ca^{2+} are the two most abundant divalent metal ions in bacterial cells. Cellular concentrations of Mg^{2+} and Ca^{2+} are 5 to 30 mM (50) and around 100 nM (51) respectively. The majority of Mg^{2+} in the cell is bound to ligands, leaving only 0.4-0.6 mM in the free, unbound form (50). It has been thought that the negatively charged polymers (teichoic acid for Gram-positive bacteria and LPS for Gram-negative bacteria) provide a reservoir of metal ions in the cell to then interact with the cell's membrane (52,53). Transport of metals into the cytoplasmic membrane is then performed through active transport by transmembrane proteins (52,54). These transmembrane proteins have been reported to rely on the electrochemical gradient across the cytoplasmic membrane to transport Mg^{2+} (55). The reliance on the membrane potential means that changes in pH and/or changes in the concentration of other ions will influence transport (52).

Chapter 2: Experimental Procedures

Preparation of LB media

Lysogeny broth was used as the growth media for *B. subtilis*. LB growth media was made by dissolving 10 g of tryptone, 5 g of yeast extract, and 5g of sodium chloride into a 1 L graduated cylinder filled with ~800mL of Milli-Q water. This mixture was allowed to stir around 5 minutes or until fully dissolved, the cylinder was filled to the 1L mark, and then allowed to stir briefly to obtain a homogenous solution. The growth media was then transferred to the flask used to grow cultures and then immediately sterilized by autoclave for 30 minutes to obtain sterility.

Cell Growth Protocol

B. subtilis 1A578 was obtained from the Bacillus Genetic Stock Center (BGSC). *B. subtilis* strain 1A578 is chloramphenicol resistant strain (up to 20 μg/mL) of parent strain *B. subtilis* 168 that is susceptible to chloramphenicol at 2 μg/mL (1). *B. subtilis* EB1451 was obtained from Eric Brown (McMaster University). EB1451 (a mutant of parent strain EB6) is deficient of WTA and has resistance to erythromycin. The growth protocol for *B. subtilis* 1A578 involved transferring 20 mL of LB through an autoclaved serological pipette to an autoclaved 125 mL Erlenmeyer flask. 20 μL of 10 mg/mL chloramphenicol solution was then added to media. A small amount of bacteria from a frozen stock was then added to the flask and allowed to sit in an incubator / shaker at 37ºC overnight. These overnight cultures were then used to inoculate larger cultures (usually of 500 mL) by transferring a volume of the overnight culture

equal to 1% of the new culture and adding an amount of chloramphenicol stock solution to create a final concentration of 10 μg/mL. A similar growth protocol was used for *B. subitlis* EB1451 with the exception of erythromycin being used in place of chloramphenicol.

Cell Wall Purification

Cell walls were purified from exponential phase cultures of *B. subtilis* 1A578 and *B. subtilis* EB1451 (WTA deficient mutant). Cells were grown in Lysogeny broth and then collected by centrifugation at 15000g for 25 minutes once the culture reached an OD_{600} of approximately 1.0. The cells were then disrupted using a Thermo® French press or an Avestin® Emulsiflex C3 high pressure homogenizer. The disrupted cells in solution were then centrifuged for 30 minutes at 20000g and the pellet containing the insoluble cell wall was retained and re-suspended in 10 mL distilled deionized water. This suspension of cell fragments were then added drop wise with stirring to 60 mL of boiling SDS in order to inactivate autolysins as well as remove the cytoplasmic membrane. The cells were then rinsed with 200 mL of distilled deionized water by centrifugation at 15000g for 20 minutes three times. The cells were then re-suspended in TRIS buffer (pH 8.2) and treated with ~1 mg trypsin and ~0.5 mg RNAse/DNAse at 37ºC in and incubator/shaker for 16-18 hours. The cells were then spun down again, washed with fresh distilled deionized water, and then re-suspended in Ammonium Acetate buffer (pH 4.7) and treated with 5 mg of pepsin at 37ºC for 2 hours. Finally, the cells were centrifuged, washed with 50 mL of 50 mM EDTA in order to remove any residual metal ion contamination,

and then washed 3 times with 200 mL of Milli-Q. The cells were then suspended in a minimal volume of Milli-Q, lyophilized, and stored in the -20ºC freezer.

Hydrolysis to Separate WTA from Peptidoglycan

Portions of the freeze dried cell wall also underwent a 10% TCA (trichloroacetic acid) treatment at 4°C for 48 hours in order to remove the WTA (2) in order to study the peptidoglycan component of *B. subtilis* 1A578. The cell wall sample was composed of peptidoglycan and covalently attached WTA as depicted in Figure 2.1. After 48 hours, the suspension of 10 mL was centrifuged at 15000 g and the supernatant was transferred to two 14 cm 500 MWCO dialysis membranes and placed in 1.5 L Milli-Q H_2O to remove the trichloroacetic acid. The water was changed every 12 hours for a total of 4 times. Swelling of bags did occur due to osmotic pressure change from the exchange of TCA in solution. The contents of the dialysis bag were then lyophilized for 1 day and then re-suspended in 1 mL of Milli-Q H_2O and placed in a 500 MWCO dialysis membrane which was then placed in jar containing 50 mL of 0.05 M EDTA to remove any metal ion contamination. This jar was placed in an incubator / shaker (200 rpm, 4°C) overnight. The dialysis membrane was transferred to a large beaker containing 1000 mL of Milli-Q H_2O in a cold room and the water was changed at 5 times at an approximate 6 hour time interval. The solution in the membrane was then transferred to a 1000 MWCO dialysis membrane and placed in 100 mL of Milli-Q H_2O and the water was removed 3 times at a 4 hour time interval. The change in dialysis membrane molecular

weight cutoff size was performed as part of a precautionary step to avoid permeation through the membrane.

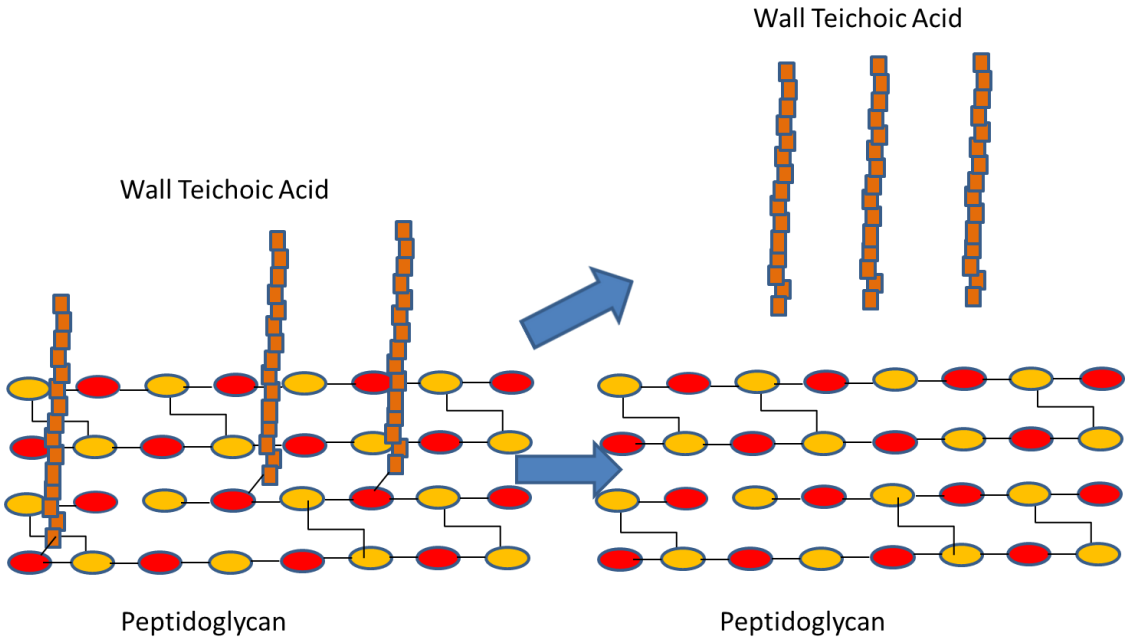


Figure 2.1: Results of the cell wall purification process and the WTA hydrolysis. The peptidoglycan component is insoluble and is separated via centrifugation, while the insoluble wall teichoic acid goes through additional membrane dialysis purifications steps to remove the TCA.

Preparation of Metal Ion Standard Solutions

The normal protocol for making metal ion standard solutions for calcium involve weighing a known amount of oven dried $CaCO_3$, dissolving it in 1 N HCl, and then diluting with distilled deionized water to the desired volume. This creates the problem of having acidic aliquots being added to the samples absorbing Ca^{2+} ions as the concentration gradient is formed, thus causing a pH gradient as well. Binding constants and metal binding capacity to teichoic acids and peptidoglycan is dependent on pH (3,4). $CaCl_2$ could not be used because of difficulties quantitatively weighing a known mass due to its hydroscopic

nature. In order to overcome these obstacles, a known mass of oven dried $CaCO_3$ was weighed and then reacted with a minimal amount of HCl to form an aqueous acidic mixture of $CaCO_3$. This solution was lyophilized to remove the H_2O and HCl. The sample was then dissolved in Milli-Q H_2O and then diluted to the desired volume.

Fundamentals of Dialysis

Dialysis is based on the selective retention of molecules based on size. A dialysis membrane is able to retain molecules of above a certain size based the average pore size of membrane and the diameter of a molecule. The dialysis membrane can structurally vary. The membrane used in this study was regenerated cellulose. The structure of a subunit of a cellulose polymer is depicted in Figure 2.2. This polymer exhibits structural symmetry and the permeability / pore size can be controlled (5). Spectrum Labs, the manufacturer of the dialysis membranes used, defines the MWCO (molecular weight cutoff) as an indirect measurement of a solute size that is retained by at least 90% during a 17 hour period. For this reason a much smaller molecular weight cutoff needs to be selected. The cell wall fragments with either peptidoglycan or peptidoglycan with covalently attached WTA are much higher than 1000 amu. Likewise, WTA has been reported to have a molecular weight in the range of 24800, which is much larger than 1000.

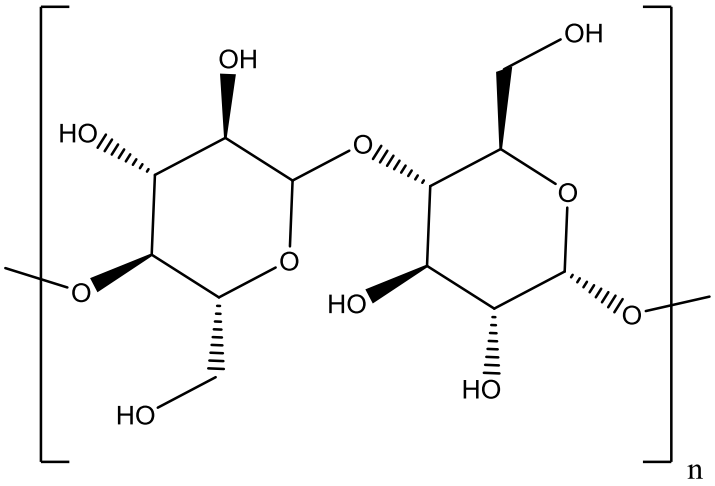


Figure 2.2: Structure of Cellulose. Cellulose is a polymer that consists of several thousands of f β(1→4) linked D-glucose units. These long strands have a tendency to aggregate and form ordered structural entities due to hydrogen bonding.

Membrane Dialysis Procedure

A known mass of around 15-40 mg of the purified cell wall material (peptidoglycan + WTA) was suspended in 1-2 ml of Milli-Q H_2O, transferred to a 6.5 cm length, 1.8 cm width, 1000 MWCO Spectra/Por® 7 dialysis membrane and placed in a closed jar with a final volume of 50 mL of Milli-Q H_2O (including the volume of H_2O in the dialysis bag). Metal ions much smaller than a molecular weight of 1000 amu could flow freely through the dialysis membrane, while cell wall fragments, much larger than 1000 amu, remained inside the dialysis membrane. This simple setup is represented by Figure 2.3. The jars with dialysis membranes were placed in a cold room (4°C) and shaken on New Brunswick G24 incubator/shaker. Equilibrium dialysis experiments indicated that full equilibration between metal ions in and out of the dialysis bag without cell wall was achieved after 12 hours. Every 12 hours a 5 mL aliquot was removed from the jar and 5 mL of a known metal ion concentration (20 ppm)

was added in order to obtain a concentration gradient. Utilizing a Varian SpectrAA 55b Flame Atomic Absorption Spectrometer, the concentration of the aliquots were determined, and that data was placed into an Excel spreadsheet in order to in order to calculate the Ca^{2+} or Mg^{2+} bound on the cell wall in dialysis membrane, the binding capacity of Ca^{2+} or Mg^{2+}, and ultimately create a Scatchard plot to extrapolate binding constants.

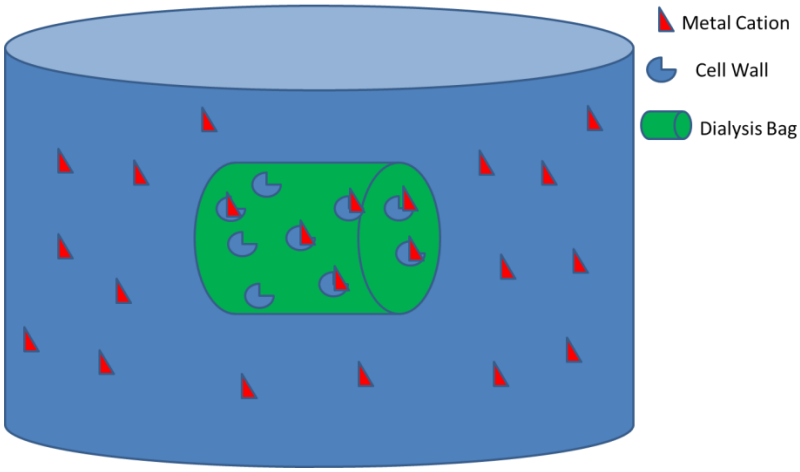


Figure 2.3: Membrane dialysis of cell wall material involved having a known quantity of cell wall material on the inside of a closed dialysis bag with a pore size that lets metal ions flow freely in and out, while keeping the cell wall material trapped inside.

General Principles of Flame AA

The fundamental principles behind atomic absorption spectroscopy have been around since the late 1800s and the first atomic absorption spectrometers have been around since the late 1950s. It has been the most widely method to quantify single element concentrations in which ultralow limits of detection are not needed. Flame atomic absorption spectroscopy has been used extensively in this dissertation to explain the metal binding characteristics of several cell components and as a result the general principles will be explained in depth.

Each atom on the periodic table has a characteristic line spectrum. Each line in the spectrum tells us about the energy levels present in the atom. Electrons gain energy and have a transition from a ground state and into an excited state. Quantum theory defines the electronic energy levels of an atom and these values are available through reference tables (6). This energy transition generates the emission spectrum. The light source of an atomic absorption instrument must produce a line spectrum with a narrow band that is as narrow as the emission spectrum. A monochromater does not have the capability to produce these narrow bands with an adequate intensity so a hollow cathode lamp with the element of interest must be utilized. These hollow cathode lamps are composed of the metal of interest at the cathode and filled with an inert gas at low pressure which ionizes when a potential is formed between the electrodes in the lamp. Gaseous metal vapor then fills the tube from ions of the inert gas colliding with metal cathode. The collisional energy causes the electrons of the metal of interest to enter into an excited state creating the aforementioned emission spectrum.

As a metal ion solution is aspirated through the system via a nebulizer that converts the analyte liquid into a fine spray. The nebulized liquid then goes into a mixing chamber to mix with the oxidant (air) and fuel (acetylene) that flows into a laminar flow burner. The laminar flow burner has a relatively long path length and a stable flame which together enhance the sensitivity and reproducibility of the instrument. The optimum flame height to observe depends on the element being analyzed and the properties of each element in terms of

how easy it is oxidized. In the flame, liquid droplets of the solvent evaporate, either thermal dissociation of molecules into atoms or reduction of ions occurs, and ground state atoms are formed. These ground state atoms then absorb the exact energy required for excitation from a hollow cathode lamp of the element being analyzed. This process is denoted on the flowchart in Figure 2.4. The incomplete dissociation of molecules or the ionization of metal ions can pose a problem in determining concentrations of a sample. However, in our simple system consisting of only H_2O and low (0-10) ppm alkaline earth metal ions with the use of an air-acetylene flame, these two factors are not of concern.

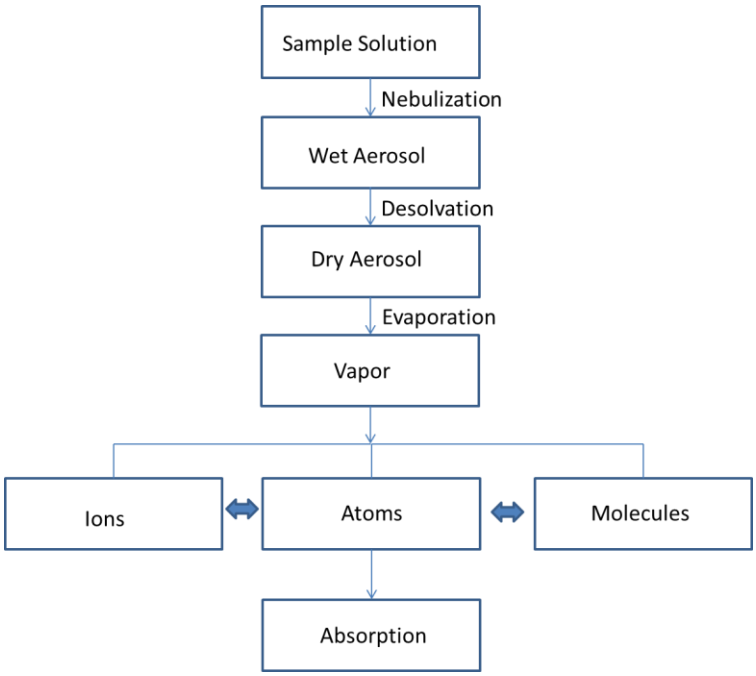


Figure 2.4: Flowchart of nebulization process leading to absorption of light energy emitted from the hollow cathode lamp.

A monochromator placed after the flame is used to disperse the light to obtain a wavelength of interest from this spectrum. A blank is aspirated through the instrument and the intensity of that wavelength selected by the

monochromator is recorded and the difference when the analyte is aspirated is calculated as a percent of transmission, which is further calculated to an absorbance value which is linear in a certain range, defined by the linear dynamic range inherent in the instrument. The concentration of analyte is directly proportional to the absorbance value. This relationship is given by Beer's law which is given by the simple equation of $A = abc$. This equation includes "A" the absorption value, "a" the absorptivity constant, "b" the path length, which in this case in the length through the laminar flame at its longest distance, and "c" which is the concentration. Since "a" and "b" are constant, "A" is the only value that is directly proportional to the concentration. A basic representation of the components of a flame atomic absorption spectrophotometer can be viewed in Figure 2.5.

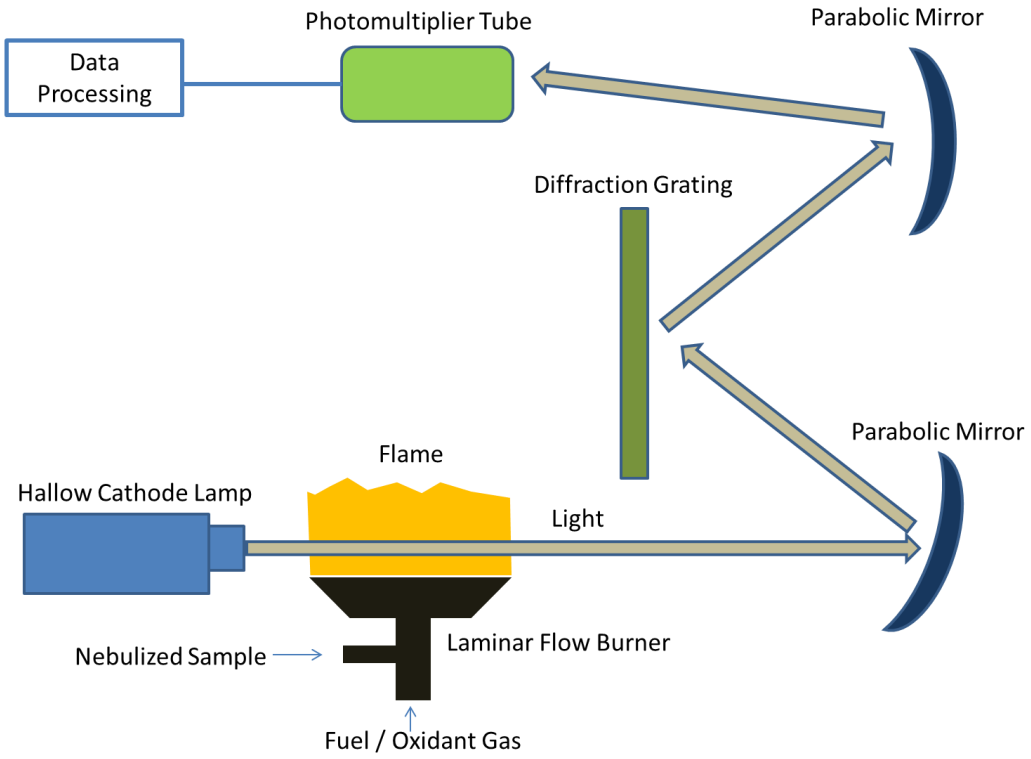


Figure 2.5: The basic representation of a flame atomic absorption spectrophotomer includes a hollow cathode lamp that produces line width wavelengths associated with the element of interest, a nebulizer, a laminar flow burner, various mirrors and gratings, as well as a photomultiplier tube to convert photons to a quantifiable signal related to absorbance. Adapted from http://www.analyticalspectroscopy.net/ap5-7.htm

Dialysis Equilibration Optimization

The optimal time between metal ion solution extractions and additions to the system was determined by monitoring the increase in Ca^{2+} outside of a dialysis bag. Spectra/Por® 7 Standard Regenerated Cellulose tubing with a molecular weight cutoff of 1000 Daltons was obtained from Spectra Labs. A 2 mL volume of 211.759 ppm Ca^{2+} was placed in a 1000 MWCO dialysis membrane which was then placed in 50 mL of Milli-Q H_2O. A 2 mL aliquot was taking from solution outside of the dialysis membrane at different time intervals and saved for Flame AA analysis. From this graph (Figure 2.6) we can

determine that a 12 hour interval between metal ion additions / extractions gives enough time for the system to equilibrate. Divalent calcium ions have been reported to have a radius 114 picometers and divalent magnesium ions have been reported to have a radius of 86 picometers. Due to the smaller radius of Mg^{2+}, it is safe to accept a 12 hour equilibration time since smaller ions have a higher rate of diffusion through a porous membrane.

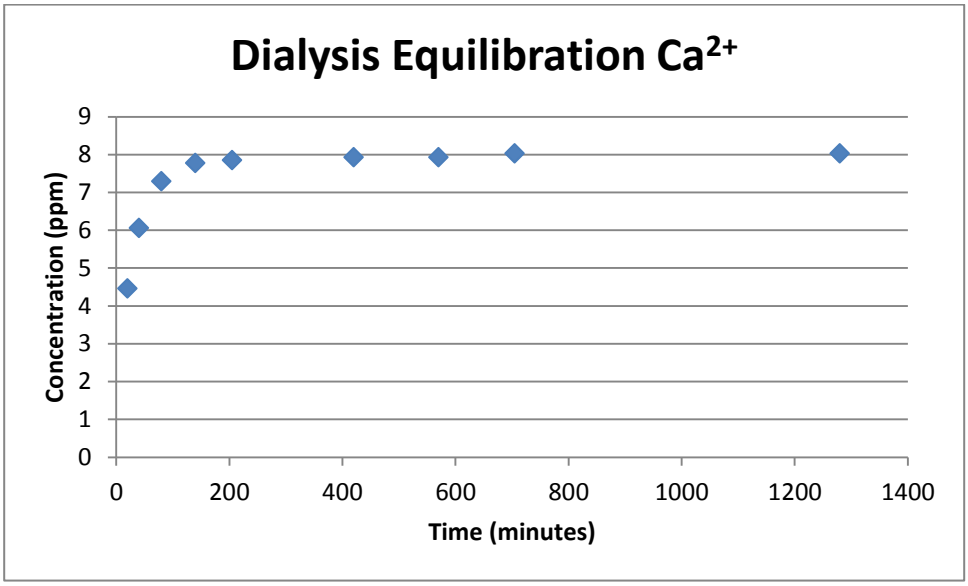


Figure 2.6: Length of time for Ca^{2+} ions to equilibrate inside and outside of the dialysis membrane.

Scatchard Plot Analysis

In order to extrapolate binding constants and metal binding capacities a Scatchard plot is utilized (3,7). Previous works in directly determining binding characteristics of metal with cell wall functional groups have utilized Scatchard plots (3,8). Scatchard plots are used to analyze both the binding constant and binding capacity from data obtained for reversible ligand and substrate binding characteristics. The purpose of the Scatchard plot is to create a linear transformation of the binding curve in a way to easily calculate the binding

slope, which is represented by the absolute value of the slope of the line and in order to calculate the binding capacity which is represented by the x-intercept of the line as seen in Figure 2.7. A non- linear optimization and regression to extract adsorption parameters could have been used but this technique would not account for changes in affinity caused by a change in the electrostatic properties of the cell wall sample due to binding events.

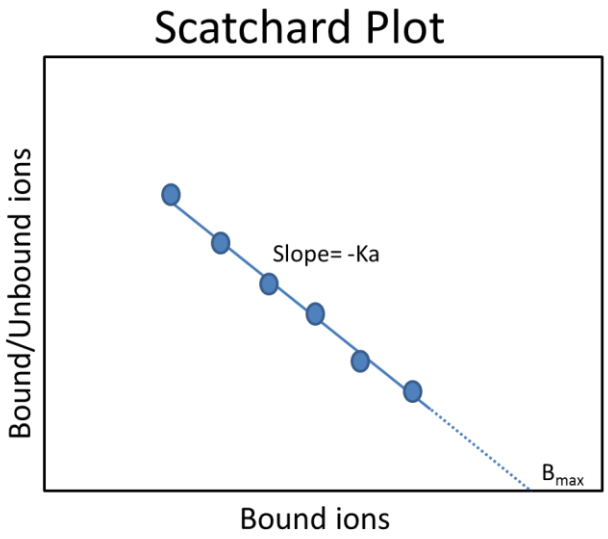


Figure 2.7: Characteristic Scatchard Plot. In a non-cooperative system, the Scatchard Plot consists of a linear regression of a straight line. The negative value of the slope is equal to the equilibrium constant K_a and the value of x-intercept is the binding capacity.

Hill Plot Analysis

Negative cooperative binding has been shown to have Scatchard plots that are shaped with a concave up curve (9). In addition, Scatchard plots that exhibit this concave up feature which deviates from linearity can also be the result of multiple classes of binding sites. We know that the cell wall has peptidoglycan with carboxyl sites as well as wall teichoic acid with phosphate metal binding sites. The combination of a low affinity binding site and high

affinity binding site could cause this deviation from linearity in the Scatchard plot. Data from individual components of the cell wall must be examined in order to determine whether cooperativity in binding exists. Due to the three dimensional polyanionic nature of the cell wall and the crosslinking present in peptidoglycan, the configuration of binding sites in the matrix might lead to binding sites with varying affinities for metal ions.

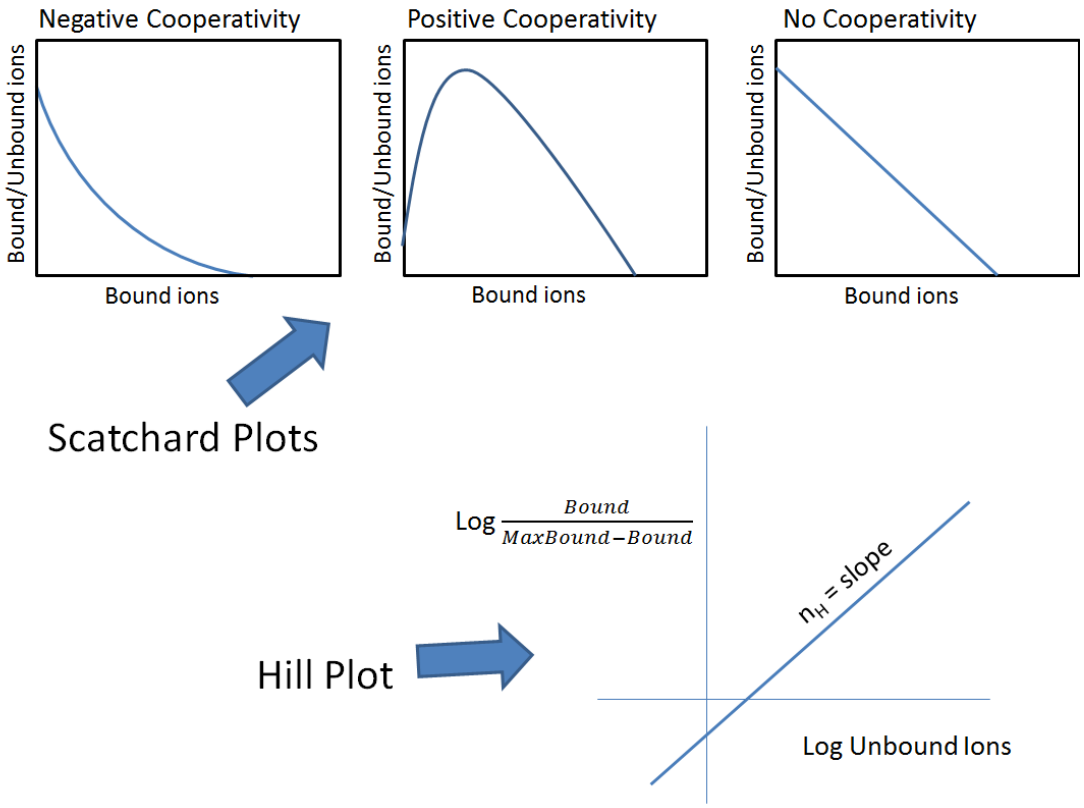


Figure 2.8: Scatchard plot shapes and associated Hill plot in cooperative and non-cooperative systems. The shape of the Scatchard Plots on the top gives an indication whether cooperative binding exists in the sample. In order to test cooperative binding a Hill Plot is created and the slope of the resulting line is examined.

In order to test for binding cooperatively a Hill plot is generally used. Specifics regarding the use and creation of a Hill plot were taken from a paper

published by Sabouri and Moosavi-Movahedi (11) concerning the use of the Hill coefficient from Scatchard and Klotz plots. A Hill plot is formed by plotting the fraction of substrate bound to ligands to the free substrate concentration. The only information obtained from a Hill plot is the presence of cooperativity when its slope is not equal to 1. In the event the slope is less than one there exists negative cooperativity in the binding system in which K_{assoc} continually decreases as the concentration of substrate increases which in this case is a metal ion.

Characterization of BPEI by Mass Spectrometry

An ESI(+) mass spectrum was taken to find the mass distribution of the polymer used in our experiments. From the mass spectrum (Figure 2.9), we can see that when this polymer is added to aqueous solution, it is not as charged as previously thought. The protonation of the amine groups is dependent on the pH and not all amine groups will be protonated at circumneutral pH. BPEI is weakly basic and a 0.1 g/L concentration yields a pH of around 9.8 in Milli-Q H_2O.

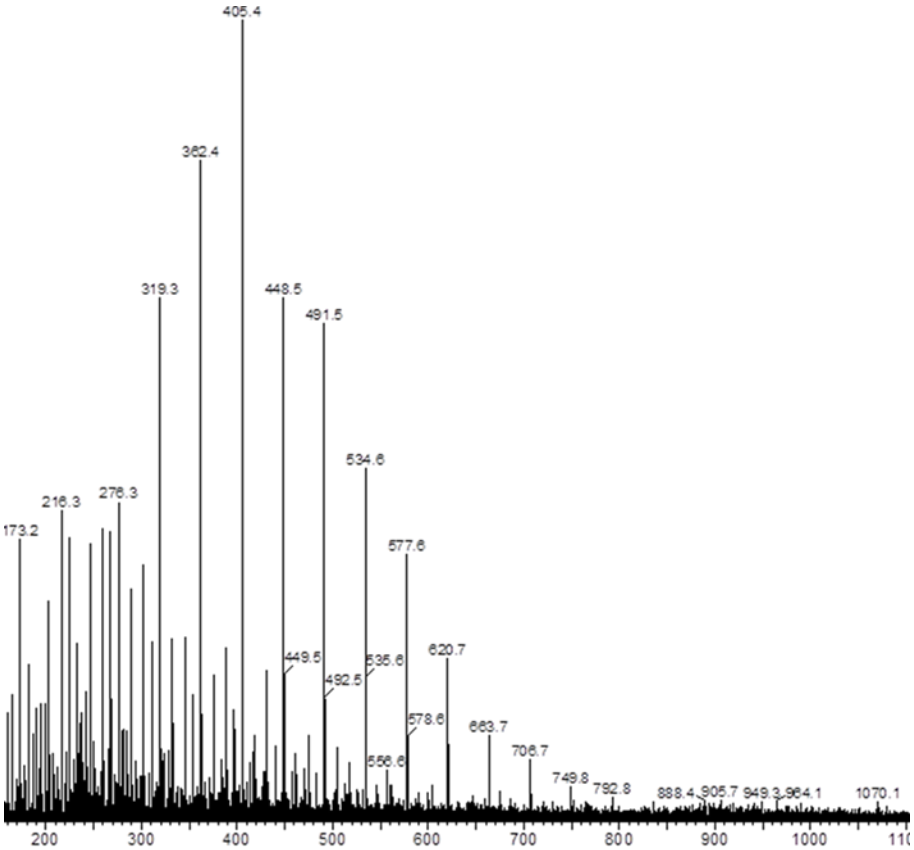


Figure 2.9: ESI(+) spectrum of the low molecular weight branched polyethyleneimine used in our experiments showing the molecular mass range of the polymer.

An example structure of BPEI corresponding to the (M+H)+ = 362.4 amu in the mass spectrum is shown in Figure 2.10. Depending on pH, the amine groups will become protonated and impart cationic properties on the polymer.

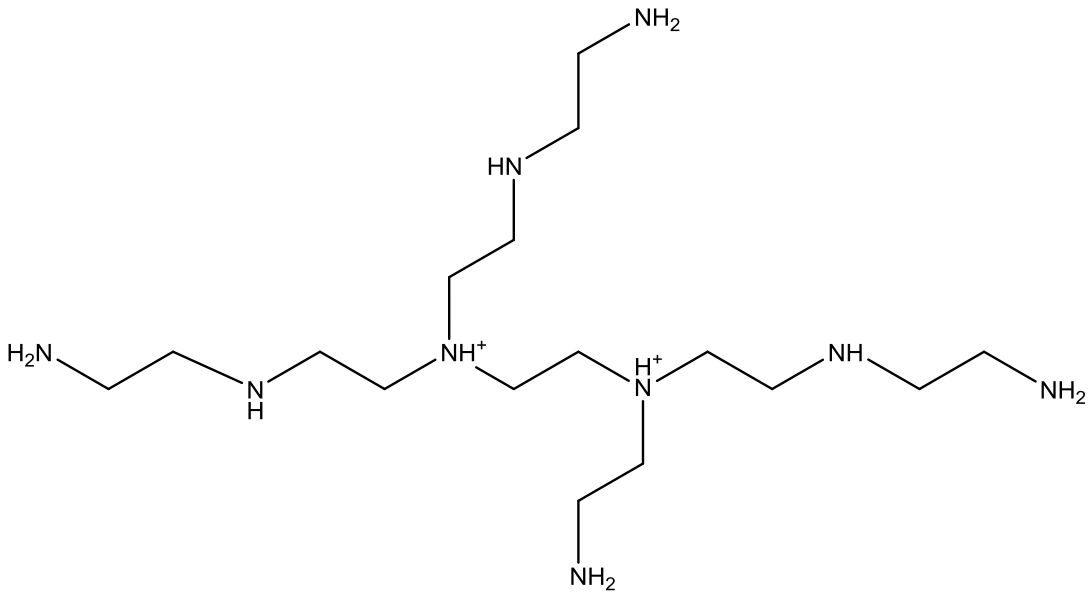


Figure 2.10: An example of one structure of low molecular weight branched polyethyleneimine. The pK_a protonation constant values for branched PEI are around 4,5 for primary, 6.7 for secondary, and 11.6 for tertiary amine groups (12).

Spectrophotometric Quantification of BPEI

Spectrometric quantification of branched polyethyleneimine was performing by adding a copper sulfate reagent to obtain a spectrophotometric complex. The spectrum of this complex is shown below in Figure 2.11. There are two wavelengths that have an absorbance that directly correlates with BPEI concentration. At 285 nm a BPEI range of 1-100 µg/mL can be quantified and at 630nm a BPEI range of 40-2000 can be quantified. The protocol of BPEI quantification includes making a calibration curve by adding between 0.1 mL to 1.9 mL of BPEI stock solution with 0.1 mL of 1M $CuSO_4$ and diluting to 2 mL in a quartz cuvette. The BPEI concentration of the stock solution and subsequent dilutions must be within the range of analyte being investigated. A different standard stock solution concentration was selected if absorbance value did not lie within the calibration curve. These measurements were taken on a Jenway

Genova UV-Vis Spectrophotometer. Calibration curves for BPEI are represented in Figures 2.12.

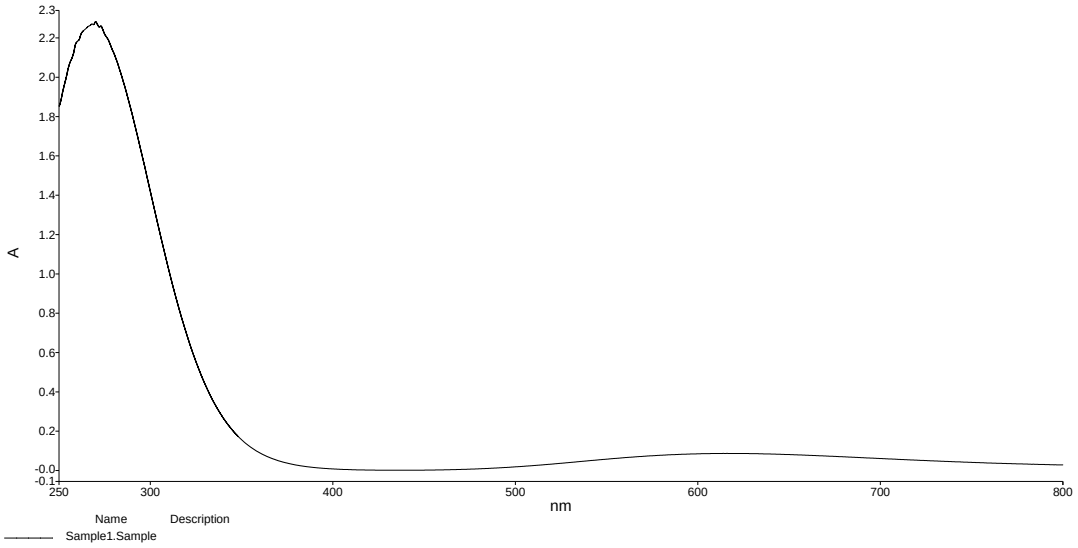
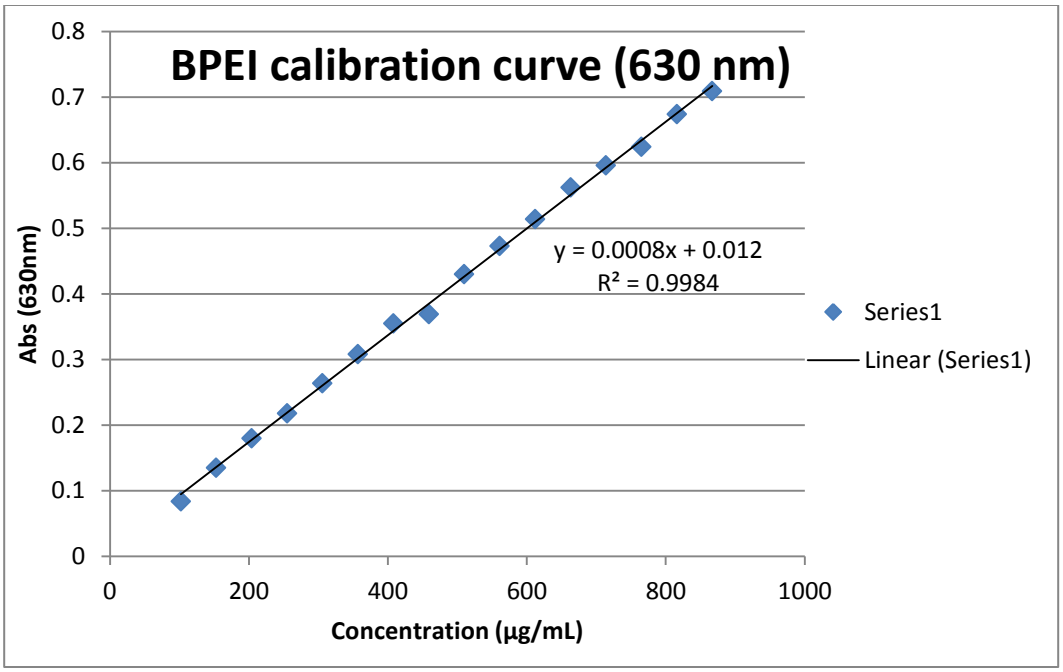


Figure 2.11: The UV-Vis Spectrum for the BPEI and Cu2+ complex displaying two peaks at 285 nm and 630 nm. The peak at 285 nm is used for low concentrations and the peak at 630 nm is used for higher concentrations of BPEI. Concentrations above 100 µg/mL of the



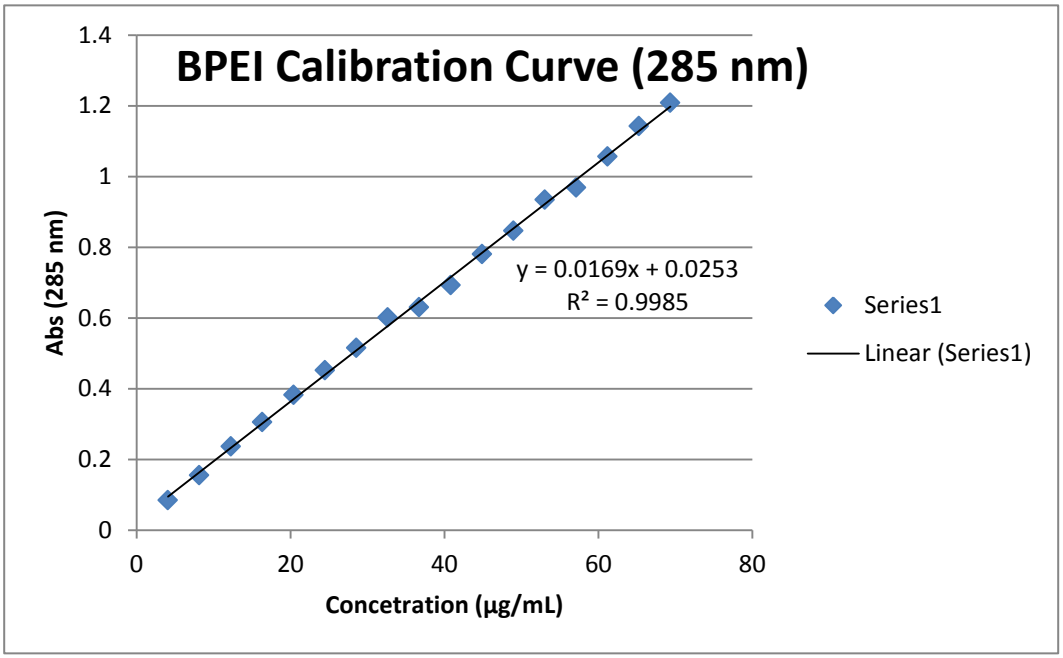


Figure 2.12: A linear relationship is obtained for concentrations of BPEI at 285 nm and 630 nm.

The absorbance values for the BPEI quantification method described above were not perturbed in the presence of 100 ppm Mg^{2+} or 100 ppm Ca^{2+}. Transition metals, such as Cu^{2+}, with incomplete sets of valence electrons have

been reported to interact with un-protonated amine groups on BPEI to produce a metal complex.

Examination of Matrix Effects Due to PEI on Flame AA Response

Up until now, all samples analyzed for metal ion content were in the simplest of matrixes containing the metal ion being analyzed in Milli-Q H_2O or with dilute HEPES buffer (0.001 M) at a pH of 7.25. Due to these simple matrixes we were able to use matrix matched standard solutions for constructing a calibration curve. In solutions containing BPEI, matrix matched standard solutions were used. However, due to lack of a static concentration of BPEI from binding events to the cell wall samples, the effect of 0.1 g/L BPEI on absorbance measurements was examined. Two sets of standard solutions were prepared: one in Milli-Q H_2O and one that contained 0.1 g/L BPEI. The results of this comparison are shown in Table 2.1. There does not appear to be an effect of BPEI on the detector response in the flame AA Mg^{2+} quantification procedure performed.

ppm Mg^{2+}	Abs Without BPEI	Abs With 0.1 g/L BPEI
0.078125	0.004	0.004
0.15625	0.007	0.008
0.3125	0.015	0.015
0.625	0.03	0.03
1.25	0.062	0.06
2.5	0.122	0.124
5	0.233	0.237

Table 2.1. Flame AA absorbance values of Mg^{2+} standard solutions with and without 0.1 g/L BPEI to examine matrix effects. The values appear to be similar and give evidence that 0.1 g/L BPEI does not affect absorbance values and that there is no reaction between BPEI and Mg^{2+} ions.

Determination of Mg^{2+} in LB Growth Media

Matrix interferences become an issue due to the high salt content in undiluted LB growth media. LB contains 5 g/L of NaCl along with high content of dissolved solids from the 10 g/L tryptone and 5 g/L yeast extract added. A high salt concentration tends to result in a decrease in signal (13). Viscosity and surface tension are directly related to salinity. As salt concentration increases, viscosity increases. This change in viscosity affects the sample uptake rate, which then leads to a decreased amount of sample reaching the system relative to the standard solutions. Larger droplets formed from high salt concentration solutions are less effectively de-solvated and can also contribute to a decreased signal. We must use the standard addition method when determining the concentration of Mg^{2+} in the LB growth media to overcome these matrix effects.

The standard addition method involves the addition of a distribution of known volumes of a known concentration of analyte to flasks containing a constant volume of the unknown sample. This process is denoted in Table 2.2 below. The absorbance values are graphed with respect to the concentration of the standard additions after dilution. The absolute value of abscissa of the graph when y is equal to zero is equal to the concentration of the unknown after dilution. To obtain the original concentration of Mg^{2+} in the sample a simple calculation using $M_1V_1=M_2V_2$ is performed. In Figure 2.13 below, the x-intercept is calculated to be 1.412 ppm Mg^{2+}, which signifies that the original concentration before the 5x dilution was 7.06 ppm Mg^{2+}. This differs from the

concentration obtained from using only a calibration curve with standard solutions in H_2O (5.86 ppm Mg^{2+}). Using the same standard addition method with LB that was sterile filtered with a 0.2 µm filter after growth of LB to an OD_{600} value of 1.0, an Mg^{2+} ion concentration of 6.85 ppm was obtained.

Volume of Fresh LB Media	Volume of 1.25 ppm Mg^{2+}	Volume of H_2O
1 mL	0 mL	4 mL
1 mL	1 mL	3 mL
1 mL	2 mL	2 mL
1 mL	3 mL	1 mL
1 mL	4 mL	0 mL

Table 2.2. Standard addition volumes and concentrations used to determine the Mg^{2+} content in fresh Lysogeny broth growth media shown in Figure 2.13.

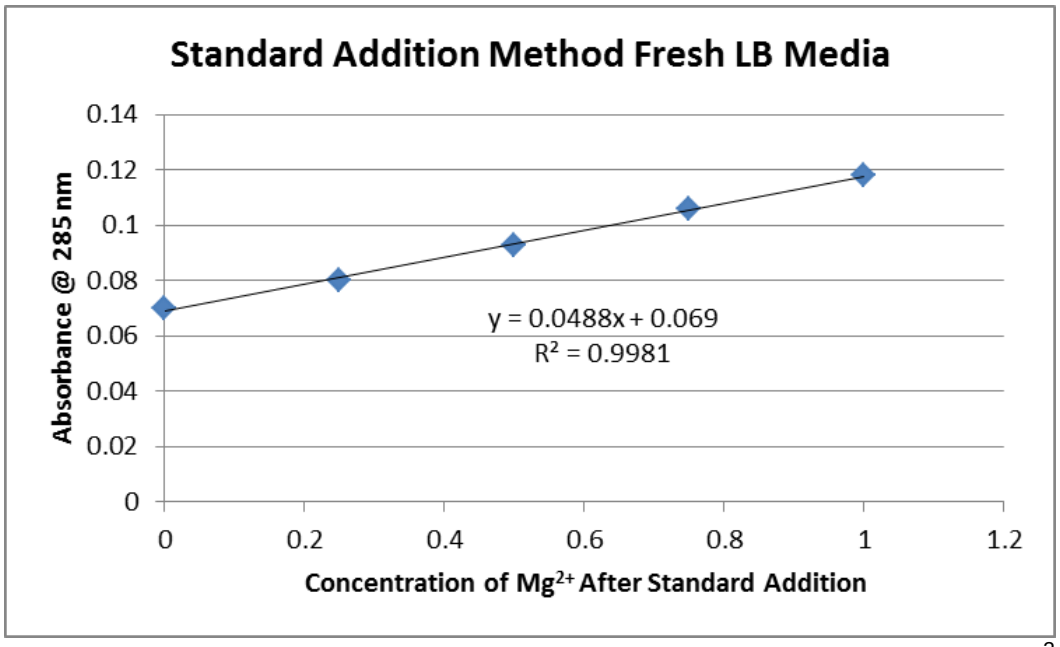


Figure 2.13. Standard addition graph of Lysogeny broth growth media Mg^{2+} content using the parameters listed in Table 2.2.

Quantity of Phosphate in WTA Sample

Our WTA sample underwent liquid state ^{31}P NMR analysis to determine the amount of phosphate on a per milligram basis. This quantity was then used to correlate Mg^{2+} binding capacity to binding stoichiometry with the phosphate groups. The NMR probe was externally calibrated with 0.0485 M triphenyl-

phosphate and one transient scan was taken with a 90° pulse and a 60 second delay time. The gain was set constant for the reference calibration standard and the sample. A 5.9 mg quantity of WTA was dissolved in 750 µL of D_2O and underwent NMR analysis for phosphate concentration. Quantitative analysis of the phosphate content in the WTA sample was performed using the qNMR tools in VnmrJ 3.1 where the integrated peak area for the reference was compared to the sample. A concentration of 21.5 mM of phosphorus was obtained in this analysis. This is equivalent to 2.7 µmol P per mg of WTA and 8.4% phosphorus on a mass percentage.

WTA Equilibrium dialysis

Due to the smaller structure of WTA when compared to the much larger cell wall fragments a 500 MWCO dialysis was used for equilibrium dialysis experiments to minimize chances of WTA diffusing through the membrane within the extended time frame they occupy the bag. The molecular weight cutoff value attributed to a dialysis membrane is an indirectly measured parameter that defines the mass at which the material is retained by at least 90%. These mass ranges are generally used as a basis for estimating the retention of globular proteins. WTA on the other hand is a long polymer which can potentially exist in linear or “folded” orientation. Nonetheless, Mg^{2+} ions have a molecular weight much smaller than 500 amu and are able to travel in and out of the dialysis membrane. In order to validate the completion of dialysis and to check if there was metal binding occurring on the membrane, a control was performed and went through the same procedures as the samples. A

known mass of 15-30 mg was suspended in 1 mL of Milli-Q H_2O and then placed in 49 mL of Milli-Q H_2O. A 5 mL volume of the solution was extracted and 5ppm Mg^{2+} solution was added every 48 hours. After 10 additions / extractions, the samples underwent flame AA analysis. Conformational rearrangement of the WTA polymer may be slower than the rate of diffusion of metal ions. Finding a conformation with the lowest potential energy would require breaking the phosphate-metal-phosphate bridges. The rate of interconversion is unknown, but is expected to be slower at 4°C, the sample temperature during dialysis process. Thus, we decided to extend the period of time between collecting flame AA samples. The metal solution addition and extraction process resumed after 21 days.

Growth Curves with Antibiotics and BPEI

In experiments examining the combination of antibiotics and BPEI, 50 mL of freshly made, un-autoclaved LB media was transferred to 125 mL Erlenmeyer flasks, covered with aluminum foil, and then immediately autoclaved for 30 minutes. Any metal supplementation occurred before autoclaving. A 1 mL volume of LB in a plastic disposable cuvette was used to blank the spectrophotometer (Jenway Genova UV-Vis Spectrophotometer) at 600 nm and 1 mL of each flask was transferred to a cuvette using sterile technique and then the sample was disposed after a measurement was taken.

Chapter 3: Mg^{2+} and Ca^{2+} Binding Characteristics of Gram-Positive Bacterial Cell Walls

Introduction

The importance of calcium and magnesium ions with regards to cell viability has been well documented (1,2). Calcium ions participate in synergistic interactions with enzymes responsible for anchoring surface proteins to the cell wall, thereby affecting the bacterium's adhesion ability (3,4). Pathogens rely on Ca^{2+} for toxin activity (5). Magnesium ions play a role in peptidoglycan synthesis, cell wall strength, and the prevention of cell lysis (6). The surfaces of Gram-positive bacteria contain carboxyl, phosphoryl, hydroxyl, and amino functional groups (7,8). At physiological pH values, these groups are deprotonated and contribute to metal binding (7,8).

For Gram-positive bacteria, WTA, LTA, and peptidoglycan are major bacterial components for sequestering metal ions from the environment. Peptidoglycan is a glycan (polysaccharide) backbone consisting of N-acetyl muramic acid and N-acetylglucosamine with peptide side chains (amino acids and diaminopimelic acid) that are cross-linked through peptide bonds to form a three dimensional structure. Teichoic acids are polysaccharides of either polyglycerol phosphate or polyribitol phosphate (depending on the bacterial strain) and are either anchored in the cytoplasmic membrane (LTA) or covalently bound to the cell wall (WTA) (9). The carboxyl groups on peptidoglycan are the anionic sites for metal binding, while phosphodiester groups are the primary metal binding sites for teichoic acids.

Previous studies on the metal binding behavior of *B. subtilis* have focused on the metal binding capacity and affinity. It was suggested through Hill plot analysis that negative cooperativity might exist (10). However, Scatchard plots reportedly do not exhibit the characteristic shape and curvature associated with negative cooperative binding (10). Nevertheless, K_A values of $4 \times 10^4 \pm 0.8 \times 10^4$ $M^{-1}$and $5.4 \times 10^4 \pm 3.3 \times 10^4$ M^{-1} for calcium and magnesium ions indicate a weak interaction (10). Binding capacities (0.75 ± 0.15 µmol/mg and 0.91 ± 0.54 µmol/mg) previously reported for calcium and magnesium have substantial error (10). These studies relied on either radioactive assays or atomic absorption spectroscopy. In contrast, an electrostatic model for metal sorption on the cell wall calculated binding constants 3 orders of magnitude stronger (6.31×10^7 M^{-1} for Ca^{2+} ions in low ionic strength solution with 0.001 M K^+ ions) (11). These experiments utilized a modeling approach to extrapolate a binding constant rather than a typical linear regression Scatchard plot analysis.

Titration experiments for most non-mutant strains of bacteria have shown that most Gram-positive and Gram-negative cell walls have similar functional groups that contribute to metal binding (7,8,10,11). Recent research with solid state NMR shows that Mg^{2+} preferentially binds to the phosphate groups, pushing the D-alanine away from the phosphate (12). Solid state NMR experiments have also been performed to estimate the binding constant of wall teichoic acid using the ^{31}P chemical shift based on the magnesium concentration used in the experiments (13). Kern et al. (13) published a dissociation constant of 600 ± 300 µM ($K_A = 1.67 \times 10^4$ M^{-1}) for WTA and Mg^{2+}

by using purified cell wall that contained peptidoglycan and covalently attached WTA through the use of 1D NMR. Nonetheless, the great disparity in K_A values suggests a complicated system that warrants further study.

Importance of WTA

Cell wall teichoic acids are essential for the virulence of Gram-positive pathogens. A *tagO* deletion mutant contradicted the belief that wall teichoic acid was necessary for the viability of Gram-positive bacteria (14). This strain grows at a considerably slower rate and has an uncharacteristic thickening of the cell wall with abnormal coccoidal cell morphology (14). The *tagO* gene is necessary for encoding the enzyme responsible for forming the wall teichoic acid linkage unit (15). The *tagO* mutant of various strains of bacteria has been investigated and this research demonstrates that WTA plays a major role in cell adhesion (16), biofilm production (16-18), and host infection (19,20).

The creation of a viable WTA deficient mutant of *B. subtilis* enables an additional method to examine the role that peptidoglycan and WTA play in bacterial uptake of the essential divalent metals such as Ca^{2+} and Mg^{2+}. Calcium and magnesium ions are both important biologically active metal ions that are some of the most abundant divalent cations in nature. We find that electrostatic effects are responsible for a strong binding between metal ions. This strength of binding decreases as the negatively charged functional groups of the cell become neutralized by divalent metal ions. Fragments of 1A578 (containing peptidoglycan and WTA) give two binding regions. For Ca^{2+}, Region I has a $K_A = (1.0 \pm 0.2) \times 10^6\ M^{-1}$ and Region II has a $K_A = (0.075 \pm 0.058) \times 10^6$

M^{-1}. This two region trend also applies to the WTA deficient mutant, EB1451. For Ca^{2+}, fragments of EB1451 give $K_{A1} = (1.2 \pm 0.1) \times 10^6$ and $K_{A2} = (0.19 \pm 0.24) \times 10^6$. Mg^{2+} ions give similar results in metal binding behavior. For Mg^{2+}, fragments of 1A578 yield a $K_{A1} = (1.5 \pm 0.1) \times 10^6$ and $K_{A2} = (0.17 \pm 0.10) \times 10^6$. For Mg^{2+}, fragments of EB1451 yield a $K_{A1} = (1.2 \pm 0.2) \times 10^6$ and $K_{A2} = (0.12 \pm 0.11) \times 10^6$. The differences in metal binding capacity of each strain are due to the contribution of WTA. EB1451 (lacking WTA) was able to bind about half as much metal as 1A578. No statistically significant difference was found with the binding capacity of either metal with each specific strain. A binding capacity (η) is reported for both regions. However, since binding is still occurring in Region II, the total binding capacity is denoted by η_2. Nonetheless, fragments of 1A578 gave binding capacities of 0.70 ± 0.04 µmol/mg and 0.67 ± 0.03 µmol/mg for Ca^{2+} and Mg^{2+} respectively. Fragments of EB1451 gave binding capacities 0.29 ± 0.03 µmol/mg and 0.25 ± 0.01 µmol/mg for Ca^{2+} and Mg^{2+} respectively.

Experimental Procedures

Cell Growth Protocol

Two strains of *B. subtilis* were used in these experiments. A chloramphenicol resistant strain of *B. subtilis* 1A578 (21), was obtained from Bacillus Genetic Stock Center (BGSC, Department of Chemistry at the Ohio State University). An erythromycin resistant, wall teichoic acid deficient mutant, *B. Subtilis* EB1451 (14), was obtained from Eric Brown (McMaster University). An overnight culture of *B. Subtilis* 1A578 was inoculated with frozen stock and grown in 20mL of LB with 10 µg/mL of chloramphenicol added. The following

day a 1L culture was inoculated from the overnight culture by transferring a volume of the overnight culture equal to 1% of the new culture and adding an amount of antibiotic stock solution (10 mg/mL) to a final concentration of 10 µg/mL. The culture was allowed to grow (200 rpm, 37°C) to an OD_{600} of 1.0 and then centrifuged at 15000*g* for 25 minutes. After centrifugation, the supernatant was decanted and the pellet was re-suspended in 10 mL of Milli-Q H_2O in preparation for cell purification. EB1451 was grown using the same method, using erythromycin in place of chloramphenicol.

Cell Wall Purification

A modified procedure by Umeda *et al.* (22) was used to purify peptidoglycan with covalently bound WTA. Only peptidoglycan was purified from EB1451 in this method due to the absence of WTA in the sample. The cells were disrupted using a French press and the resulting fragments were re-suspended in 10 mL distilled deionized water and added drop wise with stirring to 100 mL of boiling 6% (w/v) sodium dodecyl sulfate. This step inactivates autolysins (23,24) and removes the cytoplasmic membrane. In addition, the sample was kept cold (4°C) during the initial disruption procedure in order to prevent the degradation of peptidoglycan by autolytic enzymes. The sample was rinsed 3 times with 200 mL of distilled deionized water and centrifuged at 15000*g* for 20 minutes at least three times. In order to remove any remaining cell wall associated proteins, RNA or DNA, the fragments were then re-suspended in TRIS buffer (pH 8.2) and treated with trypsin (200 µg/mL) and RNAse/DNAse (100 µg/mL) at 37ºC in an incubator/shaker for 16-18 hours. The

cell wall fragments were then spun down again, washed with fresh distilled deionized water, and then re-suspended in ammonium acetate buffer (pH 4.7) and treated with pepsin (100 µg/mL) at 37ºC for 2 hours. Finally, the cell wall fragments were centrifuged and washed with 50 mL of 50 mM EDTA overnight (4 ºC) to remove any residual metal ion contamination, and then washed 3 times with 200 mL of ddH_2O. The cell wall fragments were then suspended in a approximately 5 mL of Milli-Q H_2O and then lyophilized, forming a white, charged, fluffy solid.

WTA Hydrolysis

Portions of the freeze dried cell wall also underwent a 10% TCA (trichloroacetic acid) treatment at 4°C for 48 hours in order to remove the WTA (25). After treatment with TCA, the suspension was centrifuged at 15000 g and the insoluble portion containing peptidoglycan was washed 3 times with 200 mL of Milli-Q H_2O and then lyophilized for 2 days or until the sample was dry.

Membrane Dialysis Procedure

A known mass of 10-60 mg of the purified cell wall material was suspended in 1-2 ml of Milli-Q H_2O, transferred to a 6.5 cm length, 1.8 cm width, 1000 MWCO Spectra/Por® 7 dialysis membrane and placed in a closed jar with a final total volume of 50 mL of Milli-Q H_2O. The jars with dialysis membranes were placed in a cold room and shaken on a New Brunswick G24 incubator/shaker at 4°C. Equilibrium dialysis experiments with 1.5 mL of 100 ppm Ca^{2+} ions placed inside the dialysis membrane with extractions taken at specified intervals indicated that full equilibration took place between metal ions

inside and outside of the dialysis bag after 12 hours. The time at which equilibration was achieved was determined to be at 10 hours. Every 12 hours a 5 mL aliquot was removed from the jar and 5 mL of a known metal ion concentration in the range of 5-20 ppm were added in order to obtain a concentration gradient. This range was chosen by method of trial and error. The concentration gradient had to be small enough to observe changes in the Scatchard analysis, but not so small as to have data points crowded in one region. Utilizing a Varian SpectrAA 55b Flame Atomic Absorption Spectrometer, the concentration of the aliquots was determined, and that data was used to calculate the amount of Ca^{2+} or Mg^{2+} bound to the cell wall inside the dialysis membrane. Binding constants from this data were determined with a Scatchard plot.

Results

Divalent metal cations are attracted to the negative charge of the cell wall. Initially, metal ions are strongly bound and only a small portion of metal

ions remain in solution. This is demonstrated in the binding curve (Figure 3.1).

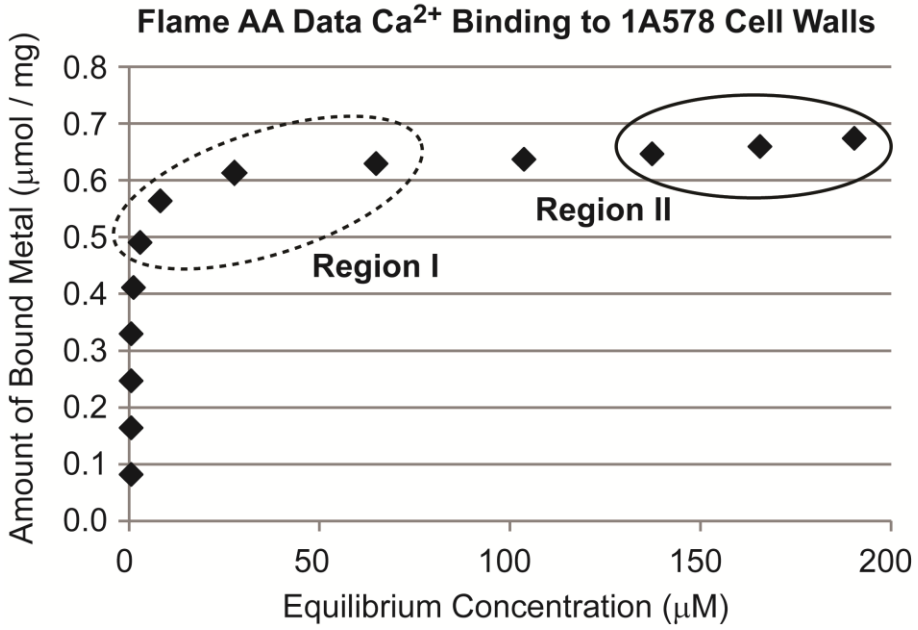


Figure 3.1. Characteristic binding curve of metal binding to purified cell wall and the points corresponding to the two regions of binding affinity shown in Figure 3.2 The cell wall binds most Ca^{2+} ions during an initial metal uptake phase, after which metal binding slows. These two regions of the binding curve were used to obtain binding constants. The equilibrium concentration was determined from the concentration of Ca^{2+} ions outside of the dialysis membrane. In this particular sample, the first four points on the binding curve correspond to the same measured concentration of 5.89×10^{-7} M^{-1}, which also correlate to an absorbance value of 0.001. These points were taken at a value near the limit of quantification and were not used in the analysis. Due to an apparent curvature in the Scatchard plot, indicative of negative cooperative binding, two bind regions are examined as presented by the dotted and solid selections. The dotted selection indicates a higher affinity region. As more metal ions become bound to the cell wall, a lower binding stability constant can be extracted with the data points in the solid circle.

Each standard addition increases the number of bound metal ions but also increases the concentration of excess ions in solution. Not only do additional cations occupy more binding sites, but the negative charge of the cell wall is partially neutralized. Attraction of free ions to the cell wall is diminished and the metal ion concentration gradient weakens. As the standard addition process continues, the unbound metal ion concentration increases and causes a

decrease in the bound/unbound ratio. This behavior is commonly referred to as negative cooperative binding and associated with a sharp upward trend to the binding curve and a concave shape to the Scatchard Plot (26). Negative cooperativity for cell-wall based metal binding has been suggested based on Hill plot analysis, but the expected curvature in the Scatchard plots was not observed in a previous report (10). Our data, obtained at lower metal ion concentrations, clearly demonstrate a concave curvature of the Scatchard plot. In this representation, the ordinate is a ratio of bound metal (micromoles per mg) over unbound metal concentration (micromoles per liter). Therefore the equilibrium concentrations determine the range of ordinate values required to find the association constant (K_A) and binding capacity (η). As described below, Scatchard plot analysis shows that metal chelation by the cell wall can be described with two distinct regions of equilibrium binding behavior. The designation of Region I and Region II are made from a Scatchard plot (Figure 3.2) which shows linear behavior and distinct slopes for each region. The first five data points of Figure 3.1 are not included in the Scatchard plot because the concentration of free ions in solution is negligible and thus the flame AA response is below the limit of quantification. Values for K_A and η are determined from the slope and x-intercept respectively. The correlation coefficient is improved if we exclude the data point in the transition between Regions I and II as shown in Figure 3.1 and Figure 3.2.

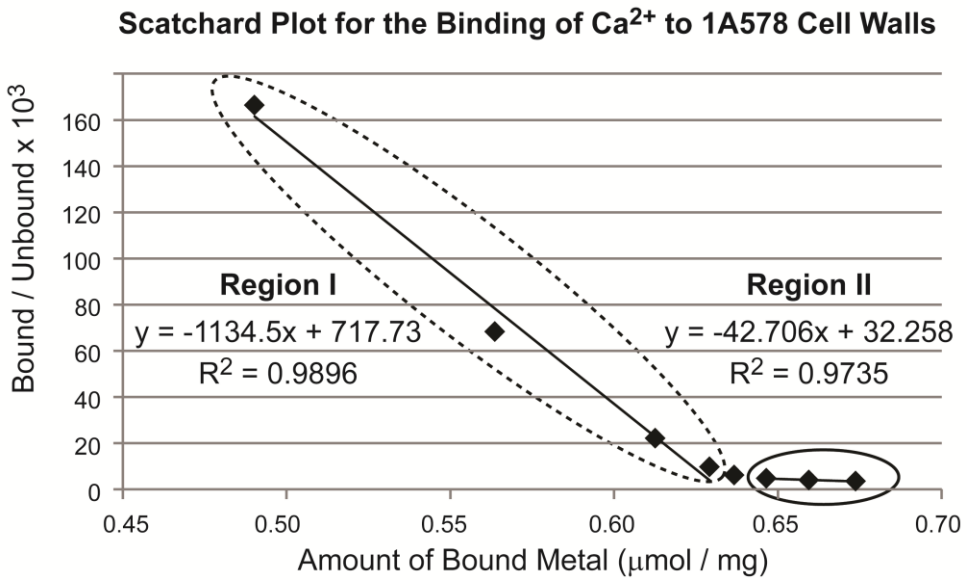


Figure 3.2. Scatchard plot associated with the binding curve in Figure 3.1 showing two regions of binding affinity. A linear transformation of the binding data provides the binding affinity (denoted by the negative value of the slope) and the binding capacity (denoted by the x-intercept). From this Scatchard plot analysis, a binding constant of 1135 x 10^3 M^{-1} is obtained from the points selected with a dotted line and a lower affinity constant of 43 x 10^3 M^{-1} is obtained from the points selected with solid line. The binding constant changes as more metal ions become bound to the sample, a property of negative cooperativity resulting from electrostatic effects in the cell wall samples. Hill plots of samples (not shown) have also pointed towards negative cooperative binding effects of the cell wall.

Table 3.1 is a compilation of K_A and η for Ca^{2+} and Mg^{2+} binding data. Equilibrium dialysis experiments were performed to evaluate the binding of Ca^{2+} to cell wall fragments of *B. subtilis* 1A578 containing both peptidoglycan and WTA. The K_A and η values were obtained from 6 trials, as presented in supplemental information Table 3.2. The average binding capacity is 0.58 ± 0.07 μmol/mg and 0.070 ± 0.04 μmol/mg for Regions I and II, respectively. The average association constant is 1.0 x 10^6 ± 0.2 x 10^6 M^{-1} and 0.075 x 10^6 ± 0.058 x 10^6 M^{-1} for Regions I and II, respectively. The results of each trial show that K_A and η are sample independent in Region I, whereas values for the

second stage of binding (Region II) are directly correlated with the bound / unbound range. Region I is characterized by higher ranges of the bound/unbound ratio and binding in Region I is stronger than binding observed in Region II. Experiments using cell wall purified from strain 1A578 were repeated to evaluate Mg^{2+} binding. The binding affinity was $1.5 \times 10^6 \pm 0.2 \times 10^6$ M^{-1} for Region I and $0.17 \times 10^6 \pm 0.10 \times 10^6$ M^{-1} for Region II while a total binding capacity (represented by η_2) of 0.67 ± 0.03 µmol Mg^{2+} per mg of sample was measured.

Metal Binding Properties of *B. subtilis* purified cell wall components at T=4°C

			Region 1		Region II	
Type of Sample	**Metal Ion**	**pH**	**η (µmol/mg)**	**$K_{assoc.}$ (M^{-1})**	**η (µmol/mg)**	**$K_{assoc.}$ (M^{-1})**
1A578 (Peptidoglycan + WTA)	Ca^{2+}	5.65	0.58 ± 0.07	(1.0 ± 0.2) x 10^6	0.70 ± 0.04	(0.075 ± 0.058) x 10^6
EB1451 (Peptidoglycan)	Ca^{2+}	5.65	0.25 ± 0.04	(1.2 ± 0.1) x 10^6	0.29 ± 0.03	(0.19 ± 0.24) x 10^6
1A578 (Purified Peptidoglycan)	Ca^{2+}	5.65	0.27 ± 0.05	(1.0 ± 0.3) x 10^6	0.33 ± 0.04	(0.080 ± 0.084) x 10^6
1A578 (Peptidoglycan + WTA)	Mg^{2+}	5.65	0.50 ± 0.10	(1.5 ± 0.1) x 10^6	0.67 ± 0.03	(0.17 ± 0.10) x 10^6
EB1451 (Peptidoglycan)	Mg^{2+}	5.65	0.17 ± 0.04	(1.2 ± 0.2) x 10^6	0.25 ± 0.01	(0.12 ± 0.11) x 10^6
1A578 (Purified Peptidoglycan)	Mg^{2+}	5.65	0.19 ± 0.05	(0.7 ± 0.5) x 10^6	0.23 ± 0.04	(0.098 ± 0.024) x 10^6
1A578 (Peptidoglycan + WTA)	Mg^{2+}	7.25	0.63 ± 0.08	(1.0 ± 0.2) x 10^6	0.77 ± 0.07	(0.26 ± 0.12) x 10^6
EB1451 (Peptidoglycan)	Mg^{2+}	7.25	0.38 ± 0.11	(1.0 ± 0.2) x 10^6	0.54 ± 0.06	(0.28 ± 0.20) x 10^6

Table 3.1. Composite data table showing the metal binding properties for each cell wall sample

A two tailed t-test was used to evaluate the statistical significance between the mean binding capacity and binding affinity of each metal ion. At a 95% confidence interval, the values of binding capacity (η) for both metals produced a t-value of 1.36 which was smaller than the critical t-value of 2.31. The smaller t-value suggests that a statistical difference in the binding capacities (η_2) cannot be accepted at a 95% confidence interval. However, for

the binding affinities, there is a statistical difference between $K_A(Ca^{2+})$ and $K_A(Mg^{2+})$ for Region I only. We attribute the apparent higher affinity of Mg^{2+} to the higher sensitivity of atomic absorption measurements towards magnesium. Magnesium produces two usable wavelengths; one at 285.2 nm, for low concentrations, with a sensitivity of 0.007 ppm and one at 202.6 nm, for higher concentration samples, with sensitivity down to 0.2 ppm. A wavelength of 422.7 nm is generally used for calcium. This wavelength produces a sensitivity in the 0.04 ppm range which is higher than that of the 285.2 nm wavelength for magnesium. As a result, we are able to observe lower Mg^{2+} concentration measurements in the limit of quantification. These lower concentrations correlate to higher bound/unbound values and an increase in the apparent binding affinity is observed. At an infinitesimal concentration, K_A would be significantly larger but unmeasurable.

Values for metal binding to peptidoglycan (isolated from *B. Subtilis* EB1451) also showed similar binding capacity and affinity for Ca^{2+} and Mg^{2+} cations. Ca^{2+} ions were found to have a total binding capacity (η_2) of 0.29 ± 0.03 µmol/mg, a binding affinity of (1.2 ± 0.1) x 10^6 M^{-1} for Region I, and a binding affinity of (0.19 ± 0.24) x 10^6 M^{-1} for Region II. Mg^{2+} ions were found to have a similar binding capacity (η_2) of 0.25 ± 0.01 µmol/mg. A binding affinity of (1.2 ± 0.2) x 10^6 M^{-1} for Region I, and a binding affinity of (0.12 ± 0.11) x 10^6 M^{-1} for Region II were obtained. When testing for a statistical difference of K_A and η for each metal ion in both regions, we cannot demonstrate that both ions have different metal binding behaviors.

Using TCA hydrolysis, we can separate WTA from peptidoglycan. Peptidoglycan purified from strain 1A578 produced similar results as the WTA deficient mutant, EB1451, as shown in Table 3.1. Results for the binding capacities of each cation showed that there was a not a statistical difference between the mutant and purified peptidoglycan at a pH of 5.65. This shows that most of the WTA from 1A578 was removed with the TCA hydrolysis method. These values are not unexpected as both should consist of peptidoglycan only.

At a buffered pH of 7.25, the metal binding capacity of the peptidoglycan increased and the metal binding capacity of the peptidoglycan with covalently bound WTA increased as well (Table 3.1). The affinity of metal to cell wall interactions in Region I remained similar at this higher pH. Individual trial results are listed in Table 3.8 and Table 3.9. The increase in binding capacity is most likely a result of the diaminopimelic acid carboxyl functional groups becoming deprotonated above their pK_a value of 6.31 (27). At a pH of 7.25, the capacity of Mg^{2+} ions to peptidoglycan from the WTA deficient mutant, EB1451, increased by 110% (from 0.25 ± 0.01 μmol/mg to 0.54 ± 0.06 μmol/mg, Table 3.1). The attraction of Mg^{2+} ions to 1A578 cell wall fragments, containing peptidoglycan and WTA, increased by 14% (from 0.67 ± 0.03 μmol/mg to 0.77 ± 0.07 μmol/mg) when the pH was increased from 5.65 to 7.25. This increase can be attributed to peptidoglycan and not WTA. We believe that the diaminopimelic acid carboxyl functional groups are becoming more deprotonated at a higher pH due to a pK_a value of 6.31 ± 0.01 (27) rather than phosphoryl groups becoming more deprotonated at a pK_a value of 6.9 ± 0.6 (8). A phosphoryl group

becoming deprotonated at this pH increase would result in additional binding sites only with samples containing WTA. The fragments of EB1451 only contain peptidoglycan, yet a change from 0.25 ± 0.01 μmol/mg to 0.54 ± 0.07 μmol/mg is observed with this pH increase. The difference in the amount gained for peptidoglycan + WTA from sample 1A578 (0.10 μmol/mg) and the amount gained from peptidoglycan alone from EB1451 (0.29 μmol/mg) can be attributed to cross-link density of diaminopimelic acid on a per milligram basis.

Discussion

Two Regions of Binding Behavior

The observance of two distinct binding regions has not been demonstrated in previous studies of metal to the cell wall. Metal binding affinities have always been represented by a single value (8,10) utilizing an experimental protocol where different samples were mixed with a single concentration of metal ions. Compared to literature reports (10), the binding affinity for Ca^{2+} in Region I ($1.0 \times 10^6 \pm 0.2 \times 10^6$ M^{-1}) is 25 times larger than previously reported ($0.040 \times 10^6 \pm 0.008 \times 10^6$ M^{-1}) for cell wall fragments containing both peptidoglycan and WTA. Additionally, Region II binding is 1.8 times larger than the previous report. The observation of Region I is important, as a misconception of weaker binding might arise if binding data is limited to only Region II. A similar trend is observed for Mg^{2+} binding to cell wall fragments. A binding affinity for Mg^{2+} in Region I is 28 times larger than previously reported ($0.054 \times 10^6 \pm 0.033 \times 10^6$ M^{-1}) (10) for fragments of cell

wall samples containing both peptidoglycan and WTA, whereas Region II binding is 3.1 times larger than the previous report.

As the cell wall gets close to saturation with metal ions, there is a gradual decrease in the slope of the Scatchard plot and thus a decrease in the apparent binding affinity. This decrease in K_A becomes more apparent as the equilibrium concentration increases (Figure 3.1). An increase in the equilibrium concentration causes a corresponding decrease in the bound/unbound ratio. Data taken from lower bound/unbound ratios will produce a line and slope that shows a weaker binding affinity. Data points were chosen for Region I based on limits of quantification and the point at which the curvature starts. Data points for Region II were chosen furthest away from the transition point at which the curvature begins in order to give the highest correlation coefficient.

The data in supplementary Tables 3.2 – 3.9 show a variation in the bound/unbound ratio range for both Regions I and II for each trial. During the standard addition process, metal ions are added and become bound to the cell wall. After the initial group of ions is added, the unbound metal ion concentration is very low and the flame AA response is below the limit of quantification of our instrument. However, the equilibrium concentration required to produce a response equal to or greater than the limit of quantification depends on cell wall mass and varies between each trial. The difference between the bound/unbound ratios after each standard addition is observed in the two highest values in Figure 3.2. For Region II, the variation in the range of bound/unbound is less dramatic and a result of variation in the

equilibrium concentration at the end of each experiment. A higher proportion of unbound metal ions in solution will cause the bound/unbound range to decrease when the cell wall sample reaches the saturation point for metal binding. Ideally, Scatchard plot analysis will provide a precise view of this equilibrium behavior independent of the bound/unbound range. The numerical values that describe the relationship between the bound and unbound metal ions should be very accurate. However, we cannot define a traditional equilibrium constant since it depends on the particulate size and electrostatic properties of each particulate. Measurements with *B. subtilis* sacculus (whole cell walls) produced a similar binding capacity of 0.62 µmol/mg but a larger binding affinity is observed. In this sample a binding affinity of 4.5×10^6 M^{-1} was obtained for Region I and a binding affinity of 1.04×10^6 M^{-1} was obtained for Region II. The bound/unbound range was much higher than with the fragment samples. Nonetheless, equilibrium remains frustrated by hindered diffusion.

The large standard deviations in binding affinity can be attributed to a combination of diffusion effects and the dependence of the affinity constant, K_A, on concentration. The process of disrupting cells with a French Press creates a distribution of particle sizes and thus each trial is expected to have a different distribution of particle sizes. Peptidoglycan forms a three dimensional mesh where diffusion of metal ions through large fragments may be significantly different than small fragments. Within the distribution of fragments, each particulate will have a unique metal ion equilibrium between the interior and exterior of the cell wall fragment. Negative cooperativity of metal binding to the

cell wall creates a situation where calculated values of K_A depend on the equilibrium concentration range. This is illustrated by the values for K_{A2} in each trial (Tables 3.2 – 3.9). The higher the bound/unbound region examined, a higher association constant is measured for Region II. The values of K_A for Region I are independent of the bound/unbound ratio.

The dependence of the Region II K_A on the bound/unbound range may lie with electrostatic interactions between the cell wall, metal cations, and counter ions. The cell wall is a polyelectrolyte in terms of the peptidoglycan and teichoic acid components, which both exhibit a strong negative charge based on deprotonated carboxyl and phosphoryl functional groups near pH = 7. The metal binding behavior of other polyelectrolytes has been investigated (28,29). However, no studies have been directed towards the cell wall. Studies with two polyelectrolytes, RNA and humic acid, have exhibited similar binding behavior when compared with our cell wall samples. Humic acid is a natural organic polyelectrolyte containing multiple carboxyl and phenolate groups. Using voltammetry, it has been shown that the stability constant of the metal ion complex decreases with increasing metal ion concentrations and decreases with increasing ionic strength values (29). Increasing Zn^{2+} concentration from 10^{-7} M to 3 x 10^{-6} M caused the stability constant to decrease from 5.01 x 10^5 M^{-1} to 1.26 x 10^5 M^{-1} (29). A gradual increase in the ionic strength of the solution from 0.001 M KNO_3 to 0.1 M KNO_3 with a constant Zn^{2+} concentration of 10^{-6} M caused a decrease in the observed stability constant from 3.16 x 10^5 M^{-1} to 7.94 x 10^4 M^{-1} (29). Additionally, just as there was little difference in the metal

binding characteristics of Mg^{2+} and Ca^{2+} in our cell wall metal binding data, there was little difference in the metal binding characteristics of Zn^{2+} and Cd^{2+} (29). RNA has a poly(ribose phosphate) backbone similar to the poly(glycerol phosphate) backbone of teichoic acid. Mg^{2+} ions binding to RNA were also found to exhibit curvature on the Scatchard plot (30). This behavior was explained as either the result of changing electrostatics, which would lead to negative cooperativity, or two classes of binding sites (30). Class 1 is a group of strongly bound ions whereas class 2 is a group of more weakly bound ions that are responsible for the trailing region of the Scatchard plot (30). As a result, a traditional equilibrium constant cannot be defined because diffuse ion binding is based on long range electrostatic interactions and does not follow the laws of mass action (31). Other studies into RNA have demonstrated that the ionic strength plays a huge role in the determination of binding affinity with RNA and metal ions, thereby providing evidence against the classification of two classes of binding sites (28). Application of this electrostatic model at low sodium concentrations has shown to be a good fit to experimental data (28). Electrostatic effects have been shown to cause a decrease in the degree of curvature of Scatchard plots, and subsequently a decrease in affinity, as the concentration of competing monovalent cations increases (28). As a result, reported stability constants for metal binding to polyelectrolytes is directly dependent on a number of variables including ionic strength, temperature, and divalent metal ion concentration (28,29). The dependence on ionic strength appears to have a greater influence on Region I in the Scatchard plot

(commonly referenced as class 1 binding sites in other publications) (28). Individual experiments at varying ionic strengths were not performed, although it is expected that the affinity within Region I would decrease as ionic strength increases, based on observations with other polyelectrolytes (28). Electrostatic effects are less prominent when the electrostatic potential of the cell wall has already been neutralized through the binding of cationic metal ions.

It has been reported that peptidoglycan contributes half of the cell's metal binding capacity by comparing the binding of both cell wall fragments (containing peptidoglycan with covalently bound WTA) and peptidoglycan alone (32). These results show that calcium has a binding constant of 25 x 10^3 M^{-1} and a binding capacity of 0.78 µmol/mg for cell walls containing both peptidoglycan and WTA (32). Peptidoglycan alone was determined to have a binding constant of 18 x 10^3 M^{-1} and a binding capacity of 0.45 µmol/mg (32). Although our binding constants are much larger for region I, the binding capacity data are similar to the Matthews *et al.* (32) report. For 1A578, peptidoglycan accounts for 47% of Ca^{2+} binding whereas it is 34% of Mg^{2+} binding. This is in contrast to previous reports that teichoic acids were solely responsible for Ca^{2+} binding to the cell wall (7).

Based on a statistical t-test analysis, we do not observe an obvious difference between the affinities or binding capacities of specific metal ions to the cell wall. In a subsequent study by Doyle *et al.* (10), Ca^{2+}, Mn^{2+}, Ni^{2+}, Sr^{2+}, Zn^{2+}, and Mg^{2+} were reported to have binding constants of 40 ± 8, 52 ± 11, 33 ± 11, 36 ± 11, 39 ± 7, and 54 ± 33 respectively (which are x 10^3 M^{-1}). Likewise the

binding capacities of all divalent metal ions appeared to be highly similar with values of 0.75 ± 0.15, 0.74 ± 0.16, 0.64 ± 0.20, 0.86 ± 0.26, 0.97 ± 0.16, and 0.91 ± 0.54 (in units of μmol/mg) for Ca^{2+}, Mn^{2+}, Ni^{2+}, Sr^{2+}, Zn^{2+}, and Mg^{2+} respectively (10). Without knowing how many samples were taken to obtain the standard deviations reported, it is impossible to perform any statistical tests on the sets of data. Nonetheless, similarity of values for divalent metal ions, coupled with large standard deviations, show that there is little preference in binding affinity or capacity between divalent cations.

Deprotonation of Binding Sites

Initially, experiments were performed at a measured pH of 5.65, which was the pH of the distilled deionized Milli-Q water due to dissolved carbon dioxide (33). Additional experiments were performed with a low concentration of HEPES buffer, 0.001 M, at an adjusted pH of 7.25 in order to examine effects of pH on the binding constant and binding capacity of Mg^{2+}. The binding capacity increases because there are more binding sites. This makes sense for both Regions I and II because of binding to the diaminopimelic acid carboxyl group. Addition of NaOH creates competition for the binding site between Na^{+} and Mg^{2+} and lowers the observed K_A. However, Mg^{2+} will overwhelm Na^{+} binding and preferentially replaces the Na^{+} due to its higher charge density, leading to a higher binding capacity. There appears to be a change in the K_A value for Region I and II when the pH is increased from 5.65 to a buffered pH of 7.25. We attribute the decrease in affinity constant for Region I to the minute addition of NaOH to adjust the pH to 7.25. The slightly higher ionic strength is expected to

cause a decrease in the electrostatic potential of the cell wall (27). However, we observe an increase in K_A for Region II though this increase is not statistically different between pH 5.65 and 7.25. When the pH was increased from 5.65 to 7.25, a more than two fold increase was seen in metal binding capacity of peptidoglycan, as shown in Table 3.1.

The two regions of binding affinity in the Scatchard plot are sometimes described as two classes of binding sites. The purified cell wall does contain two types of binding sites (carboxyl and phosphoryl groups). However, two regions of binding affinity are also seen for peptidoglycan obtained from the WTA deficient mutant and purified from 1A578 after TCA hydrolysis. A two site model predicts similar capacities for Region I between the three samples, which is not observed. Rather, the binding capacities of Region I and II are best interpreted by electrostatic effects but we cannot attribute these two regions to specific functional group.

The increase in Mg^{2+} binding at pH 7.25 is a result of the diaminopimelic acid carboxyl groups becoming deprotonated and offering additional charge density for binding metal ions. Barkleit *et al.* (27) determine three regions of pK_a values (4.55 ± 0.002, 6.31 ± 0.01, and 9.56 ± 0.03) when performing potentiometric titrations of purified peptidoglycan from *Bacillus subtilis*. These values were attributed to the carboxyl group on the glutamic acid, the carboxyl group on the diaminopimelic acid, and the amine/hydroxyl groups on the peptidoglycan sample, respectively. Site densities reported were 0.65 ± 0.17, 0.76 ± 0.02, and 1.45 ± 0.23 mmol/g of sample for the three sites. If site

densities of glutamic acid and diaminopimelic acid are similar, the pH change should double the binding capacity. This behavior is observed in our data (Table 3.1).

Binding Stoichiometry

There have been conflicting papers published on whether metal ion chelation by the cell wall occurs via a monodentate or bidentate complexation mechanism. Multidentate binding will produce binding constants with a higher affinity than monodentate binding based on the chelate effect. Bridging between two functional groups will produce a 1:2 metal to site stoichiometry where a metal ion can be bound to a single functional group and between delocalized oxygens of carboxyl or phosphoryl groups. If the binding constant is calculated indirectly with a model and equation, the calculated equilibrium constant will depend on the binding stoichiometry. Metal to cell wall binding constants have been reported using experimental methods (10,32) and model based calculations (8,11). However, models of metal binding require knowledge of binding stoichiometry, a constraint not essential for experimental determination of binding constants. Nonetheless, based on the relative amounts of carboxyl functional groups and their associated pK_a values, our data corresponds with a bridging binding mode for metal ions with peptidoglycan.

A metal binding capacity of 0.54 µmol/mg for Mg^{2+} with peptidoglycan from EB1451 is smaller than the reported binding site concentrations. The glutamic acid has a carboxyl site density of 0.65 ± 0.17 mmol/g and diaminopimelic acid had a carboxyl site density of 0.76 ± 0.02 mmol/g (27). The

contribution from terminal D-alanine carboxyl groups was not reported. The prediction of more binding sites than quantities of bound divalent metal ions is also seen in work by Borrok *et al.* (34). This supports the possibility of a binding pocket created with multiple functional groups or the possibility that every site may not become occupied. Using modeling studies, Mishra *et al.*(35) show that that 1:2 metal binding stoichiometry fits well at low concentrations (such as those used in our experiments) but there is a significantly better fit with a 1:1 binding stoichiometry when going to much higher concentrations than 200 ppm. This suggests that a different chemical environment might exist for large concentrations of metal ions and counter ions.

Peptidoglycan serves to maintain integrity in response to cellular turgor pressure. WTA contributes to cell wall stability and helps maintain cell wall shape. Wall teichoic acid deficient *B. subtilis* mutants have drastically different morphologies at the cellular level. The *B. subtilis* WTA deficient mutant EB1451 exhibits swelling and clumping that is uncharacteristic of the *B. subtilis* 1A578 (Figure 3.3). TEM images show that the absence of WTA also causes cell wall thickening (14). The spherical shape and thick cell walls are induced by internal turgor pressure.

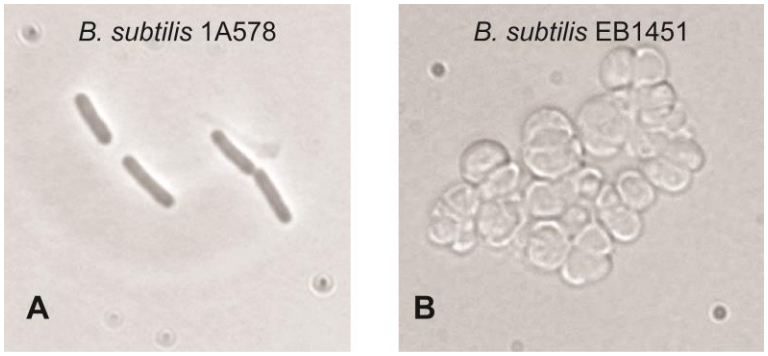


Figure 3.3. Phase contrast microscopy images of (A) *B. subtilis* 1A578 (B) and EB1451 cells grown in LB media (1000x magnification). The WTA deficient mutant EB1451 causes the cell shape to change from a narrow rod to a spherical shape. Dust particles on the microscope lens are seen in the lower right and upper left portions of the images.

The *B. subtilis* architecture relies on an amide bond between the terminal carboxyl group of D-alanine and the terminal amine of diaminopimelic acid. However, the terminus of diaminopimelic acid also contains a carboxyl group that is unaffected by cross-linking. Prior to amide bond formation, this terminus would exist as a charge neutral zwitterion and likely would have a minimal contribution to metal binding. Upon cross-linking, the terminus of diaminopimelic acid becomes negatively charged and available for metal binding. At pH 5.65 these groups are protonated and do not bind metals. Thus, the pH effects observed in our experiments can be used to indirectly evaluate the amount of diaminopimelic acid cross-linking. The binding capacity of Mg^{2+} with EB1451 cell walls increases by 0.29 µmol/mg at pH 7.25 whereas an increase of 0.10 µmol/mg is seen with 1A578 fragments. Thus, the WTA deficient mutant contains a greater fraction of diaminopimelic acid cross-links. The degree of cross-linking on peptidoglycan has been investigated with respect to a *tagO* mutant of *Staphylococcus aureus*. One report implied greater cross-linking in the *tagO* mutant through increased binding to a cell wall-targeting domain of

lysostaphin that preferentially binds to cross-linked peptidoglycan (36). Alternatively, *tagO* mutants have been reported to have a decreased degree of cross-linking (37). Further investigation into the role of cross-linked diaminopimelic acid with regards to metal binding is underway.

In these experiments, we measured the binding constants and binding capacities of metal ions (Ca^{2+} and Mg^{2+}) with purified cell wall fragments of *B. subtilis* containing either peptidoglycan or peptidoglycan with covalently attached WTA. We found much higher metal ion stability constants than previously reported. The binding of metal ions to the cell wall appears to be a largely electrostatic phenomenon at low ionic strengths. This behavior is similar to other polyelectrolytes. Even though our experiments were performed at low ionic strength conditions, bacteria can grow in a variety of extreme conditions. Many factors such as the ionic strength, amount of divalent metal ions present, and temperature must be taken into consideration when examining the cell wall's affinity toward divalent metal ions. At low ionic strength it has been demonstrated that the cell wall has a strong affinity for metal ions in solution. This property can be hypothesized as part of a survival mechanism of the cell to capture important bioactive divalent metal ions.

The data in Region I reveal the maximum amount of metal ions that are bound to this particular region. However, we are reluctant to attribute a precise chemical interpretation because binding is still occurring at Region II and there is no strong correlation between samples with and without WTA. It is possible that the initial binding events cause a reorganization of the cell wall and teichoic

acid architecture to expose additional binding sites. It is also possible that heterogeneous cell fragments with an array of metal binding groups from the carboxyl groups associated with D-alanine, D-glutamate, diaminopimelic acid, and phosphoryl groups associated with teichoic acid provide distinct binding sites that lead to different changes in the binding affinity. In the low ionic strengths of our experiments, these distinct changes would be difficult to distinguish due to the large electrostatic contribution towards binding.

There have been conflicting results published for attributing pK_a values of cell wall function groups, metal binding capacities, and metal binding affinity. We have shown that the pK_a value near 6.31 can be attributed to the diaminopimelic acid carboxyl groups associated with peptidoglycan and not phosphoryl groups. We have shown metal binding capacities similar to those reported by Doyle *et al* (10) and no significant difference between the two ions tested (Ca^{2+} and Mg^{2+}). This is in contrast to results of binding capacity published by Beveridge *et al.* (7) that showed binding capacities of 0.399 µmol/mg for Ca^{2+} and 8.226 µmol for Mg^{2+}, while also showing that teichoic acids were solely responsible for Ca^{2+} binding to the cell wall. Metal binding affinity values were found to depend on the amount of metal bound to the sample based on electrostatic effects. For the conditions used in these experiments, a binding constant much higher than previously reported was obtained.

TABLE 3.2. Metal Binding Properties of B. subtilis (1A578) with Ca^{2+} at pH 5.65 and T=4°C
Sample is composed of cell wall fragments containing peptidoglycan and WTA

Trial	Mass (mg)	η (μmol/mg) (Region II)	η (μmol/mg) (Region I)	Bound/Unbound range x 10^3 (Region I)[1]	$K_{assoc.}$ (M^{-1}) (Region I)	Bound/Unbound range x 10^3 (Region II)[1]	$K_{assoc.}$ (M^{-1}) (Region II)
#1	35.1	0.739	0.659	231-29.4	1.180×10^6	13.2-6.54	0.172×10^6
#2	34.7	0.666	0.628	146-25.9	0.660×10^6	4.41-2.67	0.031×10^6
#3	30.2	0.756	0.512	166-6.14	1.098×10^6	4.71-3.54	0.043×10^6
#4	32.4	0.681	0.633	224-14.8	0.955×10^6	7.02-3.75	0.121×10^6
#5	30.3	0.685	0.529	149-17.1	1.039×10^6	7.64-4.79	0.047×10^6
#6	11.7	0.645	0.502	84.9-5.61	1.160×10^6	5.61-2.96	0.035×10^6
	Average:	0.70	0.58		1.0×10^6		0.075×10^6
	Std. Dev. :	0.04	0.07		0.2×10^6		0.058×10^6

1. The ratio of bound ions (μmol/mg) over the unbound ion concentration (μmol/L) decreases as the amount of free ions increases at later stages of the standard addition procedure. Size effects of cell wall fragment heterogeneity causes variation in these values. These are values on the Scatchard plot denoting regions of different equilibrium behavior

TABLE 3.3. Metal Binding Properties of B. subtilis (EB1451) with Ca^{2+} at pH 5.65 and T=4°C
Sample is composed of cell wall fragments containing peptidoglycan

Trial	Mass (mg)	η (μmol/mg)	η (μmol/mg) (Region I)	Bound/Unbound range x 10^3 (Region I)[1]	$K_{assoc.}$ (M^{-1}) (Region I)	Bound/Unbound range x 10^3 (Region II)[1]	$K_{assoc.}$ (M^{-1}) (Region II)
#1	25.7	0.323	0.223	43.2-2.69	1.163×10^6	2.69-1.76	0.024×10^6
#2	67.6	0.275	0.232	80.8-14.2	1.083×10^6	14.2-4.0	0.460×10^6
#3	55.3	0.303	0.303	96-2.67	1.239×10^6	n.d.	n.d.
#4	39.2	0.249	0.228	47.4-3.29	1.110×10^6	1.97-1.1	$.071 \times 10^6$
	Average:	0.29	0.25		1.2×10^6		0.19×10^6
	Std. Dev. :	0.03	0.04		0.1×10^6		0.24×10^6

1. The ratio of bound ions (μmol/mg) over the unbound ion concentration (μmol/L) decreases as the amount of free ions increases at later stages of the standard addition procedure. Size effects of cell wall fragment heterogeneity causes variation in these values. These are values on the Scatchard plot denoting regions of different equilibrium behavior

TABLE 3.4. Metal Binding Properties of B. subtilis (1A578) purified peptidoglycan with Ca^{2+} at pH 5.65 and T=4°C
Sample is composed of cell wall fragments containing peptidoglycan

Trial	Mass (mg)	η (μmol/mg)	η (μmol/mg) (Region I)	Bound/Unbound range x 10^3 (Region I)[1]	$K_{assoc.}$ (M^{-1}) (Region I)	Bound/Unbound range x 10^3 (Region II)[1]	$K_{assoc.}$ (M^{-1}) (Region II)
#1	53.5	0.37	0.277	73.7-9.85	0.694×10^6	2.65-1.49	0.034×10^6
#2	47.9	0.337	0.315	49.5-4.63	1.082×10^6	4.63-2.27	0.178×10^6
#3	35.7	0.295	0.207	78.7-3.41	1.257×10^6	2.20-1.49	0.029×10^6
	Average:	0.33	0.27		1.0×10^6		0.080×10^6
	Std. Dev. :	0.04	0.05		0.3×10^6		0.084×10^6

1. The ratio of bound ions (μmol/mg) over the unbound ion concentration (μmol/L) decreases as the amount of free ions increases at later stages of the standard addition procedure. Size effects of cell wall fragment heterogeneity causes variation in these values. These are values on the Scatchard plot denoting regions of different equilibrium behavior

TABLE 3.5. Metal Binding Properties of B. subtilis (1A578) with Mg^{2+} at pH 5.65 and T=4°C
Sample is composed of cell wall fragments containing peptidoglycan and WTA

Trial	Mass (mg)	η (μmol/mg) (Region 2)	η (μmol/mg) (Region I)	Bound/Unbound range x 10^3 (Region I)[1]	$K_{assoc.}$ (M^{-1}) (Region I)	Bound/Unbound range x 10^3 (Region II)[1]	$K_{assoc.}$ (M^{-1}) (Region II)
#1	14.3	0.657	0.566	113-22.4	1.386×10^6	16-10.1	0.194×10^6
#2	15.4	0.661	0.523	106-20.6	1.452×10^6	14.7-10.1	0.117×10^6
#3	21.7	0.703	0.363	139-30.7	1.529×10^6	20-12.4	0.068×10^6
#4	12.9	0.64	0.567	118-27.4	1.649×10^6	17.9-10.2	0.298×10^6
	Average:	0.67	0.50		1.5×10^6		0.17×10^6
	Std. Dev. :	0.03	0.10		0.1×10^6		0.10×10^6

1. The ratio of bound ions (μmol/mg) over the unbound ion concentration (μmol/L) decreases as the amount of free ions increases at later stages of the standard addition procedure. Size effects of cell wall fragment heterogeneity causes variation in these values. These are values on the Scatchard plot denoting regions of different equilibrium behavior

TABLE 3.6. Metal Binding Properties of B. subtilis (EB1451) with Mg^{2+} at pH 5.65 and T=4°C
Sample is composed of cell wall fragments containing peptidoglycan

Trial	Mass (mg)	η (μmol/mg) (Region 2)	η (μmol/mg) (Region I)	Bound/Unbound range x 10^3 (Region I)[1]	$K_{assoc.}$ (M^{-1}) (Region I)	Bound/Unbound range x 10^3 (Region II)[1]	$K_{assoc.}$ (M^{-1}) (Region II)
#1	50.2	0.244	0.203	44.9-13.7	1.051×10^6	8.63-6.68	0.195×10^6
#2	29.4	0.259	0.14	51.0-6.45	1.301×10^6	4.76-2.15	0.044×10^6
	Average:	0.25	0.17		1.2×10^6		0.12×10^6
	Std. Dev. :	0.01	0.04		0.2×10^6		0.11×10^6

1. The ratio of bound ions (μmol/mg) over the unbound ion concentration (μmol/L) decreases as the amount of free ions increases at later stages of the standard addition procedure. Size effects of cell wall fragment heterogeneity causes variation in these values. These are values on the Scatchard plot denoting regions of different equilibrium behavior

TABLE 3.7. Metal Binding Properties of B. subtilis purified peptidoglycan with Mg^{2+} at pH 5.65 and T=4°C
Sample is composed of cell wall fragments containing peptidoglycan

Trial	Mass (mg)	η (μmol/mg) (Region 2)	η (μmol/mg) (Region I)	Bound/Unbound range x 10^3 (Region I)[1]	$K_{assoc.}$ (M^{-1}) (Region I)	Bound/Unbound range x 10^3 (Region II)[1]	$K_{assoc.}$ (M^{-1}) (Region II)
#1	29.2	0.260	0.229	26.3-9.07	0.411×10^6	4.63-2.53	0.116×10^6
#2	38.2	0.208	0.159	32.3-6.36	1.048×10^6	3.40-2.23	0.082×10^6
	Average:	0.23	0.19		0.73×10^6		0.098×10^6
	Std. Dev. :	0.04	0.05		0.45×10^6		0.024×10^6

1. The ratio of bound ions (μmol/mg) over the unbound ion concentration (μmol/L) decreases as the amount of free ions increases at later stages of the standard addition procedure. Size effects of cell wall fragment heterogeneity causes variation in these values. These are values on the Scatchard plot denoting regions of different equilibrium behavior

TABLE 3.8. Metal Binding Properties of B. subtilis (1A578) with Mg^{2+} at pH 7.25 in 0.001 M HEPES buffer and T=4°C Sample is composed of cell wall fragments containing peptidoglycan and WTA

Trial	Mass (mg)	η (μmol/mg) (Region 2)	η (μmol/mg) (Region I)	Bound/Unbound range x 10^3 (Region I)[1]	$K_{assoc.}$ (M^{-1}) (Region I)	Bound/Unbound range x 10^3 (Region II)[1]	$K_{assoc.}$ (M^{-1}) (Region II)
#1	10.2	0.826	0.642	215-68.2	0.865×10^6	22.3-6.89	0.133×10^6
#2	14.8	0.791	0.702	162-52.2	1.028×10^6	21.4-8.29	0.276×10^6
#3	17.1	0.69	0.550	385-167	1.240×10^6	45.4-8.35	0.362×10^6
	Average:	0.77	0.63		1.0×10^6		0.26×10^6
	Std. Dev. :	0.07	0.08		0.2×10^6		0.12×10^6

1. The ratio of bound ions (μmol/mg) over the unbound ion concentration (μmol/L) decreases as the amount of free ions increases at later stages of the standard addition procedure. Size effects of cell wall fragment heterogeneity causes variation in these values. These are values on the Scatchard plot denoting regions of different equilibrium behavior

TABLE 3.9. Metal Binding Properties of B. subtilis (EB1451) with Mg^{2+} at pH 7.25 in 0.001 M HEPES buffer and T=4°C
Sample is composed of cell wall fragments containing peptidoglycan and WTA

Trial	Mass (mg)	η (μmol/mg) (Region 2)	η (μmol/mg) (Region I)	Bound/Unbound range x 10^3 (Region I)[1]	$K_{assoc.}$ (M^{-1}) (Region I)	Bound/Unbound range x 10^3 (Region II)[1]	$K_{assoc.}$ (M^{-1}) (Region II)
#1	21.9	0.579	0.531	214-25.9	1.313×10^6	25.9-7.35	0.413×10^6
#2	19.3	0.521	0.286	67.3-14.1	0.828×10^6	5.07-2.41	0.047×10^6
#3	26	0.454	0.376	251-41	0.956×10^6	15.2-5.41	0.382×10^6
#4	13.5	0.596	0.31	139-31.8	0.860×10^6	11.8-4.81	0.040×10^6
	Average:	0.54	0.38		1.0×10^6		0.28×10^6
	Std. Dev. :	0.06	0.11		0.2×10^6		0.20×10^6

1. The ratio of bound ions (μmol/mg) over the unbound ion concentration (μmol/L) decreases as the amount of free ions increases at later stages of the standard addition procedure. Size effects of cell wall fragment heterogeneity causes variation in these values. These are values on the Scatchard plot denoting regions of different equilibrium behavior

Chapter 4: Mg^{2+} Binding Characteristics with Wall Teichoic Acid

Introduction

Teichoic acid is a flexible biopolymer found in the cell wall of Gram-positive bacteria. Teichoic acid participates in biofilm production, cell adhesion, cell wall development, cell to cell signaling, host infection, and metal binding(1-6). Teichoic acid also contains phosphate groups that bind external metal ions and help to keep these ions within the cell wall region (7). In this fashion, teichoic acid helps to create a reservoir of metals available for homeostatic delivery to the cytoplasm. The phosphate groups of teichoic acid have been reported to have a pK_a of 2.1 (8,9), which means that nearly all of the phosphate groups are deprotonated at physiological pH and possess anionic character.

Wall teichoic acid (WTA) is chemically bound to the peptidoglycan, as opposed to lipoteichoic acid (LTA) that is anchored to the cytoplasmic membrane. The backbone of WTA is composed of glycerol phosphate linkages having branches of D-alanine, N-acetylglucosamine, or a hydroxyl group (Figure 4.1)(10). These groups exist in random order and differing amounts dependent upon the strain and growth conditions (10,11). The D-alanine modifications have a pK_a value of 8.42 (12) and thus impart a positive charge to WTA at pH = 7. Ion pairing between D-Alanine and the phosphate is possible, leading to a charge neutral site that should not attract metals (13). However, this paradigm has been challenged and the zwitterion is a solvent separated ion pair that does not hinder metal binding (14). Solid state NMR

studies have shown that Mg^{2+} binding moves the D-alanine farther away from the phosphate and places the D-alanine group in a position(14) that allows for the repulsion of cationic antimicrobial peptides(15).

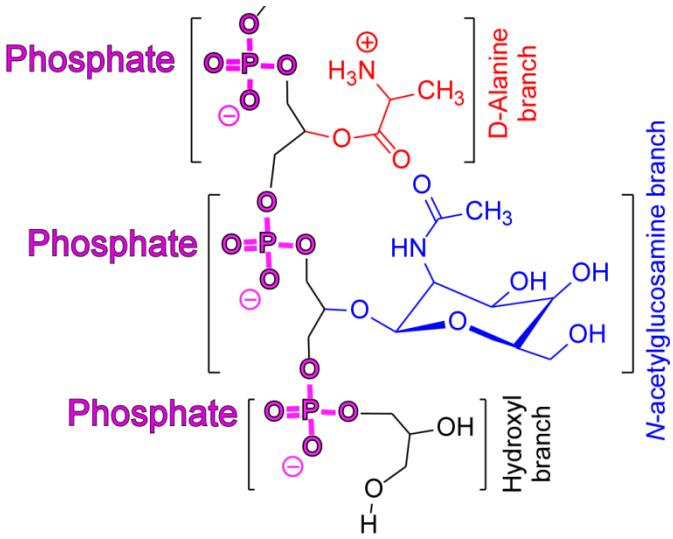


Figure 4.1: Polyglycerol backbone of wall teichoic acid. Each polyglycerol phosphate linkage can have different substituents. D-alanation of WTA is determined by growth conditions such as pH, temperature, and available metal content.

The importance of teichoic acid in cellular function is demonstrated through genetic mutation studies that remove the ability to synthesis LTA or WTA. The lack of WTA creates a *B. subtilis* cell morphology that has a loss of its rod shape, exhibits swelling, and has increased cell aggregation (16). The lack of LTA creates a cell morphology that has an increased cell or cell chain length and an increase in cell bending (17). The morphology reported on LTA deficient mutants is similar to that of Mg^{2+} deprived cells (18). Attempts to create double mutants that eliminate both WTA and LTA have shown that the lack of teichoic acids is lethal to cells (17). The lethality of this combination has

been hypothesized to be caused by a lack of divalent cation homeostasis provided by teichoic acid (17).

Here, we report data that characterizes metal binding to WTA as having a Mg^{2+}/P ratio of 1:2 and a binding affinity of 41 x 10^3 M^{-1} that slowly turns into 1.3 x 10^3 M^{-1} as the result of reduced electrostatic effects as more Mg^{2+} becomes bound to the sample. The 1:2 Mg^{2+} to phosphate ratio suggest a bridging mode between phosphates. The much lower binding affinity in comparison to that of peptidoglycan (7) also suggests that WTA facilitates movement of metal ions from outside the cell, across the peptidoglycan, and to the cell membrane.

Materials and Methods

Wall Teichoic Acid Purification

Cell wall samples from *B. subtilis* were grown, harvested, and purified as previously reported (7). These cell wall samples, containing only peptidoglycan and covalently bound WTA, underwent an additional treatment with 10 % TCA (trichloroacetic acid) at 4°C to remove the WTA. After treatment with TCA, the suspension was centrifuged at 15,000*g* and the supernatant was transferred into 1000 MWCO regenerated cellulose dialysis membrane tubing. The dialysis tubing was placed in 2 L of Milli-Q H_2O, which was changed twice at 12 hour intervals. An osmotic pressure increase inside the tubing resulted from the exchange of a large amount of TCA molecules. This required the sample to be lyophilized, re-suspended in a minimal volume of Milli-Q H_2O, and then placed into 1000 MWCO dialysis membrane tubing. The dialysis membranes were

placed in a 250 mL bath of 0.01 M EDTA at 4°C overnight to remove residual metal ion concentration. The dialysis membranes were then placed into 2L of Milli-Q H_2O at 4°C and the water bath was changed an additional 6 times during 12 hour intervals. The liquid inside the dialysis membrane was transferred to a glass vial and water removed with vacuum lyophilization to produce a white, translucent solid.

Membrane Dialysis Procedure

A known quantity (29.4 mg) of WTA was dissolved in 1 mL of Milli-Q H_2O, placed in a 500 MWCO dialysis membrane containing 74 mL of Milli-Q H_2O. A 5mL aliquot was extracted every 48 hours and a 5 mL addition of 5 ppm Mg^{2+} was performed after each extraction for the first set of data points. Additions of 25 ppm Mg^{2+} were performed with the second set of data points to create a larger concentration gradient. The Mg^{2+} concentrations of the aliquots from each extraction were analyzed with a Varian SpectraAA 55b Flame Atomic Absorption Spectrophotometer. The difference between the expected increase in unbound Mg^{2+} concentration and the observed concentration increase is attributed to Mg^{2+} binding to WTA. Binding constants of this data were determined with a Scatchard plot. A control containing a dialysis membrane filled with 1 mL of Milli-Q H_2O was subjected through the same process as the WTA sample. Flame AA analysis of the control signified that incomplete equilibrium of metal ions through the membrane and binding of Mg^{2+} to the dialysis membrane did not occur.

Phosphorus Concentration

The purified WTA underwent liquid state ^{31}P NMR analysis to quantify the phosphorus content. The probe was externally calibrated with 0.0485 M triphenyl-phosphate and one transient scan was taken with a 90° pulse and a 60 second delay time. The gain was set constant for the reference calibration standard and the sample. A 5.9 mg quantity of WTA was dissolved in 750 µL of D_2O and underwent NMR analysis for phosphate concentration. Quantitative analysis of the phosphate content in the WTA sample was performed using the qNMR tools in VnmrJ 3.1 where the integrated peak area for the reference was compared to the sample. A concentration of 21.5 mM of phosphorus was obtained in this analysis. This is equivalent to 2.7 µmol P per mg of WTA and 8.4% phosphorus on a mass percentage. This differs slightly from previous reports of wall teichoic acid from *Staphylococcus aureus* being composed of 6.4% phosphorus (19). This difference can be attributed to the wall teichoic acid being a polyribtol phosphate polymer while the *B. subtilis* used in our studies was a polyglycerol phosphate polymer.

Mg^{2+} Binding Capacity to WTA

The binding capacity of Mg^{2+} towards WTA can be extrapolated from the Scatchard plot by calculating the amount bound at sufficiently high concentrations (bound vs. unbound = 0). However, slight errors in the affinity constant and its associated slope on the Scatchard plot can produce substantial differences in the estimation of binding capacity. To mitigate this error, the metal binding capacity of WTA was also determined through a simple, one step

method of exposing WTA to a sufficiently high concentration of Mg^{2+}. A known quantity (14.8 mg) of WTA was dissolved in 1 mL of 50 ppm Mg^{2+} solution and placed in a dialysis membrane. The dialysis membrane was then placed in 49 mL of 50 ppm Mg^{2+} solution and allowed to mix in a shaker (4°C, 200 rpm). After 48 hours, the Mg^{2+} concentration outside of the dialysis membrane was examined via Flame AA analysis and it was discovered that 1.27 µmol of Mg^{2+} was bound per mg of WTA.

Results

The data presented here can be used to elucidate potential binding modes and interactions between metal ions and the cell wall. This information is essential to understand fundamental biochemical processes that precede metal ion transport through the cell membrane. By comparing the relative Mg^{2+} binding affinity and capacity with WTA, we observe that the sample initially undergoes allosteric changes caused by the addition of metal ions. This is expected since teichoic acid is reported to have a stretched rod conformation in the absence of metal ions and random coil conformation develops as the ions in solution increase (20). During this process, the fraction of metal ions remaining in solution is larger than that observed in the presence of peptidoglycan or peptidoglycan with covalently bound WTA (7). As the concentration gradient across the dialysis membrane increases, more metal becomes bound. This allows measurement of binding affinities and capacities from flame AA data.

Positive Cooperativity of Mg^{2+} Binding to WTA

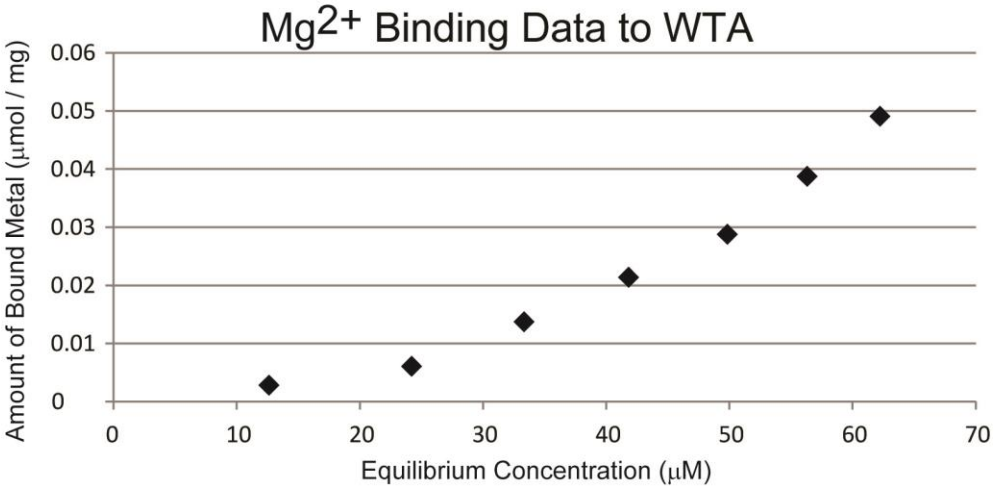


Figure 4.2: The binding curve for WTA and Mg^{2+} during the early stages of metal binding. The increase in binding at higher Mg^{2+} concentrations suggests allosteric effects to create stronger binding, perhaps caused by phosphate groups on coming closer together after prior metal binding events.

The binding of Mg^{2+} ions to WTA was measured with atomic absorption spectroscopy which provides a quantitative measurement of metal ion concentration. During equilibrium dialysis, metal ions are bound to WTA within the dialysis bag and samples for flame AA analysis are taken from the solution outside of the dialysis membrane. Differences between the equilibrium concentration in solution and the known quantity of metal ions added to the sample are used to determine the fraction of metal ions bound to WTA. The data in Figure 4.2 show that the serial addition of Mg^{2+} ions leads to increasing amounts of metal bound to WTA. However, the trend is not linear; instead metal binding appears to increase exponentially. This is in marked contrast to the metal binding behavior within the bacterial cell wall where teichoic acid works in concert with peptidoglycan to chelate metals in a logarithmic fashion (7).

The equilibrium constant for Mg^{2+} binding to WTA can be found with a Scatchard plot (7). In this representation (Figure 4.3), the positive slope indicates that metal binding has positive cooperativity. This explains why the data in Figure 4.2 show that initial binding events make it easier for subsequent metals to bind with WTA. Equilibrium constant (K_A) values are taken from the slope in the Scatchard plot. Unfortunately, the positive slope in Figure 4.3 generates a K_A with a negative value and therefore cannot be used to formulate chemical models or comparisons. The positive slope behavior in Scatchard plots has been observed in RNA samples with Mn^{2+} in low ionic strength solutions (21,22). We believe the initial upward exponential curvature and positive Scatchard plot slope is represented by allosteric effects where the binding of a previous metal ion induce an effect that creates a higher affinity for next binding ions. Such allosteric effects and associated structure changes have been reported for Mn^{2+} binding with tRNA (21). Teichoic acid has been reported to change structure with the addition of salt (20). Teichoic acid in dilute buffer or distilled water was reported to have a rigid rod conformation, while salts induced a random coil conformation based on viscosity measurements (20).

Conformational changes within WTA can affect the metal binding affinity by creating new binding sites or bringing the phosphate backbone together. In this scenario, the metal may be chelated in a bridging motif using two phosphate groups. Without metal, the two phosphate groups may be far apart but move together as initial metal binding occurs. This is analogous to the

operation of a common zipper. The electrostatic attraction between Mg^{2+} and phosphate groups can be strengthened if two phosphate groups are involved. Similarly to our zipper model, an intermolecular bidentate binding model with Ca^{2+} binding to adjacent phosphate groups on three teichoic acid strands has been proposed (23,24). It is predicted that divalent metal cations interact and form bridges between peptidoglycan, WTA, LTA, and cell wall proteins (23). There have been reports on the interaction between metal ions of wall teichoic acid and carboxyl groups on peptidoglycan which signify additional binding mechanisms when attached to the cell wall (25).

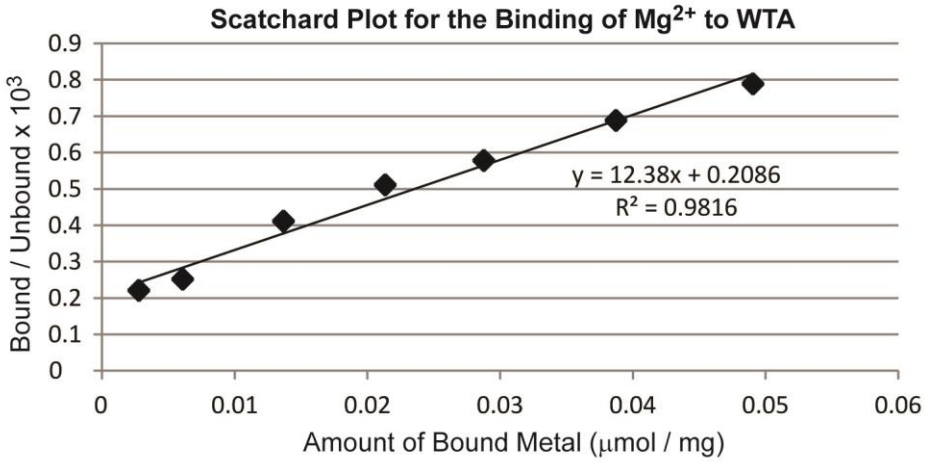


Figure 4.3: The Scatchard plot formed from the initial data points of WTA and Mg^{2+} binding shown previously in Figure 4.2. Neither binding capacity nor binding affinity parameters can be extracted from these points.

Positive cooperativity for metal binding to WTA also suggests that the system may not be at equilibrium. Equilibrium between the inside and outside of the dialysis membrane is reached quickly based on the results of control measurements of water only samples. However, conformational rearrangement of the WTA polymer may be slower. Finding a conformation with the lowest

potential energy would require breaking the phosphate-metal-phosphate bridges. The rate of interconversion is unknown, but is expected to be slower at 4°C, the sample temperature during dialysis process. Thus, we decided to extend the period of time between collecting flame AA samples. After collecting sample number 7 and adding more metal ions, we waited 21 days to collect sample number 8. To our surprise, the solution equilibrium concentration of Mg^{2+} decreased while the amount of Mg^{2+} bound to WTA increased. The additional 9 μmol/mg of bound Mg^{2+} corresponds directly to the 25 μM drop in solution concentration. These data are informative with regards to the need for additional time for WTA to reach equilibrium, which is remarkable as WTA is a single strand phosphodiester polymer. Likewise, the role of metals in causing rearrangement provides a new chemical perspective on how metals interact with Gram-positive bacteria.

After allowing 21 days for the sample to reach equilibrium, the time period between subsequent data points was reduced to 48 hours and 25 ppm was added in 5 mL quantities to cause a larger concentration gradient. Here, exponential binding behavior disappears and the data points exhibit linear behavior (Figure 4.4). Transformation into a Scatchard plot formulation gives a pattern indicative of negative cooperativity. Electrostatic effects have also been shown to be responsible for an apparent negative cooperativity in binding studies (22). The electrostatic effects are responsible for the curvature seen in Figure 4.5. As a result, an initial positive cooperativity is observed with a possible re-organization of WTA upon metal binding, leading to subsequent

negative cooperativity thereafter. Using these later sets of data, it is possible to obtain the binding affinity and metal association equilibrium constants.

Binding Affinity of Mg^{2+} to WTA

The binding affinity of Mg^{2+} to peptidoglycan has been measured (7), K_A = 1.0 x 10^6 M^{-1}. After the initial positive cooperativity observed with Mg^{2+} binding with WTA, electrostatic effects become more apparent and a concave slope is observed in the Scatchard plot with the last 7 points taken in the experiment (Figure 4.5). This behavior is also observed with Mg^{2+} binding to RNA (22,26). WTA attracts Mg^{2+} ions with a metal binding affinity of 4.07 x 10^6 M^{-1} which decreases to 1.06 x 10^3 M^{-1} as seen in Figure 4.5.

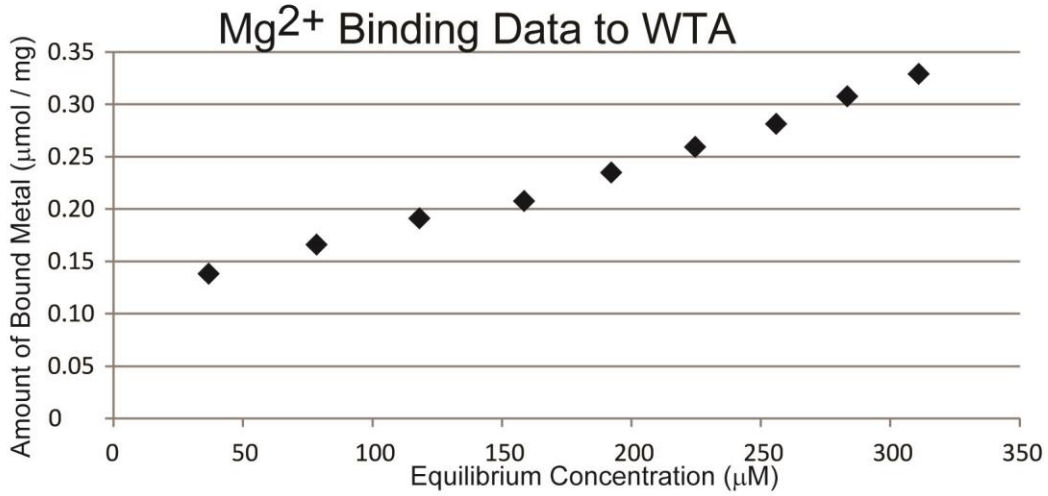


Figure 4.4: The binding curve formed from the second set of data points of WTA and Mg^{2+} that were taken 21 days later than the previous set shown previously (Figure 4.2). It appears to have a linear relationship.

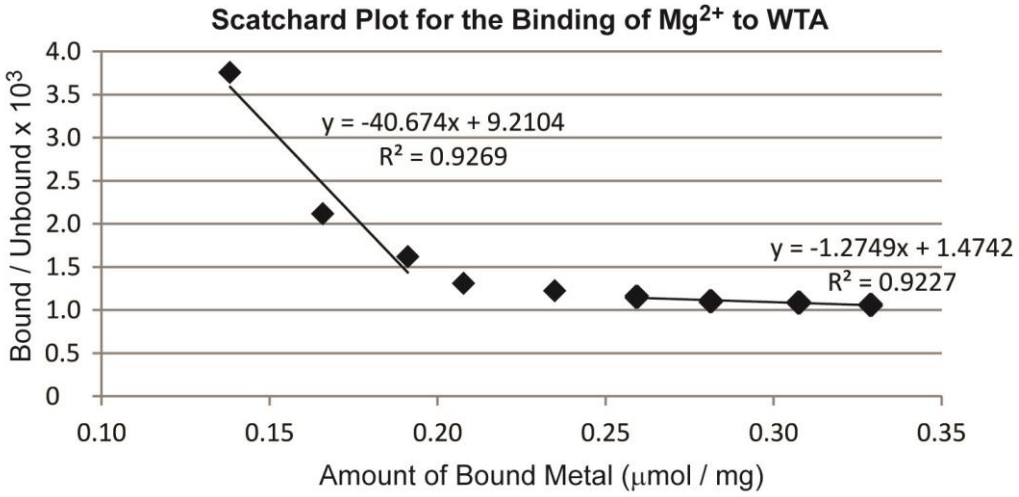


Figure 4.5: The Scatchard plot of the metal binding data from Figure 4.4 showing the gradually decreasing affinity constant as more metal is added to the system.

Both sets of binding data are represented by Figure 4.6. A distinct deviation on the curve is observed near the bound region of 0.138 μmol/mg. This data point (#8) was a result from waiting approximately 3 weeks after the final 5 ppm Mg^{2+} addition with first set of data (point #7). The shift in equilibrium concentration and bound Mg^{2+} quantity can be attributed to a potential WTA reorganization to create more binding sites. Incomplete diffusion into the dialysis membrane can be ruled out based a control that went through the same experimental procedure as the sample.

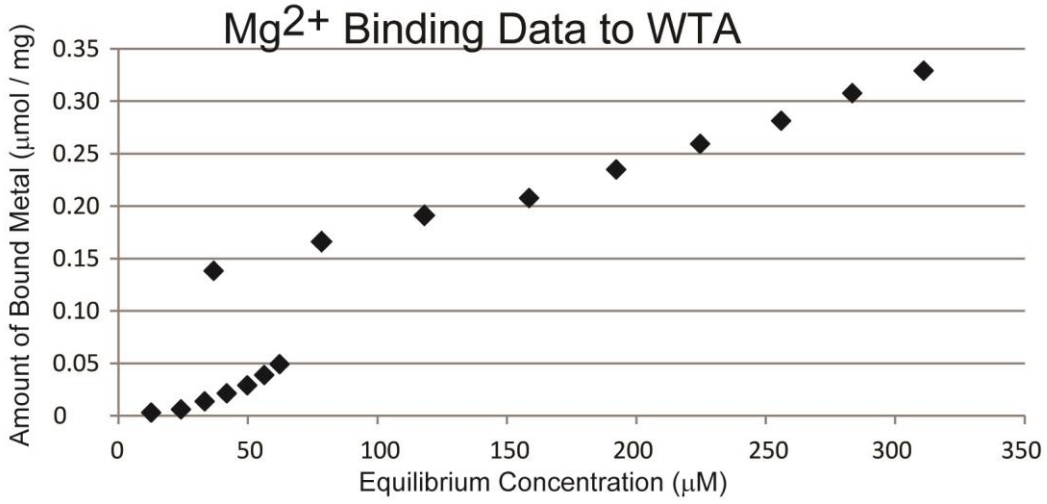


Figure 4.6: WTA Binding Curve for all data points.

The difference between data points 7 and 8 correlates well with changes in the expected equilibrium concentration and observed equilibrium concentration. The difference in amount bound between points 6 and 7 is 0.0103 µmol/mg and 0.0100 µmol/mg for points 5 and 6. Following the binding trend we can expect about an additional 0.0103 µmol/mg to be bound, leading to a total approximate bound quantity of 0.059 µmol/mg. However, with point 8, we observe 0.138 µmol/mg being bound to the sample, an increase of 0.079 µmol/mg. Likewise, we also observe a deviation from the trend in equilibrium concentration, changing from 6.22×10^{-5} M^{-1} in point 7 to 3.68×10^{-5} M^{-1} in point 8. A 5 ppm quantity of Mg^{2+} was added after point 7, as in the previous extraction and addition procedure. Taking this into account, we can predict an expected equilibrium concentration around 6.72×10^{-5} M^{-1}. This is a difference of 3.04×10^{-5} M^{-1} or 2.28 µmol Mg^{2+} in 75 mL of H_2O. With a known sample weight of 29.4 mg, the decrease in equilibrium solution concentration

corresponds to a loss of 0.078 µmol Mg^{2+} per mg WTA. This correlates strongly with the observed increase in the fraction of bound metal, 0.079 µmol Mg^{2+} per mg WTA.

Electrostatic Effects and Binding Capacity

The primary bonding force between metal ions and the phosphate groups of WTA is electrostatic, much like with purified cell wall with peptidoglycan. These electrostatic effects begin to become apparent after the initial positive cooperativity takes place where the WTA may undergo structural changes upon initial metal ion binding events. The negative cooperativity develops as more metal ions become bound to the biopolymer of WTA and charge neutralization occurs. Equilibrium dialysis measurements with 14.8 mg of WTA in 50 mL of 50 ppm Mg^{2+} solution gave a binding capacity of 1.27 µmol Mg^{2+} per mg WTA. This is equivalent to a Mg^{2+} to P ratio of 0.49 to 1 based on the phosphorus content per mg of WTA determine by NMR measurements. This supports a bridging chelation mode described earlier with LTA and Cd^{2+} (27).

Teichoic acids account for the majority of the cell's metal binding capacity due to its relative abundance in the cell and binding capacity per milligram. Previous work in our laboratory has shown the effect WTA has on metal binding to the bacterial cell wall. Composed of peptidoglycan and WTA, hydrolysis with trichloroacetic acid separates these two components. After this step, 46% of the cell wall mass remained as an insoluble peptidoglycan component. This supports previous reports that WTA accounts for 20 to 60% of

the total cell wall mass (28). Cell wall fragments of *B. subtilis* 1A578 containing peptidoglycan and WTA have a Mg^{2+} binding capacity of 0.67 μmol/mg and purified peptidoglycan has a binding capacity of 0.23 μmol/mg at a pH of 5.65. When the binding capacities of peptidoglycan (7) and WTA (this work) are combined with their relative mass percentages, we obtain a theoretical value of 0.73 μmol/mg (0.46 x 0.23 μmol/mg + 0.54 x 1.16 μmol/mg). This value compares favorably with the experimental value (0.67 μmol/mg). Thus, WTA has a higher capacity for binding metals than peptidoglycan. These data also reinforce the importance of WTA in metal binding and particularly the ability of WTA to extend past the cell wall boundary and chelate metals in extracellular space. This property would also explain why the absence of WTA leads to reduced metal uptake and distorted cell shapes from metal starvation.

Comparison of Metal Binding with RNA

WTA is a phosphodiester polymer. RNA is also a phosphodiester polymer and both molecules share metal binding properties. Comparison with previous studies of RNA metal binding can help us understand the initial positive cooperativity mode that changes to negative cooperativity. Both WTA and RNA are polymeric biomacromolecules that bind metal ions. Metal binding behavior in the Scatchard plot of RNA binding Mg^{2+} ions describe two classes of binding sites: a group of strongly site bound ions (class I sites) and more weakly bound ions (class II sites) (29). It has been proposed that each of these modes has a strong coulombic contribution responsible for binding (29). In addition, ion solvation and other nonelectrostatic contributions are said to be significant (29).

However, this designation of strong and weak sites begins to break down depending on the concentration of monovalent ions and ionic strength. This proposed model that designates specific sites as being responsible for the high and low affinity regions is not supported by evidence of “strong” sites decreasing at higher ionic strength values (22). Nonetheless, the affinity of class I sites for Mg^{2+} binding to tRNA have been reported to be 1 x 10^6 M^{-1} (30), 9 x 10^4 M^{-1} (31), 2.9 x 10^4 M^{-1} (32), and 7.5 x 10^4 M^{-1} (26). Class II sites for Mg^{2+} binding to tRNA were reported to be 1.1 x 10^4 M^{-1} (30), 6 x 10^3 M^{-1} (31), 4.2 x 10^2 M^{-1} (32), 8.3 x 10^2 M^{-1} (26). The K_A values obtained in this work (4.1 x 10^4 M^{-1} and 1.3 x 10^3 M^{-1} respectively) correlate well with these values.

Proposed Model of Facilitated Ion Movement to Membrane

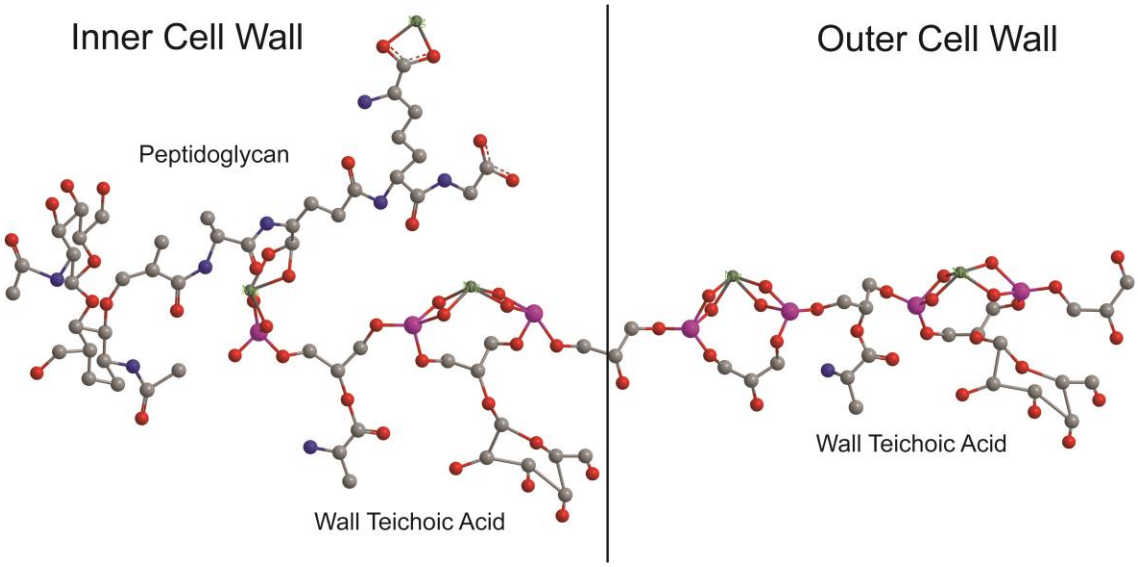


Figure 4.7. Potential binding modes between Mg^{2+} with WTA extending past the peptidoglycan layer and WTA inside the peptidoglycan layer. A fragment of the peptidoglycan repeating unit and segment of the wall teichoic acid polymer is shown above. A 1:2 Mg^{2+} to phosphate binding ratio is observed when examining the binding capacity of WTA which gives evidence towards a bridging binding mode between the phosphate groups of WTA. Interactions

among the phosphate groups and un-protonated carboxyl groups of peptidoglycan might also exist.

WTA extends past the cell wall peptidoglycan and metal ions can interact with WTA individually or they can interact with the phosphate groups of WTA and carboxyl groups of peptidoglycan simultaneously as seen in Figure 4.7. Homeostasis allows metal ions to flow from low affinity binding sites to higher affinity binding sites. In light of the binding association constants for WTA(this work), peptidoglycan (7), and cell wall fragments containing peptidoglycan and WTA (7), we suggest that the transport of metal ions from the outer cell wall to the inner cell wall can be viewed in the following manner. Metals originate outside the cell wall in the extracellular fluids, including monovalent and divalent ions. In the case of Mg^{2+} ions, the first interactions with the bacterial cell occur with WTA that extends past the cell wall. Binding to WTA is a bidentate process with an affinity constant that is “weak” compared to metalloenzymes yet necessary to allow the metal ions to traverse the phosphodiester backbone. Once the metal ions reach the cell wall, they encounter binding sites formed by peptidoglycan that have a higher affinity constant. Here, Mg^{2+} ions favor binding to the peptidoglycan component of the cell wall and are desorbed from the external WTA molecules. Nevertheless, WTA is also present within the cell wall and works in concert with peptidoglycan to form the cell wall binding sites. The peptidoglycan has a smaller binding capacity but a stronger association constant. However, WTA has a higher binding capacity but a weaker association constant. The result is two types of metal binding interactions within

the cell wall. First, strong metal binding by peptidoglycan chelates metal ions required for structural stability and rigidity of the cell wall framework. Because WTA has intimate contact with the peptidoglycan (14), WTA can also contribute to the formation of the strong metal binding site. However, WTA can form a cell wall binding site without the need for peptidoglycan. This weaker metal binding environment with a higher metal binding capacity has the potential to be the predominate environment for metal ions within the cell wall. In this way, WTA alone can create a reservoir of metal ions that are needed for various intracellular processes. Because the association constant is small, the ions can easily reach the cytoplasmic membrane. There, they can interact with lipoteichoic acid and transmembrane proteins for delivery to the cell interior. Consequently, this metal binding model presents the opportunity to interrupt cellular processes by preventing metal chelation to the phosphodiester backbone of WTA. Agents that have a stronger binding affinity constant than metals would displace the metals from the WTA polymer and perhaps lead to cell death. Effective antibiotics that function in this manner may be difficult to discover as the large fraction of WTA in the cell wall presents the need for large therapeutic doses. However, the innate immune response does include cationic antimicrobial peptides that could function by interacting with WTA to occupy metal binding sites. Antimicrobial peptides have been shown to potentially invoke WTA binding (33). Current paradigms that describe the function of cationic antimicrobial compounds do not involve the inhibition of metal chelation

(34-38). Work to re-examine the interactions of WTA, metal ions, and cationic antimicrobial peptides is currently underway.

Conclusion

In this work we determined the binding affinity and binding capacity of Mg^{2+} to WTA. WTA has a much lower binding affinity for Mg^{2+} compared to the binding affinity of Mg^{2+} to peptidoglycan. At low salt concentrations, Mg^{2+} exhibited an initial binding affinity of 41×10^3 M^{-1} that decreased to 1.3×10^3 M^{-1} as more Mg^{2+} became bound due to electrostatic effects. The binding capacity coupled with the phosphate concentration suggests a 1:2 Mg^{2+} ion to phosphate binding ratio. A binding capacity of 1.27 µmol Mg^{2+} per mg of WTA was determined. WTA and teichoic acids in general are responsible for the majority of the Mg^{2+} binding capacity of the cell wall when compared to the relative percentage of peptidoglycan in the cell wall sample. We envisage that WTA facilitates the transport of metal ions outside of the cell to regions of higher affinity near the cell wall surface. Divalent metal ions can potentially bind in a variety of modes. Metal ions might form any of the following binding modes with the phosphate groups of teichoic acid: monodentate, bidentate, mono-dentate bridging, bidentate bridging as well as bridging between adjacent strands of WTA. Metal ions can also potentially interact with interaction with both the phosphate groups of WTA and deprotonated carboxyl group of peptidoglycan. In addition, these modes can either be inner-sphere or outer-sphere depending on the hydration state when bound. Due to the chemical similarities of both WTA and LTA being polyglycerol phosphates, it is expected that they would

have similar affinity constants. Since WTA can also exist as a polyribitol phosphate polymer, we would expect that the polyribitol version would have a different binding affinity as was reported by previous studies. WTA with a polyribitol phosphate backbone and its associated binding constant have been studied by others previously. These studies utilized an equilibrium dialysis method and a binding constant of 0.61×10^3 M^{-1} as well as a Mg^{2+}/P ratio 1:1 was reported (39). This is in contrast with results of WTA with a polyglycerol phosphate backbone that was reported to have an affinity constant of 2.7×10^3 M^{-1} and Mg^{2+}/P ratio of 1:2 (9).

Chapter 5: Antimicrobial Branched Polyethyleneimine Functions by Blocking Chelation of Essential Mg^{2+} Ions

Introduction

Bacterial infections are a biochemical battle between the host and bacterial defense mechanisms. Gram-negative cells possess an outer lipid membrane with lipopolysaccharides, a periplasmic space with peptidoglycan, and an inner cytoplasmic membrane. This is in contrast to Gram-positive bacteria that possess a much thicker layer of peptidoglycan with anionic wall teichoic acid and a single cytoplasmic membrane with lipoteichoic acid. Certain antibiotics are more effective against Gram-positive bacteria due to the absence of the second lipid membrane that may prevent permeation. This trend depends on the class of a particular antibiotic and is primarily associated with hydrophobic antibiotics. To the contrary, it has been proposed that some cationic agents act as a permeabilizer of the cell by binding to the cell's membrane (1). At higher concentrations, these agents also have a bactericidal effect at a certain concentration threshold that causes the release of cytoplasmic components (1). Many clinical antibiotic treatments employ drugs that block cell wall synthesis, inhibit DNA gyrase, or prevent cell division (2). Unfortunately, these approaches allow the bacteria to develop resistance because the cell remains intact. However, it is more difficult for bacteria to counteract the effects of cationic polymers.

One bactericidal mechanism of soluble cationic compounds suggests that penetration through the thick cell wall can disrupt the cytoplasmic

membrane (3,4). Cytoplasmic permeabilization can also lead to depolarization of the cytoplasmic membrane. However, incomplete depolarization was observed when more than 90% of the bacteria have been killed in one study (5). Disruption of the cytoplasmic membrane might be primary effect in Gram-negative bacteria whereas it could be a secondary effect to the mechanism of death in Gram-positive bacteria. A live/dead two color fluorescence assay that detects damage to bacterial membranes has been reported to show immobilized N-alkylated polyethleneimine killing both Gram-positive and Gram-negative cells through membrane damage (4).

Other reports have postulated that charged molecules in solution may be able to kill through an ion exchange based killing mechanism (6). It is well known that the net negative charge of the cell-wall attracts metal cations (7-10). The negative charge comes from deprotonated phosphate groups of teichoic acids and anionic carboxyl groups in the peptidoglycan. This net negative charge allows the cell wall to form electrostatic bonds with dissolved metal ions. There is a strong likelihood that the cell wall will also attract BPEI due to its positive charge. In this situation, BPEI and metal ions must compete for cell wall binding sites. Here we are able to show that BPEI binding will displace Mg^{2+} metal ions and inhibit them from binding in competition based equilibrium. As a result of metal starvation, the bacteria experience a significant increase in lag phase growth dependent on the concentration of BPEI.

BPEI shares some electrochemical properties with natural cationic antimicrobial peptides (CAMPs) that are part of the human innate immune

response. Many antimicrobial peptides with cationic lysine and arginine residues kill bacteria by disrupting membrane integrity. Nonetheless, Gram-positive bacteria are believed to repel CAMP attack through a chemistry-based mechanism rather than genetic adaptation(11). This view originates with teichoic acid (TA), whose D-alanine groups are attached via the carboxyl group, presenting the amine group as an NH_3^+ moiety. The D-alanine of teichoic acid have a predicted pK_a value of 8.42, and are protonated at circumneutral pH (12). Bacteria without D-alanine in TA are more susceptible to killing by CAMPs.(11) However, TA contains numerous anionic phosphates that may bind cationic molecules. This contrast between repulsive and attractive forces leads to the conflicting models of structural biology and the ability of TA to attract, or repel, metal cations. With NMR spectroscopy, we have been able to resolve the structural biology questions. We showed that D-Ala does not prevent metal binding (13). This discovery also suggests that TA may not repel BPEI and presents the opportunity to employ BPEI as a chemical means of neutralizing TA molecules, thus neutralizing the ability of TA to control biochemical processes in the cell wall. Antimicrobial therapies involving BPEI may increase the effectiveness of CAMPs and reduce the MIC of antibiotics targeting the cell wall, thereby alleviating the growing risk of antibiotic-resistant strains of Gram-positive bacteria. Such therapies are possible because BPEI is chemically stable with a low cytotoxicity towards eukaryotic cells (14). An important step towards this goal is understanding the mode of action of BPEI as a antibacterial agent. Efforts to provide this information are provided below.

Experimental Procedures

Preparation and Characterization of Branched Polyethyleneimine

Low molecular weight branched polyethyleneimine was obtained from Sigma Aldrich. Serial dilutions were made using the appropriate quantitative precautions. An ESI+ mass spectrum (Figure 5.1) showed that our sample of BPEI has a maximum molecular weight of around 792 with a median weight of around 405. An example of a BPEI structure in the polymer distribution that results from the (M+H)+ peak at 362.4 is depicted in Figure 5.2. The molecule has polycationic character from the protonation of its amine functional groups based on its protonation constant (pK_a). Protonation constants for branched PEI molecules have been reported to be around 4.5 for primary amines, 6.7 for secondary amines, and 11.6 for tertiary amines (15).

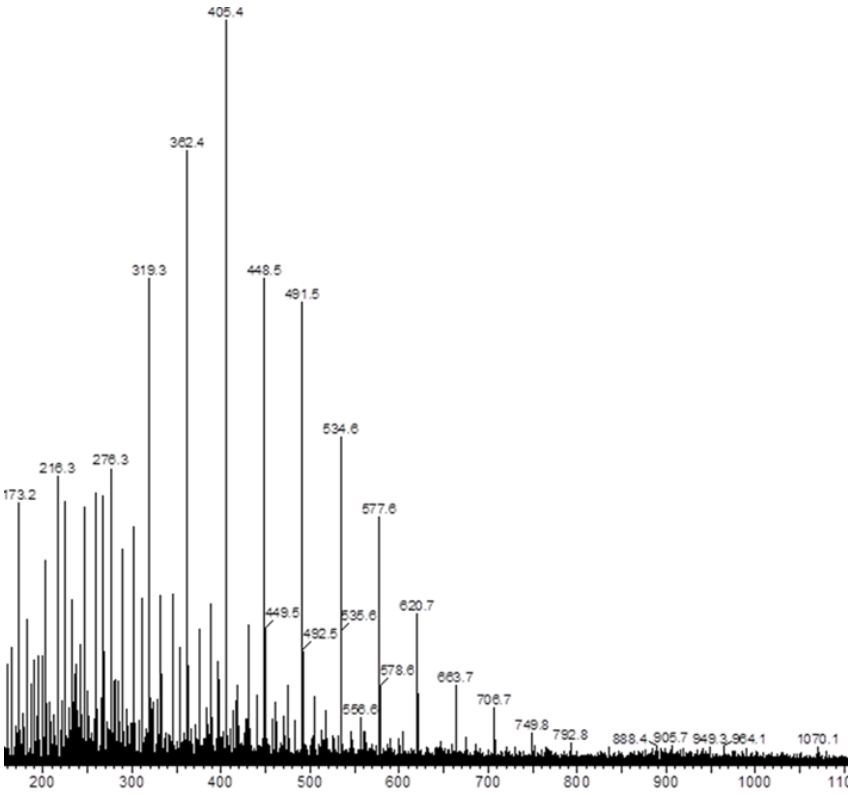
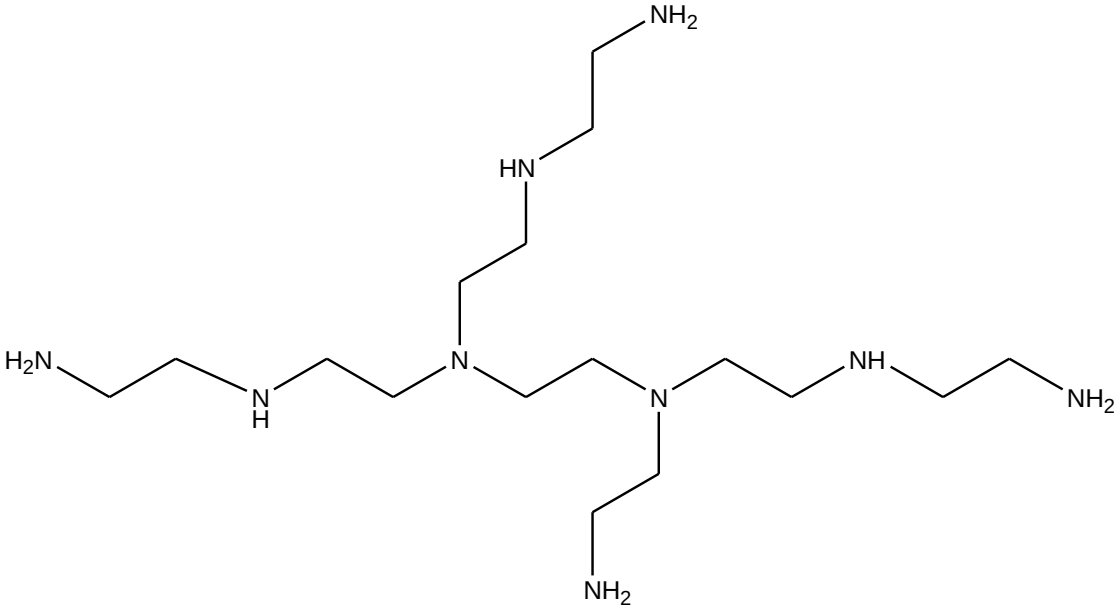


Figure 5.1. ESI(+) mass spectrum of the mass distribution of the low molecular weight branched PEI that was used in experiments.



$C_{16}H_{43}N_9$
Exact Mass: 361.36

Figure 5.2: An example of one structure of low molecular weight branched polyethyleneimine. The pK_a protonation constant values for branched PEI are

around 4.5 for primary, 6.7 for secondary, and 11.6 for tertiary amine groups (15).

Spectrophotometric Quantification of BPEI

It has been reported that polyethyleneimine can be detected spectrophotometrically with the addition of Cu^{2+} ions (16,17). A calibration curve was created by adding 0.1 mL to 1.9 mL of BPEI stock solution with 0.1 mL of 1M $CuSO_4$ and diluting to 2 mL in a quartz cuvette. From the resulting BPEI-Cu^{2+} complex we obtained two regions of absorbance. A high intensity region was observed at 285 nm which can be used to quantify samples in a concentration range of 0.5-100 µg/mL. A lower intensity region of absorbance was observed at 630 nm which can be used to quantify higher concentration PEI samples in the range of 40-2000 µg/mL.

Effect on Growth Rate of B. subtilis by BPEI and Metal Ion Supplementation

Flasks containing 50 mL of LB growth media were inoculated from an overnight culture by transferring a volume equal to 1% of the new culture. BPEI was then immediately added to each flask. The cultures were then allowed to grow (200 rpm, 37°C) and visual turbidity measurements were taken every hour for 8 hours and then again at 23 hours. *B. subtilis* was also inoculated in flasks containing combinations of 0.125 g/L BPEI. In some cases, additional $MgCl_2$ and $CaCl_2$ was added and allowed to grow under identical conditions.

Investigation of BPEI on Metal Binding

An investigation of Ca^{2+} or Mg^{2+} binding with BPEI was performed to determine if the presence of alkaline earth metal ions affected our quantification method. An estimation of the binding constants with metals other than Cu^{2+} of linear and branched PEI molecules has been investigated (18). Branched PEI molecules tend to bind metal ions more strongly than linear PEI molecules (18). A scanning UV-Vis spectrum of identical BPEI samples with and without 100 ppm Ca^{2+} or Mg^{2+} solutions and $CuSO_4$ does not show a shift in the absorbance region and the absorbance intensity did not decrease. Metal ion calibration curves performed by flame AA analysis with and without 0.1 g/L BPEI showed no difference as well. Nonetheless, calibration curves were made with identical amounts of PEI concentrations used in the experiments in Flame AA measurements.

Cell Wall Purification

Cell wall samples were produced using a modified procedure by Umeda *et al* (19). Cell wall samples purified from *B. subtilis* strain 1A578 contain peptidoglycan and WTA. Cells were grown to an OD600 of ~1.0 in mid-log phase, centrifuged at 15000g for 25 minutes, re-suspended in 10 mL of distilled deionized water, and disrupted with a French press. The resulting fragments were centrifuged (15000g, 25 minutes), re-suspended in a minimal volume of distilled deionized water and then added drop-wise with stirring to 100 mL of boiling 6% (w/v) sodium dodecyl sulfate to inactivate autolysins (20,21) and remove the cytoplasmic membrane. The sample was rinsed a minimum of 3

times with 200 mL of distilled deionized water. The sample was then re-suspended in TRIS buffer (pH 8.2) and treated with trypsin (200 µg/mL), RNAse (100 µg/mL), and DNAse (100 µg/mL) at 37°C in an incubator/shaker for 16-18 hours. The cell wall fragments were washed with distilled deionized water and then re-suspended with 25 mL of ammonium acetate buffer (pH 4.7) and treated with pepsin (100 µg/mL) at 37°C for 2 hours. The cells were then washed with H_2O and soaked in 50 mL of 50 mM EDTA overnight (4°C) to remove any residual metal ion contamination. The cell wall samples were washed with 200 mL of distilled deionized water and then lyophilized forming a white and fluffy solid.

TCA hydrolysis

Portions of the freeze dried cell wall sample was mixed with 10% trichloroacetic acid at 4°C for 48 hours (12). The sample was then centrifuged at 15000 g for 30 minutes and the insoluble portion of peptidoglycan was then washed once with Milli-Q H_2O and then allowed to sit overnight in 0.05 M EDTA at 4°C. The peptidoglycan sample was separated with centrifugation and washed 3 times before being dried with lyophilization.

Binding of BPEI to Cell Wall

Cell wall samples (~20 mg) were placed in a 1000 MWCO dialysis membrane and were left to soak in 50 mL of 0.1 g/L and 0.015 g/L BPEI for two days in a shaker (4°C). An equilibrium dialysis procedure for metal binding to the cell wall was performed. Every 24 hours a 5 mL aliquot was removed from the jar and 5 mL of a 5 ppm Mg^{2+} ion solution was added to create a

concentration gradient. The first aliquot extraction before the addition of metal ions was then analyzed for BPEI content using the spectrophotometric quantification method mentioned previously. All extractions were tested for Mg^{2+} content via flame AA analysis to determine the amount of metal bound to the cell wall sample.

Displacement of Metal Ions on the Cell Wall by BPEI

It is necessary to determine the amount of metal bound to a sample and the types of metals bound to determine the effect of BPEI. A purified cell wall sample was loaded with Mg^{2+} to quantify the displacement of metal ions. A known mass (18.4 mg) of purified cell wall was suspended in 1.5 mL of 10 ppm Mg^{2+} solution and then placed in 48.5 mL 10 ppm Mg^{2+}. After soaking in 50 mL of 10 ppm Mg^{2+} for 48 hours, a 5 mL aliquot was removed for flame AA analysis of the Mg^{2+} concentration. The dialysis membrane, with 18.4 mg of cell wall, was suspended in 1.5 mL of H_2O and transferred to a jar containing 50 mL of H_2O. The sample was mixed for 48 hours at 4°C, allowing the bound : free metal ions to reach equilibrium. A 5 mL aliquot was removed for flame AA analysis. BPEI was then placed in the solution to analyze the effect of BPEI on the bound : free metal ion equilibrium. One-half mL of a 10.044 g/L BPEI solution was added to the jar, allowed to equilibrate for 48 hours, and a 5 mL aliquot was removed for Mg^{2+} ion analysis.

Displacement of Metal Ions on Whole Cells by BPEI

A known mass (158.4 mg) of wet cells were suspended in 1.5 mL of 20 ppm Mg^{2+} solution (adjusted to pH 7.25 NaOH) and placed in a 1000 MWCO

dialysis membrane, which was then placed in a jar of 23.5 mL of H_2O (0.001 M HEPES buffer, pH 7.25) and allowed to equilibrate for 48 hours. After 48 hours, a 5mL aliquot of solution was removed for the Mg^{2+} concentration was analyzed with flame AA. Five mL of 0.8 g/L BPEI was then added to the solution to create a final concentration of 160 µg/mL BPEI. The solution of whole cells and 160 µg/mL BPEI was allowed to equilibrate for 48 hours and an aliquot of 5 mL was removed for flame AA analysis.

Results

Effect on Growth Rate of *B. subtilis* by BPEI

Displacement of metals should affect cell growth. The concentration dependence of BPEI on the growth of *B. subtlis* 1A578 is listed in Table 5.1. At a concentration of 25 µg/mL or above, there is a delay in the onset of observed growth. A more pronounced increase in the delay of visible growth is observed with increasing amounts of BPEI. A lack of metal ions in the cell wall may be responsible for this effect. Mg^{2+} ions play a role in the virulence (22), cell division(23), and cell adhesion properties (24). Ca^{2+} has been reported to catalyze sortase enzymes that anchor virulence factors to the cell wall (25).

Table 1. Growth of *B. subtilis* 1A578 with Branched Polyethyleneimine									
[BPEI] ug/ml	**1 hours**	**2 hours**	**3 hours**	**4 hours**	**5 hours**	**6 hours**	**7 hours**	**8 hours**	**23 hours**
0	-	+	+	+	+	+	+	+	+
5	-	+	+	+	+	+	+	+	+
10	-	+	+	+	+	+	+	+	+
25	-	-	+	+	+	+	+	+	+
50	-	-	+	+	+	+	+	+	+
75	-	-	+	+	+	+	+	+	+
100	-	-	-	+	+	+	+	+	+
125	-	-	-	-	-	+	+	+	+
150	-	-	-	-	-	-	-	-	+
175	-	-	-	-	-	-	-	-	+
200	-	-	-	-	-	-	-	-	-

Table 5.1. The growth of *B. subtilis* is delayed in the presence of ≥ 25 µg/mL BPEI. This effect is enhanced as the concentrations increased. A "+" signifies the appearance of growth based on the turbidity of the culture. This positive sign of growth is approximately equal to an OD_{600} of 0.15 or greater.

When *B. subtilis* is grown in the presence BPEI (125 µg/mL, 0.282 mM), the observed growth is restored when additional Mg^{2+} or Ca^{2+} ions are present. This effect is shown in Table 5.2. The delay in growth nearly disappears when 10 mM Mg^{2+} ions or 5 mM Mg^{2+} + 5 mM Ca^{2+} are supplemented in the growth media. The ability of BPEI to delay cell growth may occur by blocking sites for metal binding. Yet, cell growth is dependent on the quantity of metal ions in the system and metal binding is governed by equilibrium. An increased concentration of metal ions will shift the equilibrium to a higher amount of metal ions bound to the cell wall. Thus, cell growth can be restored by shifting equilibrium towards the remaining binding sites. The additional bound metal ions are then available for delivery into the cytoplasm where they participate in metabolic processes needed for growth.

Table 2. Growth of *B. subtilis* 1A578 with Branched Polyethyeneimine and Metal Ion Supplementation									
[BPEI]	**[Mg^{2+}]**	**[Ca^{2+}]**	**1 hours**	**2 hours**	**2.5 hours**	**3 hours**	**3.5 hours**	**4.5 hours**	**5 hours**
0	0	0	-	+	+	+	+	+	+
0.282 mM	0	0	-	-	-	-	-	-	+
0.282 mM	0.2 mM	0	-	-	-	-	-	+	+
	1.0 mM	0	-	-	-	-	-	+	+
	10 mM	0	-	-	+	+	+	+	+
0.282 mM	0	0.2 mM	-	-	-	-	-	+	+
	0	1.1 mM	-	-	-	-	+	+	+
0.282 mM	0.46 mM	0.54 mM	-	-	-	-	-	+	+
	4.9 mM	5.2 mM	-	-	+	+	+	+	+

Table 5.2. Metal ion supplementation causes lag phase to appear sooner depending on its concentration. The molarity of BPEI was estimated based on 125 µg/mL. The appearance of growth is denoted by "+" and is equivalent to an OD_{600} of 0.15 or greater.

BPEI Displaces Metal Ions on Whole Cells

If the mode of action is inhibition of metal binding, then BPEI should be able to occupy the metal binding sites and displace the metal ions. To demonstrate this mechanism, we used the data in Table 1 to select a concentration of BPEI (160 µg/mL) expected to displace a significant amount of metal ions. Samples for analysis are taken from the solution outside of the dialysis bag, but this larger volume also causes a dilution in the metal ion concentration. *B. subtilis* cells bind various metal ions, predominately Ca^{2+} and Mg^{2+}. To increase our ability to measure Mg^{2+} ions, the whole cells were isolated and transferred to a 20 ppm Mg^{2+} solution (pH = 7.25) to displace Ca^{2+} and maximize Mg^{2+} content. We are also aware that sample drying can alter the fraction of metals bound to the bacterial cells. Water molecules participate

in Mg^{2+} coordination and complete drying would give erroneous results by shifting the equilibrium towards binding. The whole cells were pelleted, extra water decanted, and the wet cell mass measured. After transfer to a dialysis membrane, but before BPEI addition, Mg^{2+} was mixed with the whole cells and 10.1 µmol were bound to 158.4 mg of wet cells. This equates to 0.0638 µmol Mg^{2+} per milligram of wet whole cells. Subsequent addition of BPEI (final concentration of 160 µg/mL) to the same sample caused a partial release of sorbed Mg^{2+} ions. After 48 hours, the amount of Mg^{2+} ions in solution increased by 4.3 µmol of Mg^{2+} with 5.81 µmol of Mg^{2+} remaining bound to the cells. Likewise, 4.87 µmol of BPEI was bound to the sample and 4.17 µmol of BPEI remained in solution. Thus, approximately 45% (0.0271 µmol Mg^{2+} per milligram of wet cells) of the Mg^{2+} originally sorbed metal ions were released into the solution. Surprisingly, there was not a complete displacement of Mg^{2+} by BPEI binding and there was BPEI that remained in solution. Equilibrium between the binding of BPEI and Mg^{2+} to whole cells is achieved after 48 hours. The competition between the binding of BPEI and Mg^{2+} to the whole cells affects cell growth as shown in Table 1. The competition also presents the opportunity to improve antimicrobial effectiveness with chemical modification of BPEI to promote polymer binding and increase Mg^{2+} release.

BPEI Binds to the Cell Wall

Using membrane dialysis, we show that BPEI causes metal ion displacement by binding to the cell wall. The large anionic charge of the cell wall attracts cationic compounds such as BPEI. This Coulombic interaction is

non-specific and there exists a competition between metal ions and cationic polyethyleneimine molecules. Table 5.3a show the amount of BPEI bound to each cell wall sample when 15 µg/mL are added to the system. At a concentration of 15 µg/mL (0.001M HEPES, pH 7.25), approximately 78% of the BPEI binds to peptidoglycan when compared to peptidoglycan and WTA within the cell wall fragments of *B. subtilis* 1A578. This suggests that BPEI interacts with both peptidoglycan and teichoic acid.

BPEI Inhibits Metal Binding

After cell walls were soaked in 50mL of 100 µg/mL BPEI solution, a complete inhibition of Mg^{2+} binding was observed within a metal ion concentration range of 0 to 0.125 mM. The concentration of BPEI in the sample solution was 0.23 mM when using the approximate mass average molecular mass (442.5 g/mol) from the mass spectrum. Flame AA data indicated no metal binding to BPEI treated samples. This is likely caused by BPEI binding to the cell wall sample to neutralize the anionic sites, and having a higher affinity for the cell wall than Mg^{2+} ions. Subsequently, the concentration of BPEI was decreased (15 µg/mL) to allow for some metal absorption and competition with BPEI. When the above procedure was repeated with 50 mL of 15 µg/mL BPEI at pH 7.25, we observe that a partial number of binding sites are occupied by BPEI (Table 5.3a). The binding affinity of Mg^{2+} drops by a factor of 4 whereas the binding capacity of Mg^{2+} is approximately 52% of that observed without BPEI addition (Table 5.3b).

Table 3a. BPEI Binding to *B. subtilis* Cell Wall (15 µg/mL BPEI, 4°C, pH 7.25)				
Sample	**mg cell wall**	**µg/mL BPEI in solution**	**mg BPEI absorbed**	**µmol BPEI / mg cell wall**
1A578	15.5	7.206	0.39	0.057
1A578	18	4.762	0.512	0.064
Peptidoglycan	15.3	8.775	0.311	0.045
EB1451	19.4	6.674	0.416	0.048

Table 5.3a. BPEI binding to the cell wall after soaking in 50 mL of 15 µg/mL BPEI for two days in Milli-Q H_2O at a buffered pH of 7.25 with 0.001 M HEPES (T=4ºC). The pH increased to 9.05 upon addition of the weakly basic BPEI. 1A578 consists of cell wall samples containing peptidoglycan and WTA.

Table 3b. Mg^{2+} Binding Properties (15 µg/mL BPEI, 4°C, pH 7.25)				
Sample	**mg cell wall**	**K_{assoc} (M^{-1})**	**µmol Mg^{2+} /mg**	**BPEI conc.**
1A578	14.0 ± 3.5	(1000 ± 200) x 10^3	0.77 ± 0.07	0
1A578	15.5	282 x 10^3	0.39	15 µg/mL
1A578	18	212 x 10^3	0.42	15 µg/mL
Peptidoglycan	15.3	198 x 10^3	0.18	15 µg/mL
EB1451	20.2 ± 5.2	(1000 ± 200) x 103	0.54 ± 0.06	0
EB1451	19.4	62 x 103	0.22	15 µg/mL

Table 5.3b. Both the binding affinity and binding capacity of Mg^{2+} ions decrease when measurements are taken after addition of 15 µg/mL BPEI (Table 3a). Metal binding data for purified peptidoglycan at pH 7.25 was not performed.

BPEI Displaces Metal Ions on the Cell Wall

After equilibrating in 50 mL of 10 ppm Mg^{2+} solution for 48 hours at a pH of 7.25, 0.75 µmol Mg^{2+} per mg of cell wall was sorbed to the *B. subtilis* 1A578 fragments. This was determined based on a decrease in the Mg^{2+} solution concentration to 3.35 ppm. Transfer of the dialysis membrane to 50 mL of Milli-Q H_2O causes equilibrium to shift. The 1.5 mL of 3.35 ppm Mg^{2+} solution inside the dialysis membrane diffuses into the total 51.5 mL of Milli-Q H_2O creating a free ion concentration of 0.098 ppm Mg^{2+}. However, a free Mg^{2+} concentration

of 0.57 ppm is observed after 5 mL is removed and undergoes flame AA analysis. This increased concentration is due to 0.05 µmol Mg^{2+} per mg of cell wall sample desorbing into solution. The sample now has 0.70 µmol Mg^{2+} per mg of cell wall in 46.5 mL of liquid and we used this sample to evaluate the effect of BPEI on metal binding. To ensure that a significant fraction of metal ions would be displaced at the cell wall, a concentration of BPEI was chosen that had a large effect on growth. Addition of 0.5 mL of BPEI (10044 µg/mL) resulted in a final system concentration of 107 µg/mL of BPEI in 47 mL. After equilibrium between the inside and outside of the dialysis membrane is established, it was determined that 0.69 µmol Mg^{2+} per mg of cell wall was desorbed as a result of BPEI binding to the cell wall. Displacing 98.6% of the Mg^{2+} ions is higher than that seen with whole cells. This results from a reduced competition for metal ion binding sites because the solution lacks additional unbound metal ions. As described above, BPEI was added to whole cells with a higher concentration of Mg^{2+} remaining in solution. In this case, the dialysis bag was placed in Milli-Q H_2O in which a minimal amount (0.098 ppm) of Mg^{2+} was able to diffuse into the solution. Additional analysis of the solution also revealed that 0.26 mg BPEI per mg of cell wall was bound to the fragments. Thus, BPEI preferentially binds to the cell wall displacing essentially metal ions such as Mg^{2+}, in a ratio of 1:1.17 BPEI:Mg^{2+}.

Discussion

This data shows that the inhibition of metal binding is one mechanism that leads to the antimicrobial properties of BPEI. This mechanism is dependent

on the concentration of metal ions in solution that compete for binding sites in equilibrium. The relatively high levels of BPEI needed to stop bacterial growth make it unfeasible to use as a standalone antibiotic. However, synergetic effects have been reported with high molecular weight linear PEI and antibiotics (26). The observation of growth when additional metal ions are added leads us to believe that disruption of the cytoplasmic membrane is not occurring. The slower growth in the presence of BPEI might also be due to a decreased apparent binding affinity of Mg^{2+} and other metals with the cell wall due to partial charge neutralization. From previous measurements without BPEI, cell wall fragments of *B. subtilis* 1A578 had a binding affinity of $(1.0 \pm 0.2) \times 10^6$ M^{-1} and a binding capacity of 0.77 ± 0.07 µmol/mg for Mg^{2+} at pH 7.25 (27). The binding affinity is decreased to 0.282×10^6 M^{-1} and the binding capacity is decreased to 0.39 µmol/mg in the presence of 15 µg/mL BPEI, Electrostatic interactions are responsible for BPEI binding to the cell wall. The electrostatic potential of the cell wall is generated by anionic groups formed after the de-protonation of functional groups in both the peptidoglycan and teichoic acid components. The charge density of BPEI at physiological conditions also enables interactions with phosphates of the lipid membrane, perhaps contributing to the molecule's antimicrobial characteristic. The relationship between cell charge polarity and cell death using a cationic antimicrobial compound have been reported(28).

Charge density is used also to predict the effectiveness of cationic antimicrobials (29,30). Polycationic polymers have been reported to have a

significantly higher antimicrobial activity than their monomeric and single charged counterparts (29). It is possible to optimize cationic antimicrobial compounds by adjusting the charge properties and hydrophobicity of specific molecules to enhance its bactericidal effect while minimizing their hemolytic activity (30). LB media has been measured to have pH around 6.97. The pH changes to a value of around 8.56 after an overnight growth of *B. subtilis*. This increase in pH can be due to the production of alkaline proteases (31). An increase in pH would decrease the fraction of protonated amine groups with BPEI. The resulting decrease in charge density should cause a decrease in the antimicrobial characteristics of BPEI. However, due to the polycationic nature of BPEI, the electrostatic properties are not governed by a single pK_a value. One study has reported that 60% of amine groups are protonated at pH 5.65 (32)and 30% are protonated at pH 7.25 (32). Another study reported a pH of 5.65 enables 40% of the amine groups to be protonated (33) while approximately 15-20% are protonated at pH 7.25 (33). In contrast, another study denoted that pK_a values decrease with increasing molecular weight and that low molecular weight PEI has pK_a values around 9.94 (34,35). Regardless, only a fraction of the amine groups are protonated at physiological pH. An increase in the pH increases the negative charge character of the cell wall, but decreases the positive charge character of BPEI. This is consistent with results from Campanha *et al(28).* that described the change of the cell wall from negative to positive as correlating with cell death. A charge density threshold with respect to preventing biofilm deposition and optimizing the efficacy of cationic

antimicrobials grafted on surfaces was reported (6). Inflammatory response to pathogenic microorganisms has been reported to be associated with a decrease in extracellular pH (36). This decrease in extracellular pH should have a twofold advantage in both decreasing the anionic character of the infectious bacteria and increasing the charge character of BPEI in that region.

The antimicrobial efficacy of BPEI decreases with an increasing concentration of metal ions in the system. In a clinical setting, the ability to change the free metal ion concentration is limited. Blood plasma magnesium and calcium levels have been reported to be around 0.95 ± 0.17 mM and 2.51 ± 0.28 mM (37). The LB growth media was found to have a Mg^{2+} concentration of 0.29 mM using flame AA and a standard addition method. The addition of metal ions, especially Ca^{2+} and Mg^{2+} ions has also been shown to decrease the efficacy of two cationic antimicrobial peptides investigated against both *B. subtilis* and *E. coli* (38). This decrease in efficacy was reported to be more pronounced as the metal ion concentration increased (38). Similarly, a salt sensitive effect was shown on the BPEI to remove metal ions from the cell wall through binding events. In our data, the ability of BPEI to displace metal ions decreased in the presence of a higher metal ion concentration.

Conversely, magnesium deprivation creates a bacteriostatic effect, facilitating easier bacterial killing by immune response and/or antibiotics. Even though bactericidal antibiotics perform better in a laboratory setting, there is little clinical relevance between bacteriostatic and bactericidal antibiotics (37). Clinical tests have shown that bactericidal antimicrobials are not superior over

bacteriostatic antimicrobials when treated the majority of Gram-positive infections involving in individuals with uncompromised immune systems (37). Gram-positive bacteria subjected to magnesium deprived growth media remain viable but growth does not take place until the addition of Mg^{2+} (39). Likewise, magnesium ion concentration in growth media has been reported to influence the growth rate of *bacilli* bacteria (23). An increase in magnesium ion concentration within magnesium depleted growth media caused an increase in growth (23). The connection between magnesium ion concentration and growth rate is also observed in our experimental results. Instead of limiting cellular access to metal by lowering the total magnesium concentration, cellular access to magnesium ions and other essential metal ions to the cell wall is limited by the presence of BPEI. This mechanism causes a decreased binding affinity and capacity that result from partial charge neutralization and binding sites occupied by BPEI.

Conclusion

In these experiments, we measured the effect of low molecular weight branched polyethyleneimine on metal binding to cell wall. We found that BPEI can displace metals bound to cells and inhibit metal binding to whole cell bacteria and the bacterial cell wall. The addition of BPEI decreases the binding affinity and capacity of Mg^{2+} to the cell wall, thus decreasing the available metal ions to be transported into the cell. The deprivation of essential metal ions such as Mg^{2+} can be a factor in weakening the cell and causing a slower growth rate. A bactericidal mechanism was not observed and the addition of metal ions

restored growth. As a result, the effect of bacteriostatic effect caused by BPEI is dependent on the concentration of metal ions in solution.

BPEI has been shown to have a low cytotoxicity (40,41). Branched and linear PEI's cytotoxicity is dependent on dose, time, molecular weight of polymer, and cell line (14). HeLa cells and Vero cells have been utilized to examine cytotoxicity (14). BPEI was shown to have an IC_{50} toxicity level above 2.4 g/L. In order to be safe in a clinical setting there must be a significant difference between concentrations required to kill bacterial cells and concentrations that are cytotoxic towards mammalian cells. Our experiments were performed at lower concentrations of 0.16 g/L BPEI. A study has shown synergy between clinically resistant Gram-negative bacteria and different classes of antibiotics (26). A potential opportunity to decrease the concentration of BPEI further exists if a similar synergy with antibiotics can be observed with Gram-positive organisms.

Chapter 6: Antimicrobial Synergy of BPEI with Antibiotics and Morphological Changes Associated with BPEI Exposure

Introduction and Background

Branched polyethyleneimine has been reported to possess an antimicrobial effect. In order to be effective at killing bacteria and safe in a clinical setting, the cytotoxicity towards mammalian cells must be significantly lower than the range at which it is effective at killing bacterial cells. When used alone, concentrations of 180 µg/mL or greater were needed to inhibit cell growth after an overnight inoculation. However, the possibility exists to lower concentrations of PEI (branched or linear) when used in conjunction with traditional antibiotics to produce a synergetic inhibition of growth effect.

LMW (low molecular weight) BPEI has been shown to have a low cytotoxicity (1,2). Insight into the cytotoxicity of BPEI towards mammalian cells were provided by one study that utilized HeLa cells and Vero cells (3). These two cell lines were chosen to determine if cytotoxicity was dependent on the type of mammalian cells and a colorimetric MTT toxicity assay was used to determine cytotoxicity. LMW-BPEI was shown to have an IC_{50} toxicity level above 2400 µg/mL (3). However, in addition to concentration, it was also reported that the cytotoxicity of PEI is dependent on whether it is linear or branched, as well as the exposure time, molecular weight of PEI polymer, and cell line (3).

Synergetic Effect of PEI on Gram-Negative Bacteria

It has been reported that high molecular weight (10kDa) PEI increases the efficacy of some antibiotics to a clinical resistant strain of *P. aeruginosa* (4). Synergy between antiobiotics and PEI refers to the ability to reduce minimum inhibitory concentration (MIC) values of antibiotics in the presence of PEI. *P. aeruginosa* infections are difficult to overcome due to its resistance to antibiotics which can be caused by reduced permeability of the outer membrane (5,6). Chloramphenicol, ampicillin, novobiocin, ceftazidime, ticarcillin, carbenicillin, piperacillin, cefotaxime, rifampin, or norflaxacin were reported to have reduced MICs by 1.5 to 56 fold when combined with 250 nM PEI, which by itself was neither bacteriostatic or bactericidal (4). The efficacy of other antibiotics such as erythromycin, ciprofloxacin, and ofloxacin were not affected by PEI, while the efficacy of aminoglycosides, polymyxins, and vancomycins decreased (4). Antibiotics have a variety of killing mechanisms as seen in Figure 6.1. The synergetic effects appear to differ even within the same family of antibiotics. For example, ofloxacin, ciprofloxacin, and norflaxacin are all fluoroquinolones, yet only norflaxacin was reported to have a synergetic effect with PEI. However, the lack of synergetic behavior by some of the antibiotics examined is not explained. It is possible that cationic antibiotics such as aminoglycosides and polymyxins compete for binding sites with PEI(7). The binding of Mg^{2+} to the bacterial cell reduces vancomycin adsorption (8). Increased cell wall permeability is believed to be the cause of the synergetic effect with some antibiotics due to PEI binding.

Mechanisms of action	Antibiotic families
Inhibition of cell wall synthesis	Penicillins; cephalosporins; carbapenems; daptomycin; monobactams; glycopeptides
Inhibition of protein synthesis	Tetracyclines; aminoglycosides; oxazolidonones; streptogramins; ketolides; macrolides; lincosamides; amphenicols
Inhibition of DNA synthesis	Fluoroquinolones
Competitive inhibition of folic acid synthesis	Sulfonamides; trimethroprim
Inhibition of RNA synthesis	Rifampin
Other	Metronidazole

Table 6.1. Mechanism of action of different antibiotic families. Adapted from Levy et al. (9)

Polyethyleneimine has been reported to be an effective permeabilizer of Gram-negative bacteria (10). EDTA is also an effective permeabilizer of Gram-negative bacteria. The permeabilizing effect of EDTA is based on the chelation of divalent metal ions from the outer membrane of Gram-negative bacteria. Metal ions such as Mg^{2+} and Ca^{2+} provide structural integrity of the outer membrane (11). The basis of the structural integrity that metal ions provide lies in the lipopolysaccharides that are linked electrostatically by divalent metal ions. The cell wall of Gram-negative bacteria is less permeable than the cell wall of Gram-positive bacteria (12). The ability to increase permeabilization of Gram-positive bacteria is more difficult due to its single cytoplasmic membrane and thick layer of peptidoglycan when compared to Gram-negative bacteria. Peptidoglycan provides minimal effect towards permeability. However, it does provide the cell additional protection against osmotic stress.

BPEI's Mode of Action toward Gram-Positive Bacteria

The specific mode of action that polycationic antimicrobials exert on Gram-positive bacteria is not fully known. The biocidal mechanism of cationic polymers may involve a disturbance of the cell membrane which also leads to an increased permeability towards foreign molecules (13). Similarly, a mechanism of polycationic antimicrobials involving penetration through the cell wall to disrupt the cytoplasmic membrane has been proposed (14,15). However, it has also been reported that cytoplasmic membrane permeation did not appear to be a mechanism of action that is based on an incomplete depolarization of the membrane (16). An ion exchange based killing mechanism based on electrostatic charge density has also been proposed (17). In earlier experiments (Chapter 5), it was demonstrated that the inhibition of metal ion binding contributes to its antimicrobial effect. Our data supports a model that involves an ion exchange based killing mechanism with BPEI.

The reversal of antibiotic resistance has also been reported with combinations of permeabilizers such as EDTA and antibiotics (18,19). Cationic quaternary ammonium compounds were found to be more effect against Gram-negative bacteria in the presence of 100 µg/mL EDTA (20). Additionally, antibiotic MIC values have been examined for β-lactam resistant Gram-positive bacteria with variable concentrations of EDTA (21). Decreased MIC values were obtained with β-lactam antibiotics when in the presence of EDTA at a concentration 100 times less than its MIC. However, no antibiotic resistance reversal studies have been performed with Gram-positive bacteria with

combinations of antibiotics and branched polyethyleneimine. Here, we will present data regarding the synergetic effect of low molecular weight BPEI and resistant strains of the Gram-positive bacteria, *B. subtilis.* This chapter will primarily focus on the effect of varying concentrations of BPEI with a constant concentration of antibiotic has with *B. subtilis*. The motive in choosing resistant strains was to observe if antibiotic resistance could be overcome with sub-lethal concentrations of BPEI. As multi-drug resistance continues to increase while the discovery new antibiotics decrease, it becomes important to investigate methods that enable the use of current antibiotics without regards to a bacteria's particular resistance.

Experimental

Investigation of BPEI and Antibiotics on Growth Rate

Concentrations of low molecular weight branched polyethyleneimine were placed in LB growth media and bacterial growth was measured by examining the absorbance value at 600nm. The absorbance value represents an arbitrary number that corresponds to the density of cells in the sample. Although specific cell densities cannot be extracted without correlating known cells densities to OD_{600} values, this measurement gives information of the rate of growth and the point at which cell replication begins. The absorbance value enables the creation of growth curves where the value is graphed against time and the growth phases can be determined. The growth behavior was compared with a control, with different concentrations of BPEI, and with varying concentration of BPEI combined with antibiotics. *B. subtilis* 1A578 is resistant to

chloramphenicol at a higher concentration than the parent strain. *B. subtilis* 1A578 has a MIC of approximately 20 µg/mL, while the parent strain *B. subtilis* 168 has a chloramphenicol MIC of 2 µg/mL (22). The existence of synergy between BPEI and resistant antibiotics was examined by combining a sub-MIC concentration of chloramphenicol (10 µg/mL) with gradually increasing concentrations of BPEI (0.12-0.18 g/L). The results of this combination was compared with growth measurement of *B. subtilis* grown in media with the addition of BPEI alone. A teichoic acid deficient strain of *B. subtilis* (EB1451) with an increased level of erythromycin resistance was also investigated. Unfortunately, because the MIC of *B. subtilis* EB1451 was not reported, an erythromycin concentration of 10 µg/ml was used in our experiments.

Morphology Examination with Phase Contrast Microscopy

Phase contrast microscopy was employed to observe any morphological changes in the bacterium in the presence of BPEI. Growth took place in the same conditions that were used in the formation of growth curves. LB growth media was used and cultures were placed in an incubator/shaker at 200 rpm and 37°C. Microscopy images were taken under a 1000x magnification after 6 µL of growth media was taken from a flask in the incubator/shaker and placed on a glass slide with a cover slip.

Morphology Examination with Scanning Electron Microscopy

A 1 mL aliquot *B. subtilis* cells were harvested at an OD_{600} = 0.216 after 2 hours and 20 minutes. These cells were centrifuged at 5000*g* for 3 minutes and then rinsed with 1 mL of sterile Milli-Q H_2O. The water was then decanted

and the cells were re-suspended in 350 µL of Milli-Q H_2O. A volume of 40 µL of this suspension was then placed on an autoclaved sterile glass cover slip and was allowed to dry for approximately 5 hours in a dish that was placed near a Bunsen burner and loosely covered with aluminum foil to allow for airflow to mitigate the chances of contamination. The *B. subtilis* sample grown with 150 µg/mL of BPEI was harvested at an OD_{600} =0.212 after 7 hours and 30 minutes and was prepared under identical conditions.

Results

In this work we tested for synergetic effects with the use of spectrophotometric optical density measurements to measure the onset of cellular growth and the subsequent rate of growth. Cell morphologies were examined with phase contrast microscopy. Once a distinct change in morphology was observed, a higher magnification was needed to investigate the presence of septa formation and a scale was needed to measure the size. Scanning electronic microscopy was employed to satisfy these requirements.

Synergy with Resistant Bacteria and Antibiotics

Results with and without 10 µg/mL of chloramphenicol are shown in Figures 6.1 and 6.2. There is a noticeable difference between the growth rate with and without chloramphenicol at sub-lethal doses of BPEI. Taking an absorbance value of 0.5 at 600 nm as an arbitrary reference point associated with bacterial density, there is an approximate 70 minute difference (a 47% increase) between *B. subtilis* 1A578 with and without chloramphenicol. A noticeable difference is observed when the same concentration of

chloramphenicol is combined with near MIC levels of BPEI. When concentrations of BPEI near its MIC range are added this effect is intensified. For BPEI at a concentration of 0.12 g/L there is a 100% increase in the time to grow to a reference density corresponding to 0.5 absorbance units for samples with chloramphenicol at the same BPEI concentration. For 0.14 g/L BPEI, there is a 150% time increase for the growth containing chloramphenicol. A complete inhibition of growth is seen at a concentration of 0.16 g/L BPEI and 10 µg/mL of chloramphenicol. Growth is still observed with 10 µg/mL of chloramphenicol and 0.18 g/L separately. The combination of these two antimicrobials proves effective in inhibiting growth.

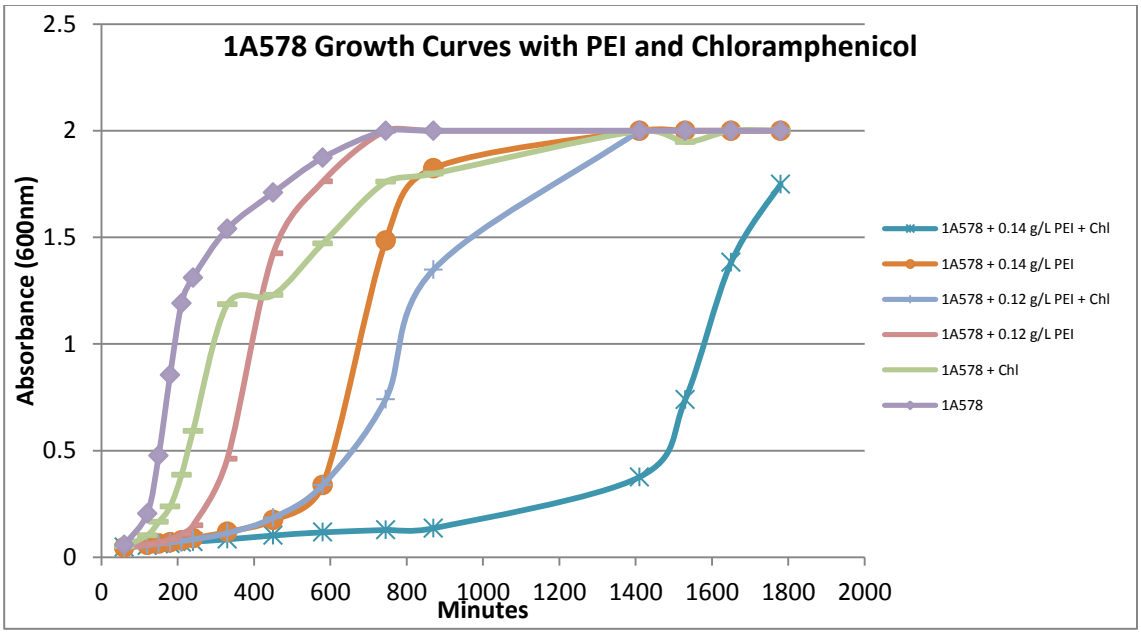


Figure 6.1: Growth curves for *B. subtilis* 1A578 with combinations of 10 µg/mL chloramphenicol with 0.12 and 0.14 g/L BPEI. Note: the signal becomes saturated at an absorbance value of 2.

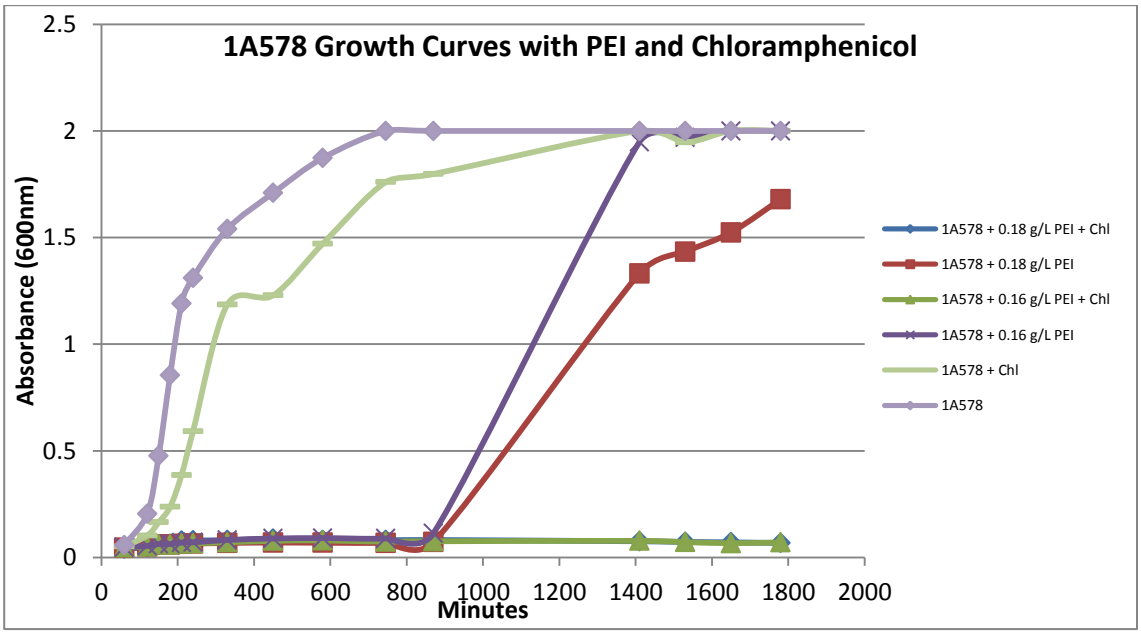


Figure 6.2: Growth curves for *B. subtilis* 1A578 with combinations of 10 ug/mL chloramphenicol with 0.16 and 0.18 g/L BPEI. Note: the signal becomes saturated at an absorbance value of 2.

A synergetic effect is also observed for a WTA deficient mutant that has resistance to erythromycin. The difference in the increased lag time for *B. subtilis* EB1451 with and without 10 µg/mL of erythromycin is small compared to the cumulative effect with different concentrations of BPEI. The individual time increases in lag phase added together is much less than the increase in time in lag phase of experiments containing the same components together as observed in Figure 6.3

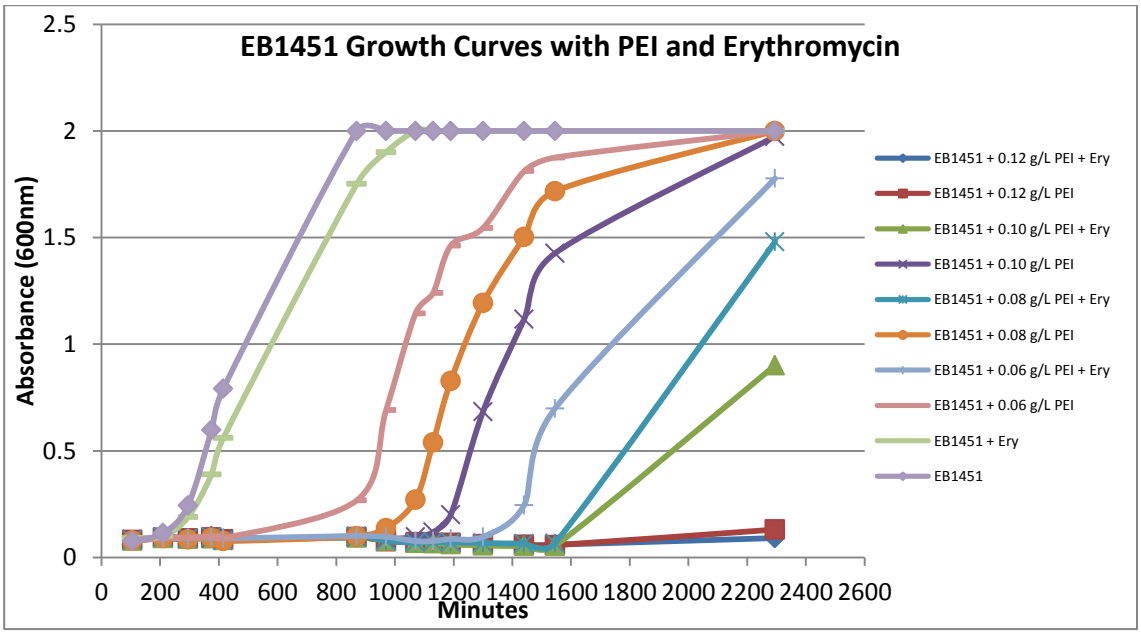


Figure 6.3: Growth curves showing a synergetic effect with combinations of 10 µg/mL erythromycin and varying concentrations of BPEI against an erythromycin resistant strain, WTA deficient mutant of *B. subtilis* (EB1451)

When observing growth for an extending time we see that bacterial death is not occurring. This leads us to believe that BPEI is causing a bacteriostatic affect and that growth can begin 2.5 days later as is seen with 0.21 g/L BPEI and 10 µg/mL of chloramphenicol as seen in Figure 6.4. This is significantly longer than the approximately 3 hours it takes to observe growth entering exponential phase for cultures with only 10 µg/mL of chloramphenicol. Traditionally, MIC (minimum inhibitory concentration) values are defined as the concentration required to inhibit cell growth with a 1% inoculation of an overnight culture (23). MIC values should not be confused to MBC (minimum bactericidal concentration) values that describe cell death and not a bacteriostatic effect that slows or completely stops growth.

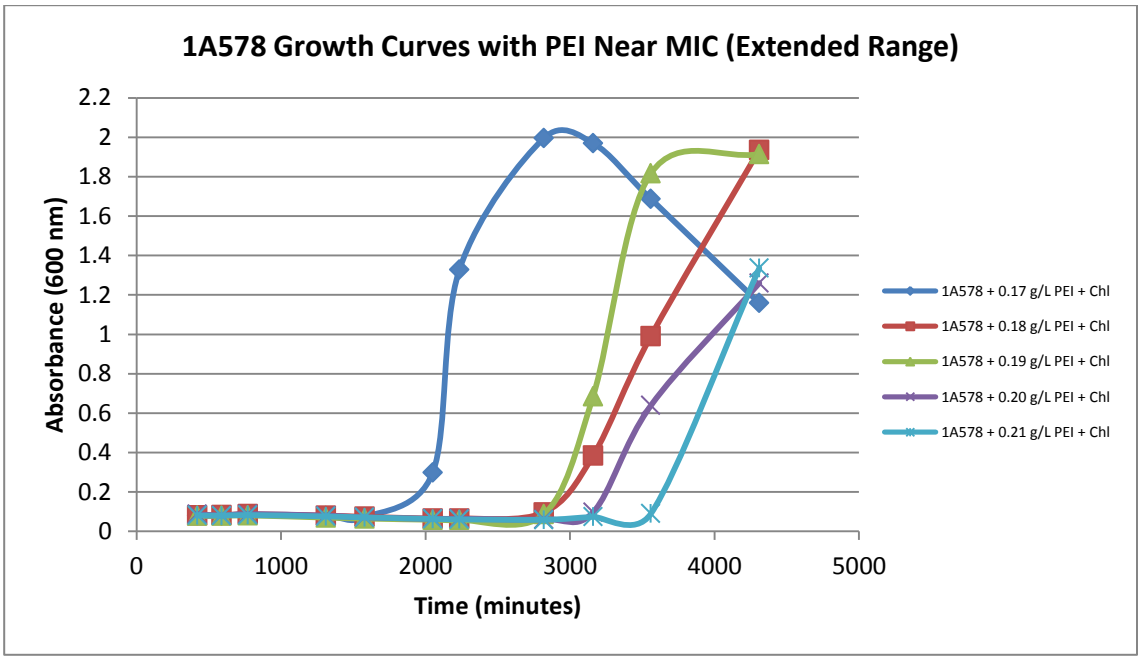


Figure 6.4: Growth of *B. subtilis* 1A578 with BPEI and chloramphenicol (extended time range).

Morphology Changes in the Presence of BPEI

Cell morphologies were examined to investigate if the cells were undergoing any changes during the period of increased lag phase. BPEI has been found to inhibit binding of Mg^{2+} to the cell wall (Chapter 5). Deprivation of essential metal ions has been reported to cause filamentous bacterial morphologies (24). A control set of images were taken with *B. subtilis* 1A578 without exposure to BPEI to observe any morphological changes (Figures 6.5 – 6.10). Growth is still taking place during the extended lag phase in cultures with BPEI, although division is not occurring (Figures 6.11 – 6.16). Increased cell length is also observed with the control culture not containing BPEI (Figures 6.6 - 6.10). This is phenomenon has been reported as the result of a delay between growth and cell division that is common with *B. subtilis* (25). However this becomes increasingly uncommon as growth continues. Eventually, these large

interlinked cells for both samples, the BPEI exposed sample and the control, divide to produce a normal morphology. Changes present in both samples are solely the result of BPEI and chloramphenicol was excluded.

Phase contrast images at 2 hours for the control sample (with no BPEI added) displayed the characteristic rod shape associated with *Bacillus* bacteria as seen in Figure 6.5 below. Distributions of images were taken to be representative of the entire sample and not just an uncommon occurrence. The following images show the morphological changes as a result of elapsed time and growth for both a control set of *B. subtilis* cells and *B. subtlis* cells growth in the presence of 150 µg/mL BPEI. Each phase contrast image is taken under 1000x magnification.

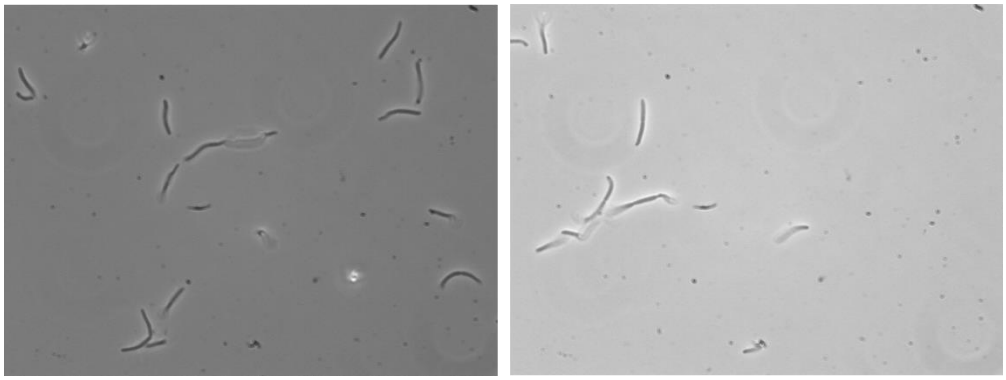


Figure 6.5: Phase contrast images of *B. subtilis* 1A578 (No BPEI, OD_{600} = 0.174)

At 2 hours and 20 minutes and an OD_{600} absorbance value of 0.216 (early exponential phase) the bacteria begin to display long chains of bacteria (Figure 6.6). These chains of cells have been reported to be associated with a delay between growth and cell division is common with *B. subtilis* (25). However, the observance of these long chains of cells is not common and mostly the cells

such as that in the top left of Figure 6.6 are seen in the majority of microscope slides. A similar morphology is observed at 2 hours 30 minutes and an OD of 0.270 (Figure 6.7) where there are elongated cells, but the majority of them are shorter, individual cells. At mid-exponential phase, there are even less elongated cells and there is an even greater majority separated individual cells. This trend continues as the cells continue to reproduce and increase in density.

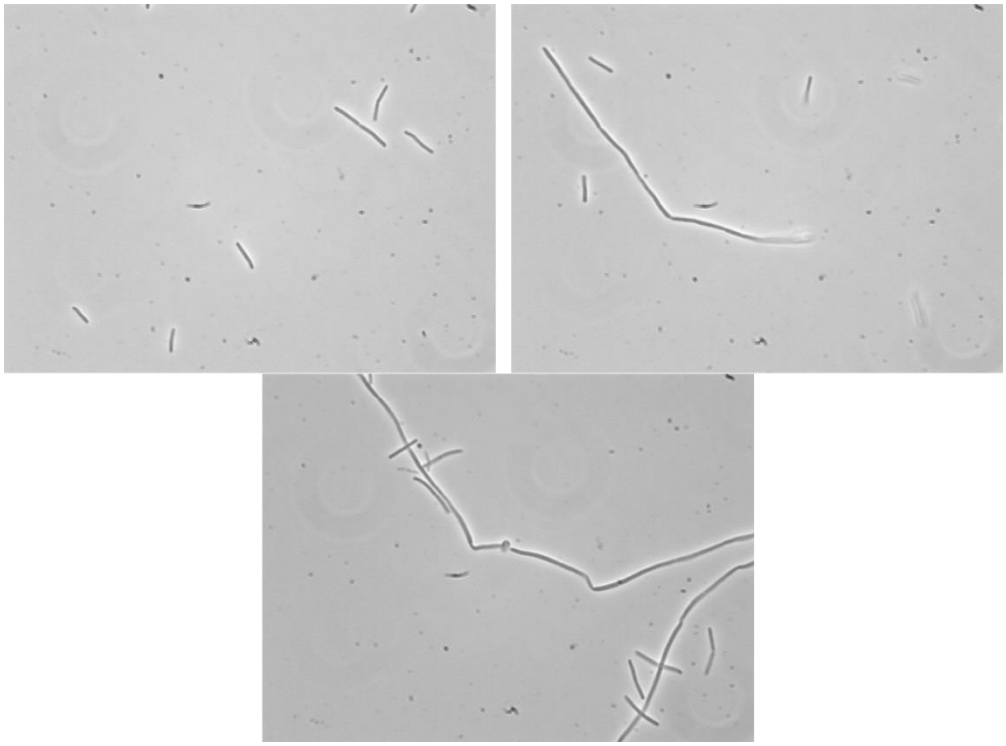


Figure 6.6: Phase contrast images of *B. subtilis* 1A578 (No BPEI, OD_{600} = 0.216)

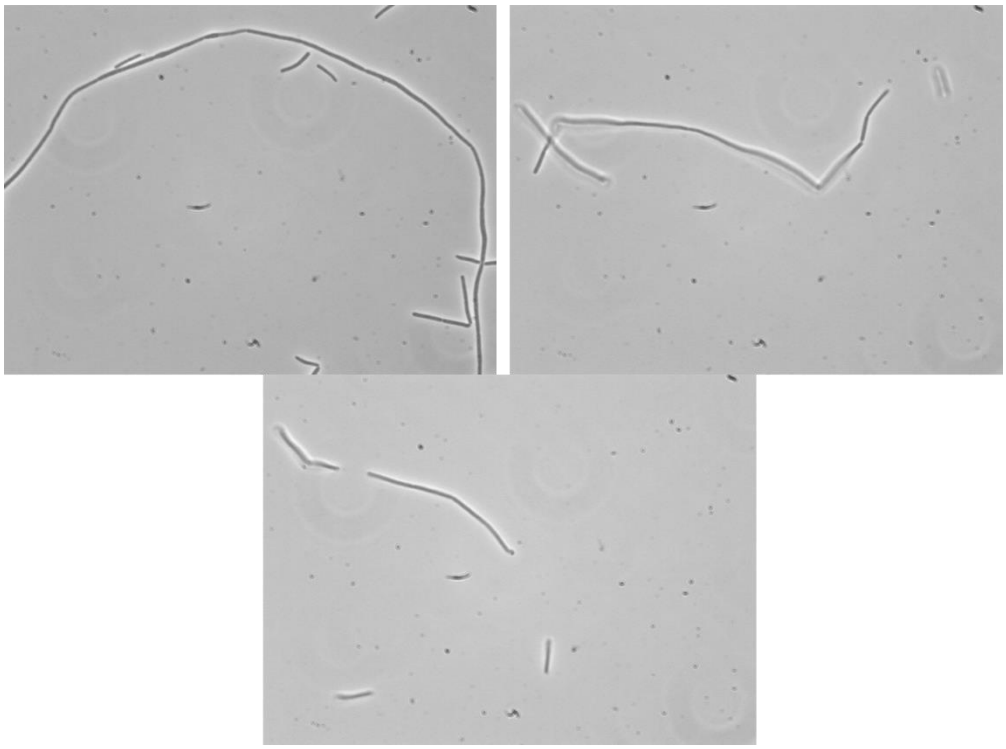


Figure 6.7: Phase contrast images of *B. subtilis* 1A578 (No BPEI, OD_{600} = 0.270)

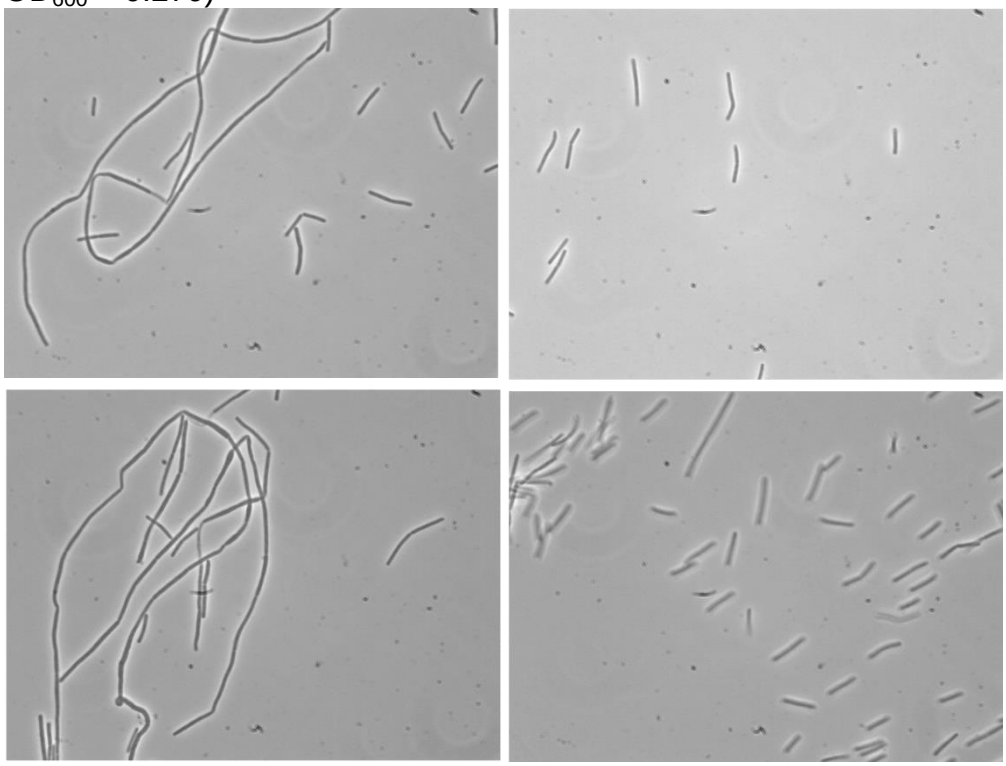


Figure 6.8: Phase contrast images of *B. subtilis* 1A578 (No BPEI, OD_{600} = 0.488)

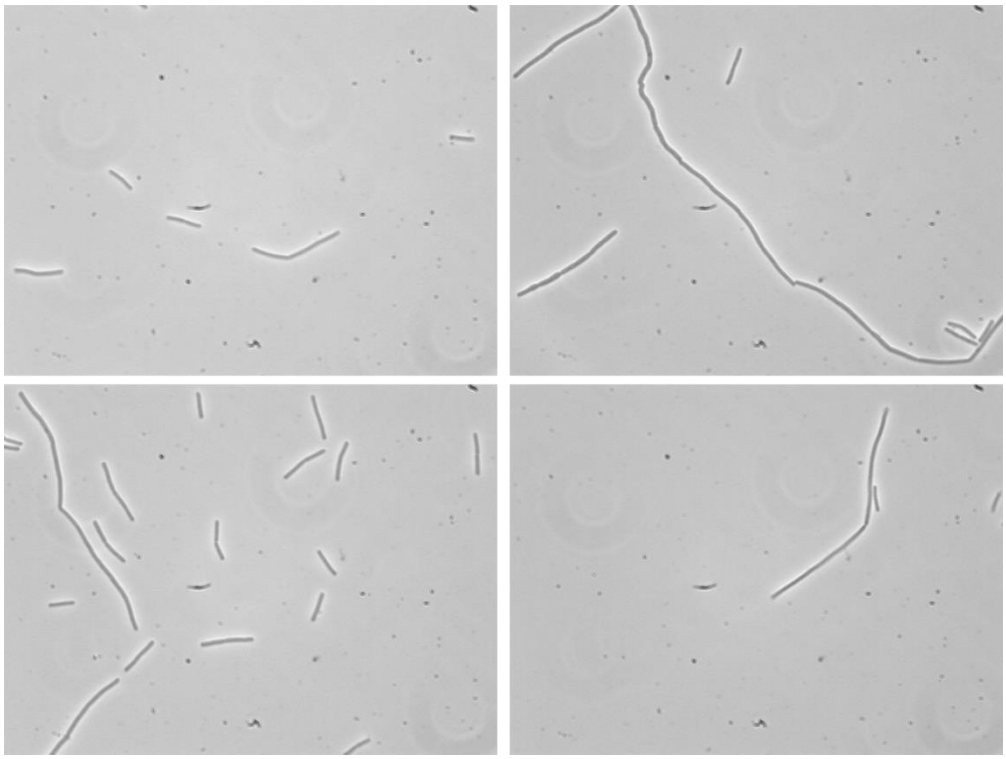


Figure 6.9: Phase contrast images of *B. subtilis* 1A578 (No BPEI, OD_{600} = 0.822)

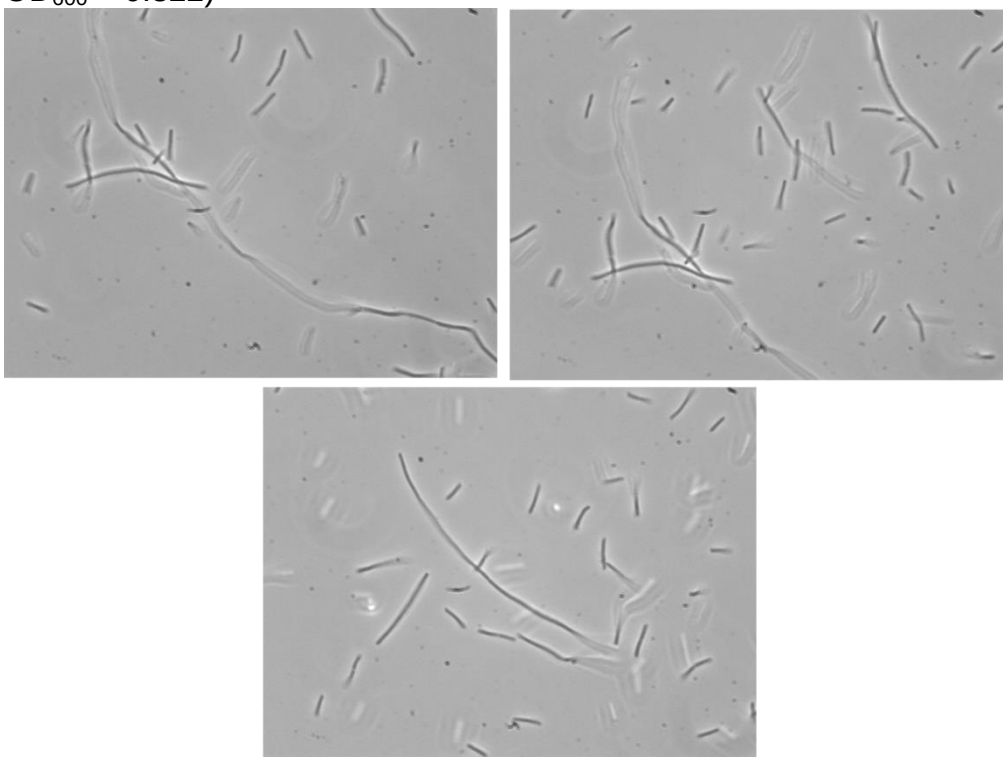


Figure 6.10: Phase contrast images of *B. subtilis* 1A578 (No BPEI, OD_{600} = 1.153)

The addition of BPEI at 150 ug/mL creates cells that have an extended lag phase and exhibit a twisted, random coil morphology. Unlike the control with no BPEI, this twisted and elongated cell morphology predominates. Although at an OD_{600} of 0.091 (Figure 6.11), these cells are difficult to locate due to the shear lack of density.

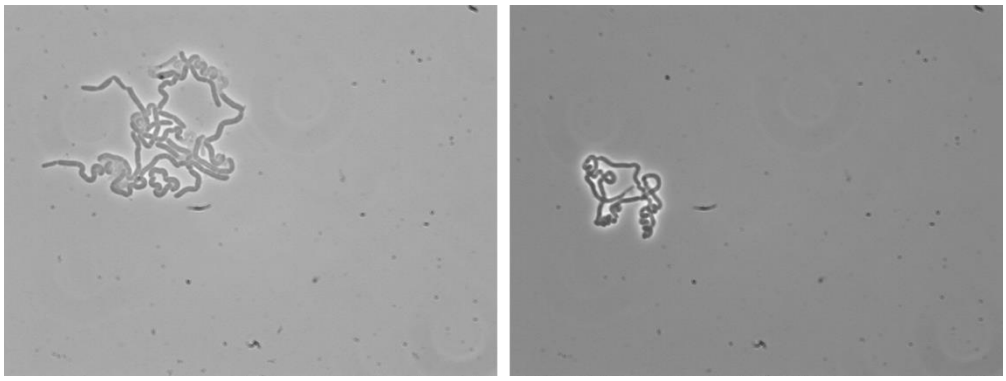


Figure 6.11: Phase contrast images of *B. subtilis* 1A578 (150 µg/mL BPEI, OD_{600} = 0.091)

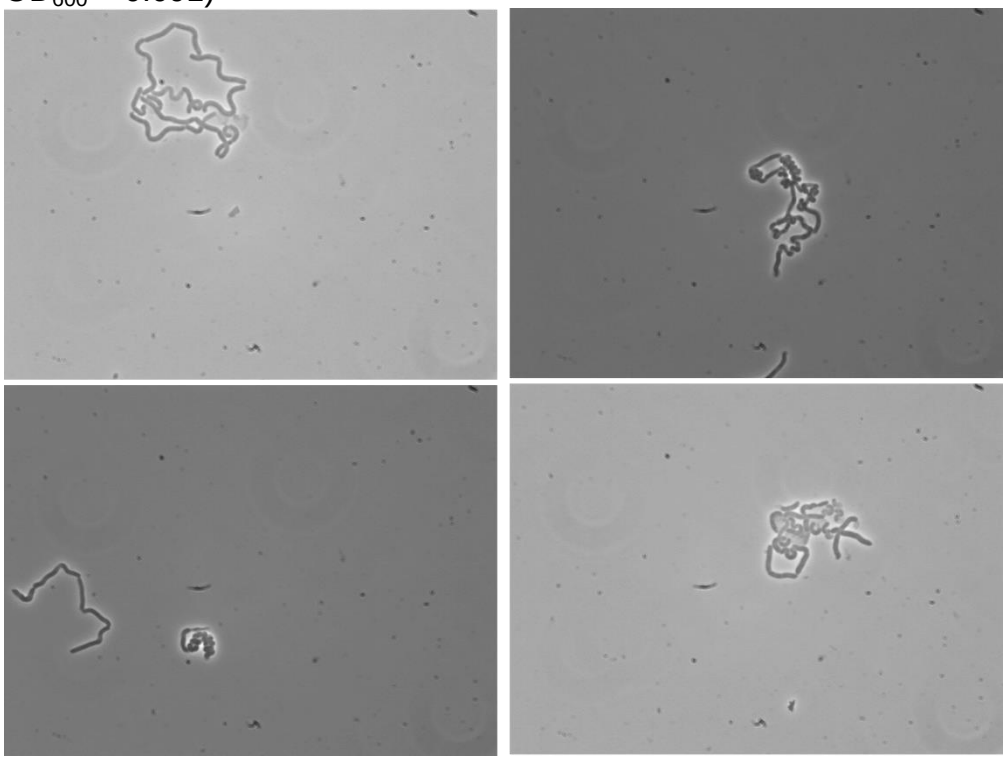


Figure 6.12: Phase contrast images of *B. subtilis* 1A578 (150 µg/mL BPEI, OD_{600} = 0.113)

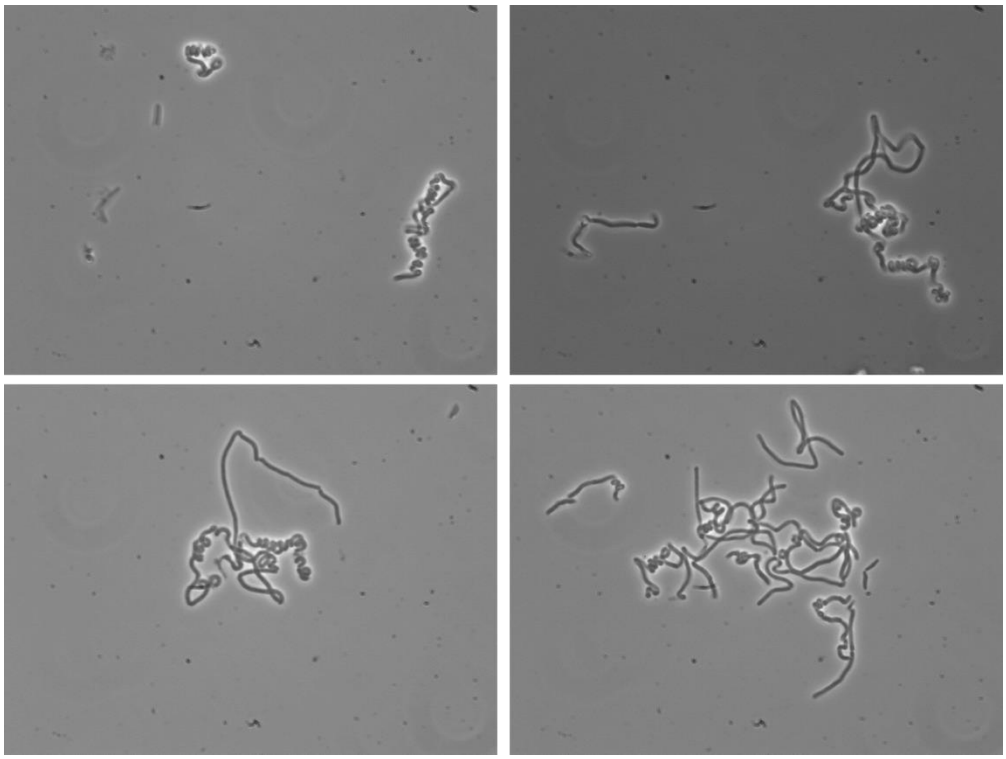


Figure 6.13: Phase contrast images of *B. subtilis* 1A578 (150 µg/mL BPEI, OD_{600} = 0.164)

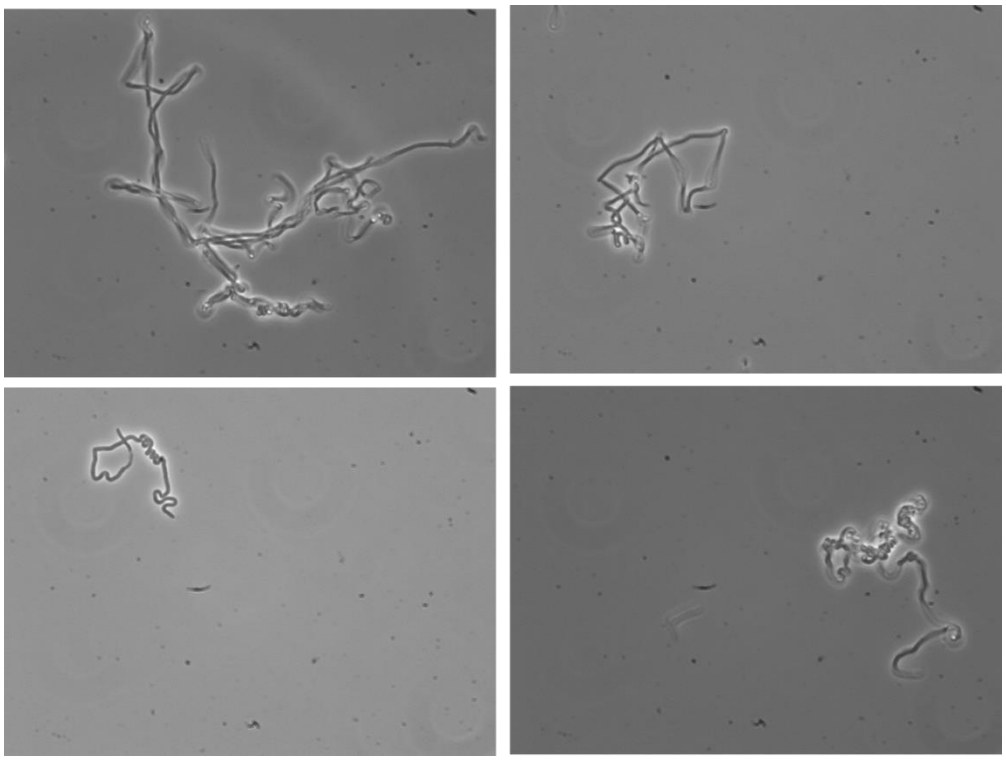


Figure 6.14: Phase contrast images of *B. subtilis* 1A578 (150 µg/mL BPEI, OD_{600} = 0.181)

As cell growth increases, the morphology of the majority of cells begins to diminish. Although septa formation is not clearly visible, the cells do eventually divide. This is supported by phase contrast images taken the following morning (Figure 6.16).

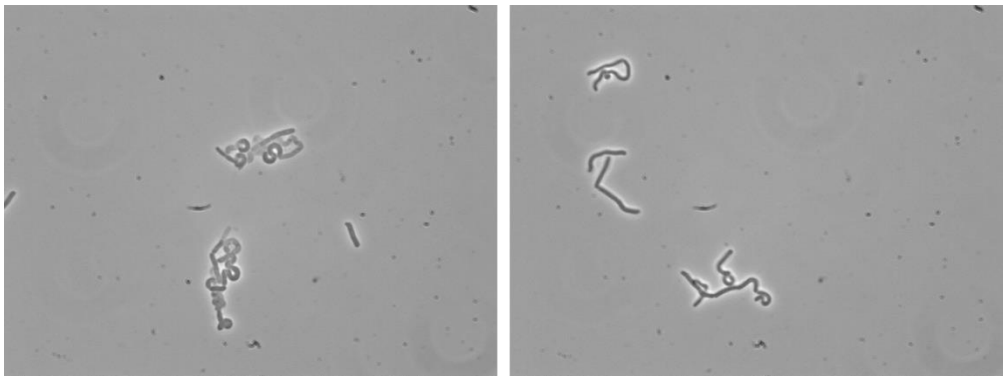


Figure 6.15: Phase contrast images of *B. subtilis* 1A578 (150 µg/mL BPEI, OD_{600} = 0.243)

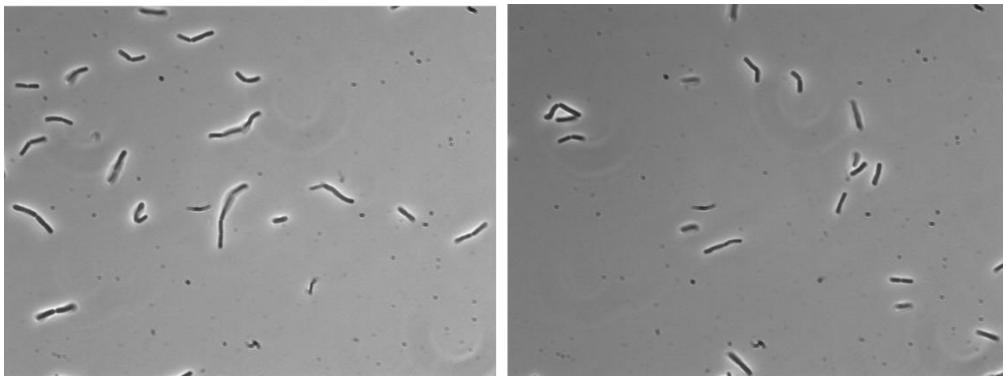


Figure 6.16: Phase contrast images of *B. subtilis* 1A578 (150 µg/mL BPEI, OD_{600} = 1.246)

Scanning Electron Microscopy of Cells

SEM offers higher magnifications, a better three dimension view of cells, and a scale to gauge the size of cells. Similarly to what we observed with phase contrast, we observed long chains of bacteria (not exposed to BPEI) that were in the process of cell division during early exponential phase as seen in Figure

6.18 below. We can observe septa formations in certain regions from the SEM images of cells grown in LB containing 150 µg/mL BPEI (Figures 6.18 - 6.20). However, it is more difficult to observe with the random spiral morphologies and aggregation of cells. This random coil and bending morphology might arise from electrostatic interactions between the flexible strands of teichoic acid on nearby cells. Other possibilities for these abnormal shapes can be related to gene expression associated with peptidoglycan synthesis. In a very few instances an more extreme thickening of the cell wall was observed that gave rise to somewhat spherical shapes such as those in Figure 6.21. Since this was the only occurrence of this morphology that was observed, it was excluded from the following cell width calculations.

Width of the cells can be calculated by correlating the pixel length of 1 um provided in the image to the pixel length of the cells using Adobe Photoshop. Various cell thicknesses were calculated from different cells at different sections of the cover slip on two separate samples taken at similar OD_{600} absorbance values. The calculated cell widths are listed in Table 6.2 below.

Cell Thickness with and without BPEI (µm)							
No BPEI	0.694	0.729	0.700	0.754	0.667	Average	0.657
	0.631	0.684	0.667	0.554	0.616	StdDev	0.055
	0.649	0.685	0.602	0.578	0.638		
150 µg/ml BPEI	1.029	0.824	1.038	1.013	0.973	Average	0.925
	0.902	0.849	0.887	0.813	0.751	StdDev	0.105
	0.845	1.056	1.042				

Table 6.2 Cell Thickness with and without BPEI. All values above are in units of micrometers.

A two tailed t-test was used to evaluate the statistical significance between the cell wall thickness of both cells grown with 150 µg/mL BPEI and a control group of cells at a similar OD_{600} value. At a 99% confidence interval, the cell width values of both group produced a t-value of 8.65 which is larger than the critical t-value of 2.78. The larger t-value suggests that a statistical difference in the thickness values can be accepted at a 99% confidence interval.

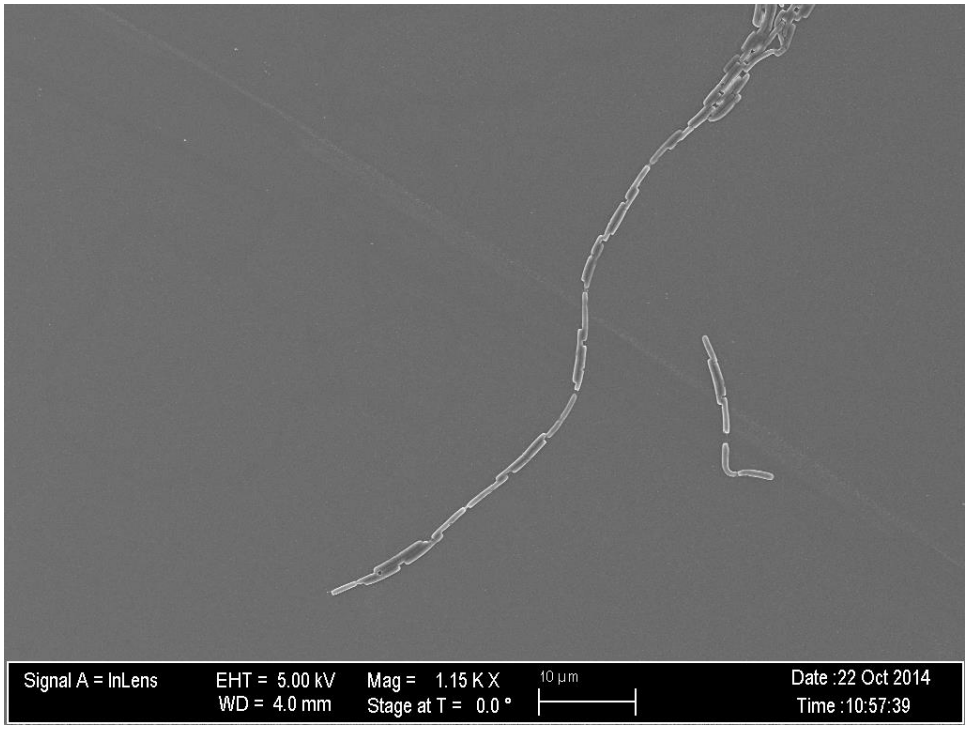


Figure 6.17 SEM image, *B. subtilis* 1A578, No BPEI, OD_{600}=0.174, 1150x

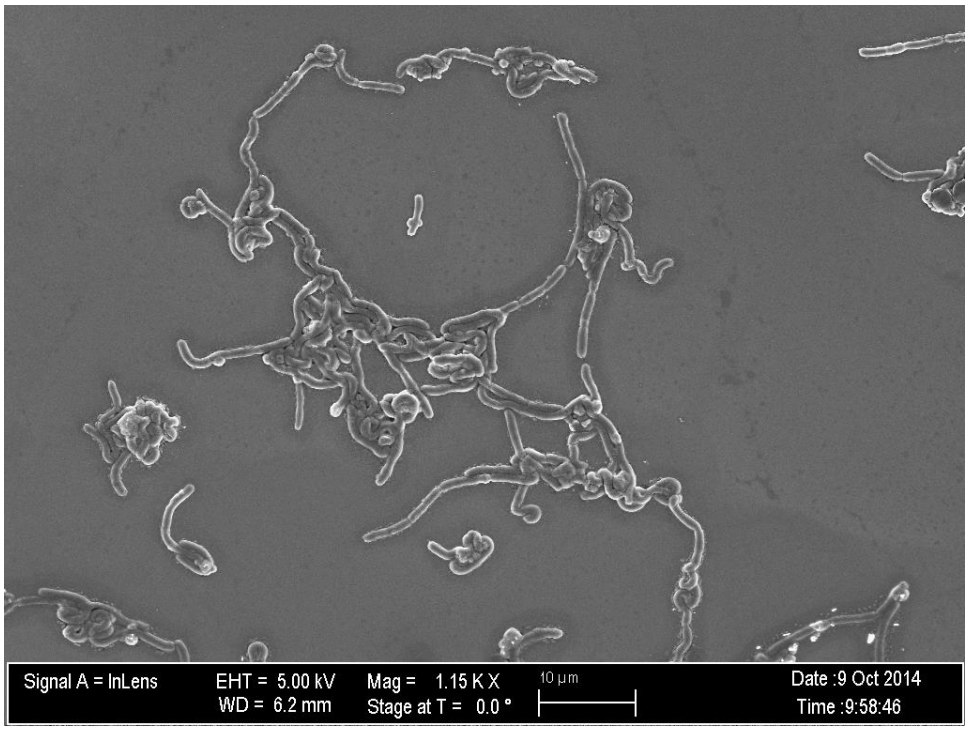


Figure 6.18 SEM image, *B. subtilis* 1A578, 150 µg/mL BPEI, OD_{600}=0.212, 1150x

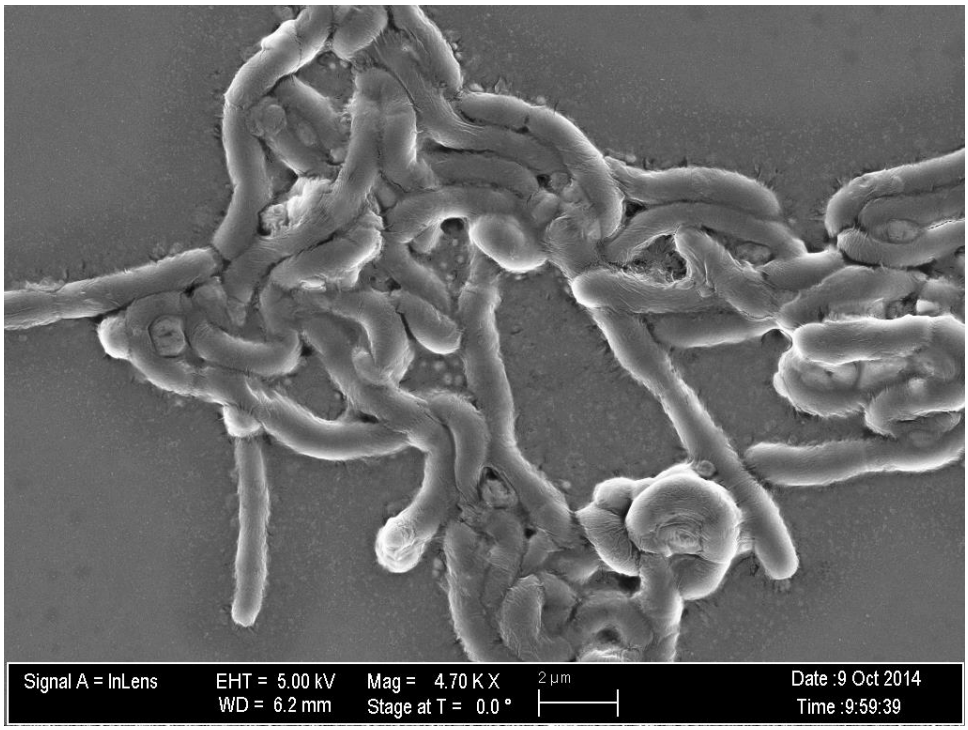


Figure 6.19 SEM image, *B. subtilis* 1A578, 150 µg/mL BPEI, OD_{600}=0.212, 4700x

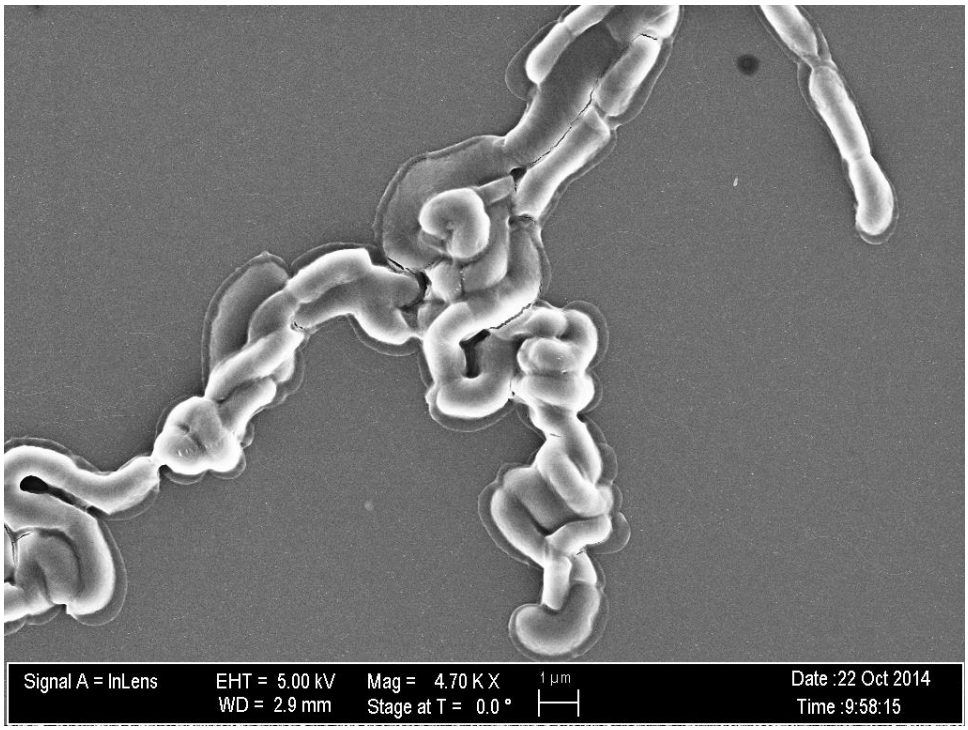


Figure 6.20 SEM image, *B. subtilis* 1A578, 150 µg/mL BPEI, OD_{600}=0.187, 4700x

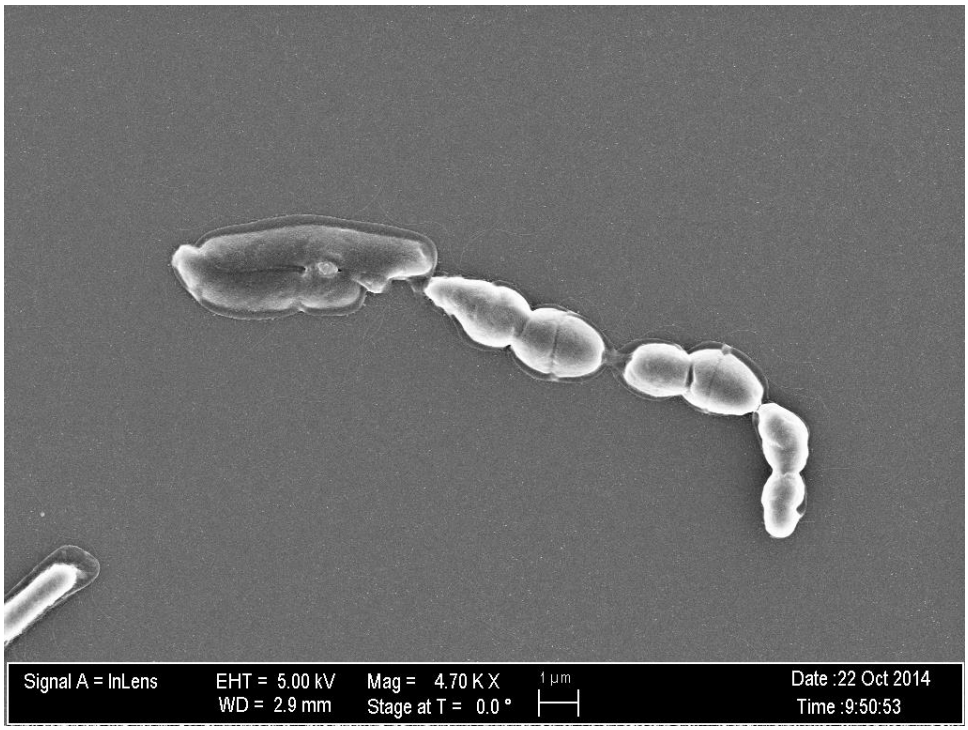


Figure 6.21 SEM image, *B. subtilis* 1A578, 150 µg/mL BPEI, OD_{600}=0.187, 4700x

Morphology Changes in Presence of EDTA and Supplemented Mg^{2+}

Different morphological changes occur when the LB bacterial growth media is supplemented with sub-lethal concentrations of EDTA, a metal chelator, or 0.01 M $MgCl_2$ combined with 150 µg/mL of BPEI. The addition of 0.0002 M EDTA causes an increase in cell length and a perturbation of cell division (Figure 6.22). This morphology is only partly similar to that of cell exposed to BPEI and lacks tight helical twisting. Attempts to rescue the cells to a normal morphology with the addition of 0.01 M Mg^{2+} ions proved unsuccessful. However, a distinct uneven thickening and thinning were observed in cells that were exposed to 150 µg/mL BPEI and supplemented with 0.01 M Mg^{2+} ions (Figure 6.23 and Figure 6.24). This combination of non-uniform thickening of the cells wall was not observed with BPEI exposed samples.

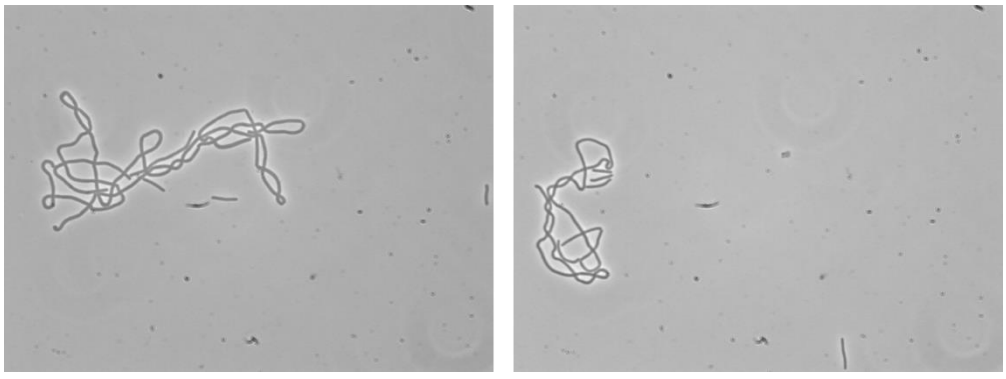


Figure 6.22: Phase contrast images of *B. subtilis* 1A578 (0.0002 M EDTA, OD_{600} = 0.183)

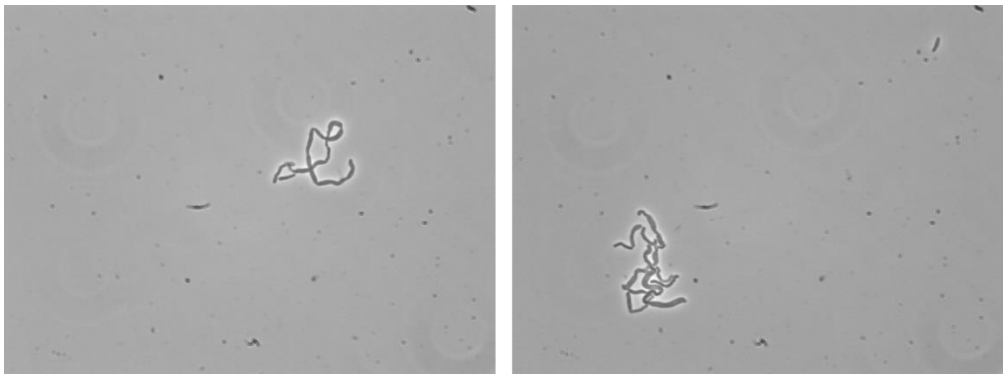


Figure 6.23: Phase Contrast images of *B. subtilis* 1A578 (150 µg/mL BPEI and 0.01 M $MgCl_2$, OD_{600} = 0.066)

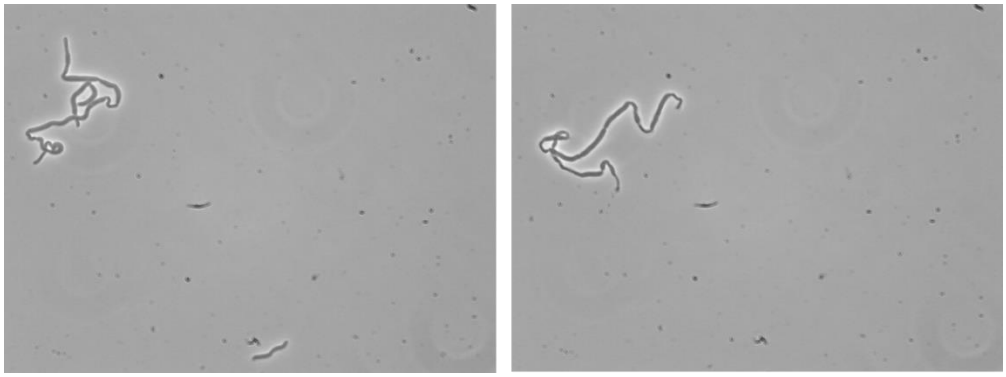


Figure 6.24: Phase Contrast images of *B. subtilis* 1A578 (150 µg/mL BPEI and 0.01 M $MgCl_2$, OD_{600} = 0.133)

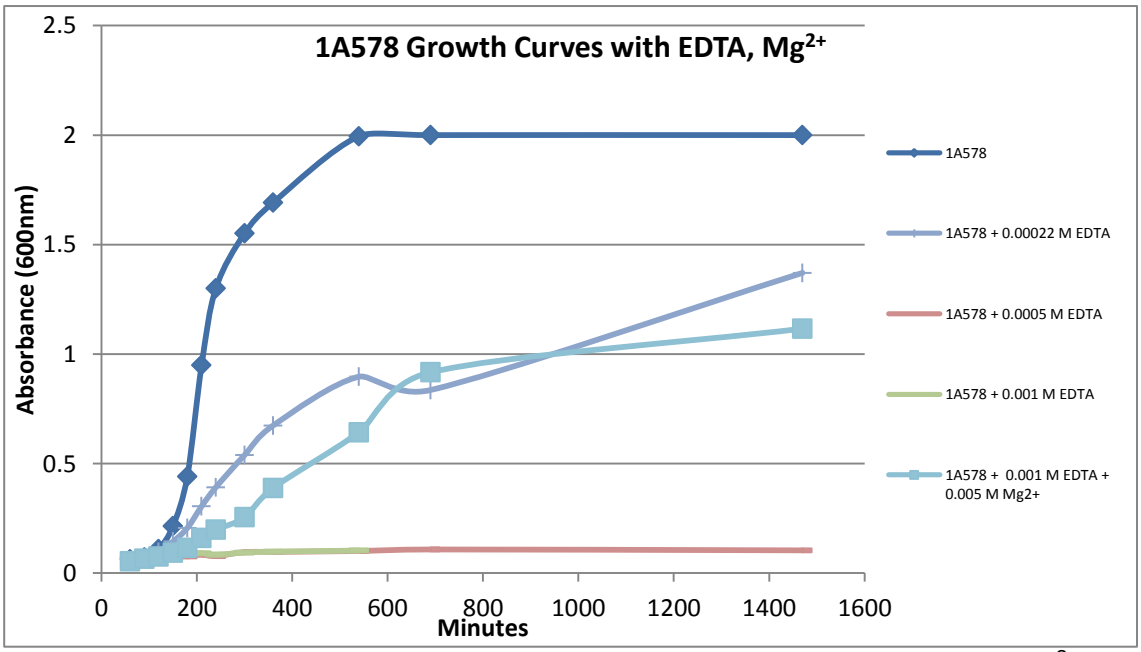


Figure 6.25: The inhibition of growth by EDTA and rescue of growth by Mg^{2+} supplementation

Discussion

Antibiotic resistant bacteria can be killed by a sufficiently high concentration of antibiotic (26). However, these sufficiently high concentrations of antibiotics cannot be achieved safely in the human body (26). Weakening antibiotic resistant cells with BPEI has been shown to decrease the MIC to some antibiotics. Although a direct mechanism for this increased susceptibility is not fully known, it is known that BPEI inhibits metal binding to the bacterial cell walls and that cell growth is limited in the presence of the metal ion chelator, EDTA as seen with the growth curve on Figure 6.25.

Chloramphenicol must permeate through the membrane to complete its mechanism of action. It binds to residues in the 23S rRNA to inhibit protein synthesis by preventing peptide bond formation (27). Similarly, erythromycin also binds to the 23S rRNA nucleotide where peptidyl transferase activity resides (27). Resistance to chloramphenicol can be a result of one or a combination of four mechanisms: the production of the enzyme chloramphenicol acetyletransferase (28), target site modification/mutant of the nucleotide sequence of 23S rRNA (29), multidrug efflux systems which use the proton motive force to transport antibiotics out of the cell (30), and decreased outer membrane permeability (31). The chloramphenicol resistant strain used in our experiments, *B. subtilis* 1A578, was reported to have no difference in ribosomal proteins when compared to the wild type strain (22). In addition, a lack of chloramphenicol acetyltransferase was observed with B. *subtilis* 1A578 (22). Most likely an altered uptake mechanism that is normally exploited by

chloramphenicol is responsible for the increased resistance. *B. subtilis* 1A578 is resistant to up to 20 µg/mL chloramphenicol whereas the parent strain had an MIC of 3 µg/mL (22). A constant concentration of 10 µg/mL of chloramphenicol was used in these studies. It has been reported that dissipation of the proton motive force (PMF) is a common mechanism for cationic antimicrobial proteins (32). The PMF is based on an electrostatic gradient and the binding of cationic antimicrobial compounds would cause this force to dissipate. A potential dissipation of the PMF would make it more difficult for antibiotics to be removed from the cell through efflux systems.

BPEI binding to the cell wall have previously been shown to remove metal ions as well as inhibit further metal binding to the cell wall (Chapter 5). As a result of BPEI binding to whole cells, the reservoir of metal ions decreases and the bacteria grow more slowly. This bacteriostatic effect has the potential to make the bacteria easier to kill by immune response and/or antibiotics. There is little clinical relevance between bacteriostatic and bactericidal antibiotics in patients without compromised immune systems (33). Gram-positive bacteria subjected to magnesium deprived growth media remain viable but growth does not take place until the addition of Mg^{2+} (34). This depletion of magnesium from the growth media can thus be considered to have a bacteriostatic effect on the bacteria. Magnesium ion concentration in growth media has also been reported to influence the growth rate of bacilli bacteria (24). The addition of magnesium to magnesium depleted growth media causes a restoration in growth (24). The connection of magnesium ions to growth rate is also observed in our

experiments. Instead of total magnesium concentration being limited, the access to magnesium ions and other essential metal ions are limited due to BPEI binding. As a result, the cell morphology changes from rods, to chains, and then to filamentous shapes. These effects are also observed as the Mg^{2+} content in the growth media was decreased (24). This data suggest a biochemical connection between BPEI, metal deprivation, and cell morphology.

Lag phase growth prepares bacteria for exponential growth by the accumulation of metals and other nutrients (35). It has been reported that bacteria are metabolically active in lag-phase (36). As seen in Figure 6.11, the bacteria continue to grow in the presence of 150 µg/mL BPEI during lag phase, but division does not occur. Septum formation is somewhat visible in some locations. Magnesium deprivation has caused the formation of long filamentous cells with *bacilli* bacteria that have yet to complete cellular division (24). It has been reported that a long chain polyphosphate also causes a change in the morphology of *Bacilli* cells when added at sub-lethal concentrations (37). *Bacilli* bacteria also exhibit inhibited septum formation when exposed to long chained polyphosphate (37). This morphological change is reversed and septum formation resumes on the addition of divalent cations (37).

In these experiments, we believe that metal ion binding is strongly inhibited, but not entirely inhibited in the presence of 150 µg/mL BPEI. Since metal binding and BPEI binding is an equilibrium mediated process, there will be a continuous binding, unbinding, and selective uptake of different components. A slower uptake of nutrients leads to a slower growth rate. This

behavior is also observed in the WTA deficient mutant of *B. subtilis* (EB1451). WTA is a significant metal binding component of the cell (Chapter 4) and loss of it would presumably decrease the bacterium's ability to gather metal ions needed for metabolic activity. Up-regulation or down-regulation of proteins responsible for cell division may be linked to metal ion deprivation. Additional work in this area is underway.

Conclusion

In our experiments we found that BPEI can decrease the MIC of an antibiotic resistant strain of *B. subtilis*. Both BPEI and sub-lethal concentrations of antibiotics increased the lag phase of *B. subtilis*. When used in conjunction, this increase in lag phase is more than an additive effect. During lag phase the cell is still growing, but septa formation is slow and cellular division is inhibited. This change in morphology and increased duration in lag phase and can originate from a decreased uptake of metal ion nutrients from BPEI occupying binding sites that are responsible for metal ion homeostasis. Further experiments are needed to elucidate the mechanisms of antibiotic synergy and morphological changes produced by BPEI exposure.

References

Chapter 1: Background Information of Gram-Positive Cell Wall

1. Naik, M. T., Suree, N., Ilangovan, U., Liew, C. K., Thieu, W., Campbell, D. O., Clemens, J. J., Jung, M. E., and Clubb, R. T. (2006) Staphylococcus aureus Sortase A Transpeptidase: Calcium Promotes Sorting Signal Binding by Altering the Mobility and Structure of an Active Site Loop. *Journal of Biological Chemistry* **281**, 1817-1826

2. Van Nhieu, G. T., Clair, C., Grompone, G., and Sansonetti, P. (2004) Calcium signalling during cell interactions with bacterial pathogens. *Biology of the Cell* **96**, 93-101

3. Tanaka, H., Oiwa, R., Matsukura, S., Inokoshi, J., and Omura, S. (1982) Studies on bacterial cell wall inhibitors. X. Properties of phosph-N-acetylmuramoyl-pentapeptide-transferase in peptidoglycan synthesis of Bacillus megaterium and its inhibition by amphomycin. *The Journal of antibiotics* **35**, 1216

4. Rayman, M. K., and MacLeod, R. A. (1975) Interaction of Mg-2+ with peptidoglycan and its relation to the prevention of lysis of a marine pseudomonad. *Journal of Bacteriology* **122**, 650-659

5. Beveridge, T. J., and Murray, R. G. (1980) Sites of metal deposition in the cell wall of Bacillus subtilis. *Journal of Bacteriology* **141**, 876-887

6. Borrok, D., Fein, J. B., Tischler, M., O'Loughlin, E., Meyer, H., Liss, M., and Kemner, K. M. (2004) The effect of acidic solutions and growth conditions on the adsorptive properties of bacterial surfaces. *Chemical Geology* **209**, 107-119

7. Fein, J. B., Daughney, C. J., Yee, N., and Davis, T. A. (1997) A chemical equilibrium model for metal adsorption onto bacterial surfaces. *Geochimica et Cosmochimica Acta* **61**, 3319-3328

8. Yee, N., Fowle, D. A., and Ferris, F. G. (2004) A Donnan potential model for metal sorption onto Bacillus subtilis. *Geochimica et Cosmochimica Acta* **68**, 3657-3664

9. Josset, S., Keller, N., Lett, M.-C., Ledoux, M. J., and Keller, V. (2008) Numeration methods for targeting photoactive materials in the UV-A photocatalytic removal of microorganisms. *Chemical Society Reviews* **37**, 744-755

10. Schleifer, K. H. (1985) Analysis of the chemical composition and primary structure of murein. *Methods Microbiol* **18**, 123-156

11. Vollmer, W., Blanot, D., and De Pedro, M. A. (2008) Peptidoglycan structure and architecture. *FEMS Microbiology Reviews* **32**, 149-167

12. Meroueh, S. O., Bencze, K. Z., Hesek, D., Lee, M., Fisher, J. F., Stemmler, T. L., and Mobashery, S. (2006) Three-dimensional structure of the bacterial cell wall peptidoglycan. *Proceedings of the National Academy of Sciences of the United States of America* **103**, 4404-4409

13. Delcour, J., Ferain, T., Deghorain, M., Palumbo, E., and Hols, P. (1999) The biosynthesis and functionality of the cell-wall of lactic acid bacteria. *Antonie Van Leeuwenhoek* **76**, 159-184

14. Bhavsar, A. P., Erdman, L. K., Schertzer, J. W., and Brown, E. D. (2004) Teichoic Acid Is an Essential Polymer in Bacillus subtilis That Is Functionally Distinct from Teichuronic Acid. *Journal of Bacteriology* **186**, 7865-7873

15. MacArthur, A. E., and Archibald, A. R. (1984) Effect of culture pH on the D-alanine ester content of lipoteichoic acid in Staphylococcus aureus. *Journal of Bacteriology* **160**, 792-793

16. Bernal, P., Zloh, M., and Taylor, P. W. (2009) Disruption of d-alanyl esterification of Staphylococcus aureus cell wall teichoic acid by the β-lactam resistance modifier (−)-epicatechin gallate. *Journal of Antimicrobial Chemotherapy* **63**, 1156-1162

17. Gross, M., Cramton, S. E., Götz, F., and Peschel, A. (2001) Key Role of Teichoic Acid Net Charge inStaphylococcus aureus Colonization of Artificial Surfaces. *Infection and Immunity* **69**, 3423-3426

18. Baddiley, J., Hancock, I. C., and Sherwood, P. M. A. (1973) X-ray Photoelectron Studies of Magnesium Ions bound to the Cell Walls of Gram-positive Bacteria. *Nature* **243**, 43-45

19. Garimella, R., Halye, J. L., Harrison, W., Klebba, P. E., and Rice, C. V. (2009) Conformation of the Phosphate d-Alanine Zwitterion in Bacterial Teichoic Acid from Nuclear Magnetic Resonance Spectroscopy. *Biochemistry* **48**, 9242-9249

20. Gründling, A., and Schneewind, O. (2006) Cross-Linked Peptidoglycan Mediates Lysostaphin Binding to the Cell Wall Envelope of Staphylococcus aureus. *Journal of Bacteriology* **188**, 2463-2472

21. Kobayashi, S., Hiroishi, K., Tokunoh, M., and Saegusa, T. (1987) Chelating properties of linear and branched poly(ethylenimines). *Macromolecules* **20**, 1496-1500

22. Kohler, T., Weidenmaier, C., and Peschel, A. (2009) Wall Teichoic Acid Protects Staphylococcus aureus against Antimicrobial Fatty Acids from Human Skin. *Journal of Bacteriology* **191**, 4482-4484

23. Oku, Y., Kurokawa, K., Matsuo, M., Yamada, S., Lee, B.-L., and Sekimizu, K. (2009) Pleiotropic Roles of Polyglycerolphosphate Synthase of Lipoteichoic Acid in Growth of Staphylococcus aureus Cells. *Journal of Bacteriology* **191**, 141-151

24. Peschel, A., Otto, M., Jack, R. W., Kalbacher, H., Jung, G., and Gotz, F. (1999) Inactivation of the dlt operon in Staphylococcus aureus confers sensitivity to defensins, protegrins, and other antimicrobial peptides. *Journal of biological chemistry* **274**, 8405-8410

25. Vergara-Irigaray, M., Maira-Litrán, T., Merino, N., Pier, G. B., Penadés, J. R., and Lasa, I. (2008) Wall teichoic acids are dispensable for anchoring the PNAG exopolysaccharide to the Staphylococcus aureus cell surface. *Microbiology* **154**, 865-877

26. Weidenmaier, C., Kokai-Kun, J. F., Kristian, S. A., Chanturiya, T., Kalbacher, H., Gross, M., Nicholson, G., Neumeister, B., Mond, J. J., and Peschel, A. (2004) Role of teichoic acids in Staphylococcus aureus nasal colonization, a major risk factor in nosocomial infections. *Nat Med* **10**, 243-245

27. Weidenmaier, C., Peschel, A., Xiong, Y. Q., Kristian, S. A., Dietz, K., Yeaman, M. R., and Bayer, A. S. (2005) Lack of wall teichoic acids in Staphylococcus aureus leads to reduced interactions with endothelial cells and to attenuated virulence in a rabbit model of endocarditis. *J Infect Dis* **191**, 1771-1777

28. Collins, L. V., Kristian, S. A., Weidenmaier, C., Faigle, M., van Kessel, K. P. M., van Strijp, J. A. G., Götz, F., Neumeister, B., and Peschel, A. (2002) Staphylococcus aureus Strains Lacking d-Alanine Modifications of Teichoic Acids Are Highly Susceptible to Human Neutrophil Killing and Are Virulence Attenuated in Mice. *J Infect Dis* **186**, 214-219

29. Bera, A., Biswas, R., Herbert, S., Kulauzovic, E., Weidenmaier, C., Peschel, A., and Götz, F. (2007) Influence of Wall Teichoic Acid on Lysozyme Resistance in Staphylococcus aureus. *Journal of Bacteriology* **189**, 280-283

30. Hoover, D. G., and Gray, R. J. (1977) Function of cell wall teichoic acid in thermally injured Staphylococcus aureus. *Journal of Bacteriology* **131**, 477-485

31. Bierbaum, G., and Sahl, H.-G. (1985) Induction of autolysis of staphylococci by the basic peptide antibiotics Pep 5 and nisin and their

influence on the activity of autolytic enzymes. *Arch. Microbiol.* **141**, 249-254

32. Fedtke, I., Mader, D., Kohler, T., Moll, H., Nicholson, G., Biswas, R., Henseler, K., Götz, F., Zähringer, U., and Peschel, A. (2007) A Staphylococcus aureus ypfP mutant with strongly reduced lipoteichoic acid (LTA) content: LTA governs bacterial surface properties and autolysin activity. *Mol. Microbiol.* **65**, 1078-1091

33. Greenberg, J. W., Fischer, W., and Joiner, K. A. (1996) Influence of lipoteichoic acid structure on recognition by the macrophage scavenger receptor. *Infection and Immunity* **64**, 3318-3325

34. Dunne, D. W., Resnick, D., Greenberg, J., Krieger, M., and Joiner, K. A. (1994) The type I macrophage scavenger receptor binds to gram-positive bacteria and recognizes lipoteichoic acid. *Proceedings of the National Academy of Sciences* **91**, 1863-1867

35. Polotsky, V. Y., Fischer, W., Ezekowitz, R. A., and Joiner, K. A. (1996) Interactions of human mannose-binding protein with lipoteichoic acids. *Infection and Immunity* **64**, 380-383

36. Lynch, N. J., Roscher, S., Hartung, T., Morath, S., Matsushita, M., Maennel, D. N., Kuraya, M., Fujita, T., and Schwaeble, W. J. (2004) L-Ficolin Specifically Binds to Lipoteichoic Acid, a Cell Wall Constituent of Gram-Positive Bacteria, and Activates the Lectin Pathway of Complement. *The Journal of Immunology* **172**, 1198-1202

37. Nahid, A. M., and Sugii, S. (2006) Binding of porcine ficolin-α to lipopolysaccharides from Gram-negative bacteria and lipoteichoic acids from Gram-positive bacteria. *Developmental & Comparative Immunology* **30**, 335-343

38. Morath, S., Geyer, A., and Hartung, T. (2001) Structure–Function Relationship of Cytokine Induction by Lipoteichoic Acid fromStaphylococcus aureus. *The Journal of Experimental Medicine* **193**, 393-398

39. Chatterjee, A. N. (1969) Use of Bacteriophage-resistant Mutants to Study the Nature of the Bacteriophage Receptor Site of Staphylococcus aureus. *Journal of Bacteriology* **98**, 519-527

40. Park, J. T., Shaw, D. R. D., Chatterjee, A. N., Mirelman, D., and Wu, T. (1974) MUTANTS OF STAPHYLOCOCCI WITH ALTERED CELL WALLS*. *Annals of the New York Academy of Sciences* **236**, 54-62

41. Koprivnjak, T., Peschel, A., Gelb, M. H., Liang, N. S., and Weiss, J. P. (2002) Role of charge properties of bacterial envelope in bactericidal

action of human group IIA phospholipase A(2) against Staphylococcus aureus. *Journal of Biological Chemistry* **277**, 47636-47644

42. Peschel, A., Vuong, C., Otto, M., and Götz, F. (2000) The d-Alanine Residues ofStaphylococcus aureus Teichoic Acids Alter the Susceptibility to Vancomycin and the Activity of Autolytic Enzymes. *Antimicrobial Agents and Chemotherapy* **44**, 2845-2847

43. Weidenmaier, C., Kokai-Kun, J. F., Kulauzovic, E., Kohler, T., Thumm, G., Stoll, H., Götz, F., and Peschel, A. (2008) Differential roles of sortase-anchored surface proteins and wall teichoic acid in Staphylococcus aureus nasal colonization. *International Journal of Medical Microbiology* **298**, 505-513

44. Xia, G., Kohler, T., and Peschel, A. (2010) The wall teichoic acid and lipoteichoic acid polymers of Staphylococcus aureus. *International Journal of Medical Microbiology* **300**, 148-154

45. Holland, L. M., Conlon, B., and O'Gara, J. P. (2011) Mutation of tagO reveals an essential role for wall teichoic acids in Staphylococcus epidermidis biofilm development. *Microbiology* **157**, 408-418

46. Saar-Dover, R., Bitler, A., Nezer, R., Shmuel-Galia, L., Firon, A., Shimoni, E., Trieu-Cuot, P., and Shai, Y. (2012) D-Alanylation of Lipoteichoic Acids Confers Resistance to Cationic Peptides in Group B <italic>Streptococcus</italic> by Increasing the Cell Wall Density. *PLoS Pathog* **8**, e1002891

47. Campbell, J., Singh, A. K., Swoboda, J. G., Gilmore, M. S., Wilkinson, B. J., and Walker, S. (2012) An antibiotic that inhibits a late step in wall teichoic acid biosynthesis induces the cell wall stress stimulon in Staphylococcus aureus. *Antimicrobial Agents and Chemotherapy*

48. Rose, R. K., Matthews, S. P., and Hall, R. C. (1997) Investigation of calcium-binding sites on the surfaces of selected Gram-positive oral organisms. *Archives of Oral Biology* **42**, 595-599

49. Maresso, A. W., and Schneewind, O. (2008) Sortase as a Target of Anti-Infective Therapy. *Pharmacological Reviews* **60**, 128-141

50. Romani, A., and Scarpa, A. (1992) Regulation of cell magnesium. *Archives of Biochemistry and Biophysics* **298**, 1-12

51. Iida, H., Yagawa, Y., and Anraku, Y. (1990) Essential role for induced Ca2+ influx followed by [Ca2+]i rise in maintaining viability of yeast cells late in the mating pheromone response pathway. A study of [Ca2+]i in single Saccharomyces cerevisiae cells with imaging of fura-2. *Journal of Biological Chemistry* **265**, 13391-13399

52. Groisman, E. A., Hollands, K., Kriner, M. A., Lee, E.-J., Park, S.-Y., and Pontes, M. H. (2013) Bacterial Mg2+ Homeostasis, Transport, and Virulence. *Annual Review of Genetics* **47**, 625-646

53. Hughes, A., Hancock, I., and Baddiley, J. (1973) The function of teichoic acids in cation control in bacterial membranes. *Biochem. J* **132**, 83-93

54. Moore, C. M., and Helmann, J. D. (2005) Metal ion homeostasis in Bacillus subtilis. *Current Opinion in Microbiology* **8**, 188-195

55. Maguire, M. E. (2006) Magnesium transporters: properties, regulation and structure. *Frontiers in bioscience : a journal and virtual library* **11**, 3149-3163

Chapter 2: Experimental Procedures

1. Anderson, L. M., Henkin, T. M., Chambliss, G. H., and Bott, K. F. (1984) New chloramphenicol resistance locus in Bacillus subtilis. *Journal of Bacteriology* **158**, 386-388

2. DeHart, H. P., Heath, H. E., Heath, L. S., LeBlanc, P. A., and Sloan, G. L. (1995) The lysostaphin endopeptidase resistance gene (epr) specifies modification of peptidoglycan cross bridges in Staphylococcus simulans and Staphylococcus aureus. *Applied and Environmental Microbiology* **61**, 1475-1479

3. Doyle, R. J., Matthews, T. H., and Streips, U. N. (1980) Chemical basis for selectivity of metal ions by the Bacillus subtilis cell wall. *Journal of Bacteriology* **143**, 471-480

4. Lambert, P. A., Hancock, I. C., and Baddiley, J. (1975) The interaction of magnesium ions with teichoic acid. *Biochem. J.* **149**, 519-524

5. Sakai, K. (1994) Determination of pore size and pore size distribution: 2. Dialysis membranes. *Journal of Membrane Science* **96**, 91-130

6. Haynes, W. M. (2014) *CRC Handbook of Chemistry and Physics, 95th Edition*, Taylor & Francis

7. Scatchard, G. (1949) THE ATTRACTIONS OF PROTEINS FOR SMALL MOLECULES AND IONS. *Annals of the New York Academy of Sciences* **51**, 660-672

8. Leroy, J. L., and Guéron, M. (1977) Electrostatic effects in divalent ion binding to tRNA. *Biopolymers* **16**, 2429-2446

9. Alvarado, D., Klein, D. E., and Lemmon, M. A. (2010) Structural Basis for Negative Cooperativity in Growth Factor Binding to an EGF Receptor. *Cell* **142**, 568-579

10. Mishra, B., Boyanov, M., Bunker, B. A., Kelly, S. D., Kemner, K. M., and Fein, J. B. (2010) High- and low-affinity binding sites for Cd on the bacterial cell walls of Bacillus subtilis and Shewanella oneidensis. *Geochimica et Cosmochimica Acta* **74**, 4219-4233

11. Sabouri, A. A., and Moosavimovahedi, A. A. (1994) Evaluation of the hill coefficient from scatchard and klotz plots. *Biochemical Education* **22**, 48-49

12. Demadis, K. D., Paspalaki, M., and Theodorou, J. (2011) Controlled Release of Bis(phosphonate) Pharmaceuticals from Cationic Biodegradable Polymeric Matrices. *Industrial & Engineering Chemistry Research* **50**, 5873-5876

13. Sneddon, J., and Haley, F. W. (1988) Discrete Nebulization for Sample Introduction of High Salt Solutions in Flame Atomic Absorption Spectrometry. *Spectroscopy Letters* **21**, 183-191

Chapter 3: Mg^{2+} and Ca^{2+} Binding Characteristics of Gram-Positive Bacterial Cell Walls

1. Shooter, R. A., and Wyatt, H. V. (1955) Mineral requirements for growth of Staphylococcus pyogenes; effect of magnesium and calcium ions. *British journal of experimental pathology* **36**, 341-350

2. Webb, M. (1949) The Influence of Magnesium on Cell Division: The Effect of Magnesium on the Growth and Cell Division of Various Bacterial Species in Complex Media. *Journal of General Microbiology* **3**, 410-417

3. Naik, M. T., Suree, N., Ilangovan, U., Liew, C. K., Thieu, W., Campbell, D. O., Clemens, J. J., Jung, M. E., and Clubb, R. T. (2006) Staphylococcus aureus Sortase A Transpeptidase: Calcium Promotes Sorting Signal Binding by Altering the Mobility and Structure of an Active Site Loop. *Journal of Biological Chemistry* **281**, 1817-1826

4. Ilangovan, U., Ton-That, H., Iwahara, J., Schneewind, O., and Clubb, R. T. (2001) Structure of sortase, the transpeptidase that anchors proteins to the cell wall of Staphylococcus aureus. *Proceedings of the National Academy of Sciences* **98**, 6056-6061

5. Van Nhieu, G. T., Clair, C., Grompone, G., and Sansonetti, P. (2004) Calcium signalling during cell interactions with bacterial pathogens. *Biology of the Cell* **96**, 93-101

6. Rayman, M. K., and MacLeod, R. A. (1975) Interaction of Mg-2+ with peptidoglycan and its relation to the prevention of lysis of a marine pseudomonad. *Journal of Bacteriology* **122**, 650-659

7. Beveridge, T. J., and Murray, R. G. (1980) Sites of metal deposition in the cell wall of Bacillus subtilis. *Journal of Bacteriology* **141**, 876-887

8. Fein, J. B., Daughney, C. J., Yee, N., and Davis, T. A. (1997) A chemical equilibrium model for metal adsorption onto bacterial surfaces. *Geochimica et Cosmochimica Acta* **61**, 3319-3328

9. Bhavsar, A. P., Erdman, L. K., Schertzer, J. W., and Brown, E. D. (2004) Teichoic Acid Is an Essential Polymer in Bacillus subtilis That Is Functionally Distinct from Teichuronic Acid. *Journal of Bacteriology* **186**, 7865-7873

10. Doyle, R. J., Matthews, T. H., and Streips, U. N. (1980) Chemical basis for selectivity of metal ions by the Bacillus subtilis cell wall. *Journal of Bacteriology* **143**, 471-480

11. Yee, N., Fowle, D. A., and Ferris, F. G. (2004) A Donnan potential model for metal sorption onto Bacillus subtilis. *Geochimica et Cosmochimica Acta* **68**, 3657-3664

12. Garimella, R., Halye, J. L., Harrison, W., Klebba, P. E., and Rice, C. V. (2009) Conformation of the Phosphate d-Alanine Zwitterion in Bacterial Teichoic Acid from Nuclear Magnetic Resonance Spectroscopy. *Biochemistry* **48**, 9242-9249

13. Kern, T., Giffard, M., Hediger, S., Amoroso, A., Giustini, C. c., Bui, N. K., Joris, B., Bougault, C., Vollmer, W., and Simorre, J.-P. (2010) Dynamics Characterization of Fully Hydrated Bacterial Cell Walls by Solid-State NMR: Evidence for Cooperative Binding of Metal Ions. *Journal of the American Chemical Society* **132**, 10911-10919

14. D'Elia, M. A., Millar, K. E., Beveridge, T. J., and Brown, E. D. (2006) Wall Teichoic Acid Polymers Are Dispensable for Cell Viability in Bacillus subtilis. *Journal of Bacteriology* **188**, 8313-8316

15. Soldo, B., Lazarevic, V., and Karamata, D. (2002) tagO is involved in the synthesis of all anionic cell-wall polymers in Bacillus subtilis 168. *Microbiology* **148**, 2079-2087

16. Vergara-Irigaray, M., Maira-Litrán, T., Merino, N., Pier, G. B., Penadés, J. R., and Lasa, I. (2008) Wall teichoic acids are dispensable for anchoring the PNAG exopolysaccharide to the Staphylococcus aureus cell surface. *Microbiology* **154**, 865-877

17. Gross, M., Cramton, S. E., Götz, F., and Peschel, A. (2001) Key Role of Teichoic Acid Net Charge inStaphylococcus aureus Colonization of Artificial Surfaces. *Infection and Immunity* **69**, 3423-3426

18. Holland, L. M., Conlon, B., and O'Gara, J. P. (2011) Mutation of tagO reveals an essential role for wall teichoic acids in Staphylococcus epidermidis biofilm development. *Microbiology* **157**, 408-418

19. Kohler, T., Weidenmaier, C., and Peschel, A. (2009) Wall Teichoic Acid Protects Staphylococcus aureus against Antimicrobial Fatty Acids from Human Skin. *Journal of Bacteriology* **191**, 4482-4484

20. Weidenmaier, C., Kokai-Kun, J. F., Kristian, S. A., Chanturiya, T., Kalbacher, H., Gross, M., Nicholson, G., Neumeister, B., Mond, J. J., and Peschel, A. (2004) Role of teichoic acids in Staphylococcus aureus nasal colonization, a major risk factor in nosocomial infections. *Nat Med* **10**, 243-245

21. Anderson, L. M., Henkin, T. M., Chambliss, G. H., and Bott, K. F. (1984) New chloramphenicol resistance locus in Bacillus subtilis. *Journal of Bacteriology* **158**, 386-388

22. Umeda, A., Yokoyama, S., Arizono, T., and Amako, K. (1992) Location of Peptidoglycan and Teichoic Acid on the Cell Wall Surface of Staphylococcus aureus as Determined by Immunoelectron Microscopy. *Journal of Electron Microscopy* **41**, 46-52

23. Schleifer, K. H. (1985) Analysis of the chemical composition and primary structure of murein. *Methods Microbiol* **18**, 123-156

24. Majcherczyk, P. A., Langen, H., Heumann, D., Fountoulakis, M., Glauser, M. P., and Moreillon, P. (1999) Digestion of Streptococcus pneumoniae Cell Walls with Its Major Peptidoglycan Hydrolase Releases Branched Stem Peptides Carrying Proinflammatory Activity. *Journal of Biological Chemistry* **274**, 12537-12543

25. Bernal, P., Zloh, M., and Taylor, P. W. (2009) Disruption of d-alanyl esterification of Staphylococcus aureus cell wall teichoic acid by the β-lactam resistance modifier (−)-epicatechin gallate. *Journal of Antimicrobial Chemotherapy* **63**, 1156-1162

26. Koshland, D. E., and Hamadani, K. (2002) Proteomics and Models for Enzyme Cooperativity. *Journal of Biological Chemistry* **277**, 46841-46844

27. Barkleit, A., Moll, H., and Bernhard, G. (2009) Complexation of uranium(vi) with peptidoglycan. *Dalton Transactions*, 5379-5385

28. Leroy, J. L., and Guéron, M. (1977) Electrostatic effects in divalent ion binding to tRNA. *Biopolymers* **16**, 2429-2446

29. van den Hoop, M. A. G. T., Porasso, R. D., and Benegas, J. C. (2002) Complexation of heavy metals by humic acids: analysis of voltammetric data by polyelectrolyte theory. *Colloids and Surfaces A: Physicochemical and Engineering Aspects* **203**, 105-116

30. Misra, V. K., and Draper, D. E. (1998) On the role of magnesium ions in RNA stability. *Biopolymers* **48**, 113-135

31. Wyman, J., and Gill, S. J. (1990) *Binding and linkage: Functional chemistry of biological macromolecules*, University Science Books, Mill Valley, Calif.

32. Matthews, T., Doyle, R., and Streips, U. (1979) Contribution of peptidoglycan to the binding of metal ions by the cell wall ofBacillus subtilis. *Current Microbiology* **3**, 51-53

33. Bradfield, R. (1942) Calcium in the Soil: I. Physico-Chemical Relations1. *Soil Sci. Soc. Am. J.* **6**, 8-15

34. Borrok, D., Fein, J. B., Tischler, M., O'Loughlin, E., Meyer, H., Liss, M., and Kemner, K. M. (2004) The effect of acidic solutions and growth conditions on the adsorptive properties of bacterial surfaces. *Chemical Geology* **209**, 107-119

35. Mishra, B., Boyanov, M., Bunker, B. A., Kelly, S. D., Kemner, K. M., and Fein, J. B. (2010) High- and low-affinity binding sites for Cd on the bacterial cell walls of Bacillus subtilis and Shewanella oneidensis. *Geochimica et Cosmochimica Acta* **74**, 4219-4233

36. Gründling, A., and Schneewind, O. (2006) Cross-Linked Peptidoglycan Mediates Lysostaphin Binding to the Cell Wall Envelope of Staphylococcus aureus. *Journal of Bacteriology* **188**, 2463-2472

37. Atilano, M. L., Pereira, P. M., Yates, J., Reed, P., Veiga, H., Pinho, M. G., and Filipe, S. R. (2010) Teichoic acids are temporal and spatial regulators of peptidoglycan cross-linking in Staphylococcus aureus. *Proceedings of the National Academy of Sciences of the United States of America* **107**, 18991-18996

Chapter 4: Mg^{2+} Binding Characteristics with Wall Teichoic Acid

1. Fedtke, I., Mader, D., Kohler, T., Moll, H., Nicholson, G., Biswas, R., Henseler, K., Götz, F., Zähringer, U., and Peschel, A. (2007) A Staphylococcus aureus ypfP mutant with strongly reduced lipoteichoic acid (LTA) content: LTA governs bacterial surface properties and autolysin activity. *Mol. Microbiol.* **65**, 1078-1091

2. Gross, M., Cramton, S. E., Götz, F., and Peschel, A. (2001) Key Role of Teichoic Acid Net Charge inStaphylococcus aureus Colonization of Artificial Surfaces. *Infection and Immunity* **69**, 3423-3426

3. Vergara-Irigaray, M., Maira-Litrán, T., Merino, N., Pier, G. B., Penadés, J. R., and Lasa, I. (2008) Wall teichoic acids are dispensable for anchoring the PNAG exopolysaccharide to the Staphylococcus aureus cell surface. *Microbiology* **154**, 865-877

4. Weidenmaier, C., Kokai-Kun, J. F., Kristian, S. A., Chanturiya, T., Kalbacher, H., Gross, M., Nicholson, G., Neumeister, B., Mond, J. J., and Peschel, A. (2004) Role of teichoic acids in Staphylococcus aureus nasal colonization, a major risk factor in nosocomial infections. *Nat Med* **10**, 243-245

5. Weidenmaier, C., Kokai-Kun, J. F., Kulauzovic, E., Kohler, T., Thumm, G., Stoll, H., Götz, F., and Peschel, A. (2008) Differential roles of sortase-anchored surface proteins and wall teichoic acid in Staphylococcus aureus nasal colonization. *International Journal of Medical Microbiology* **298**, 505-513

6. Weidenmaier, C., Peschel, A., Xiong, Y. Q., Kristian, S. A., Dietz, K., Yeaman, M. R., and Bayer, A. S. (2005) Lack of wall teichoic acids in Staphylococcus aureus leads to reduced interactions with endothelial cells and to attenuated virulence in a rabbit model of endocarditis. *J Infect Dis* **191**, 1771-1777

7. Thomas, K., III, and Rice, C. (2014) Revised model of calcium and magnesium binding to the bacterial cell wall. *Biometals* **27**, 1361-1370

8. Dawson, R. M. C., and Elliott, W. H. (1989) *Data for Biochemical Research*, Clarendon Press

9. Lambert, P. A., Hancock, I. C., and Baddiley, J. (1975) The interaction of magnesium ions with teichoic acid. *Biochem. J.* **149**, 519-524

10. Brown, S., Xia, G., Luhachack, L. G., Campbell, J., Meredith, T. C., Chen, C., Winstel, V., Gekeler, C., Irazoqui, J. E., Peschel, A., and Walker, S. (2012) Methicillin resistance in Staphylococcus aureus requires glycosylated wall teichoic acids. *Proceedings of the National Academy of Sciences* **109**, 18909-18914

11. MacArthur, A. E., and Archibald, A. R. (1984) Effect of culture pH on the D-alanine ester content of lipoteichoic acid in Staphylococcus aureus. *Journal of Bacteriology* **160**, 792-793

12. Bernal, P., Zloh, M., and Taylor, P. W. (2009) Disruption of d-alanyl esterification of Staphylococcus aureus cell wall teichoic acid by the β-

lactam resistance modifier (−)-epicatechin gallate. *Journal of Antimicrobial Chemotherapy* **63**, 1156-1162

13. Lambert, P. A., Hancock, I. C., and Baddiley, J. (1975) Influence of Alanyl Ester Residues on Binding of Magnesium-Ions to Teichoic-Acids. *Biochem J* **151**, 671-676

14. Garimella, R., Halye, J. L., Harrison, W., Klebba, P. E., and Rice, C. V. (2009) Conformation of the Phosphate d-Alanine Zwitterion in Bacterial Teichoic Acid from Nuclear Magnetic Resonance Spectroscopy. *Biochemistry* **48**, 9242-9249

15. Kovács, M., Halfmann, A., Fedtke, I., Heintz, M., Peschel, A., Vollmer, W., Hakenbeck, R., and Brückner, R. (2006) A Functional dlt Operon, Encoding Proteins Required for Incorporation of d-Alanine in Teichoic Acids in Gram-Positive Bacteria, Confers Resistance to Cationic Antimicrobial Peptides in Streptococcus pneumoniae. *Journal of Bacteriology* **188**, 5797-5805

16. D'Elia, M. A., Millar, K. E., Beveridge, T. J., and Brown, E. D. (2006) Wall Teichoic Acid Polymers Are Dispensable for Cell Viability in Bacillus subtilis. *Journal of Bacteriology* **188**, 8313-8316

17. Schirner, K., Marles-Wright, J., Lewis, R. J., and Errington, J. (2009) Distinct and essential morphogenic functions for wall- and lipo-teichoic acids in Bacillus subtilis. *The EMBO Journal* **28**, 830-842

18. Webb, M. (1949) The Influence of Magnesium on Cell Division: The Effect of Magnesium on the Growth and Cell Division of Various Bacterial Species in Complex Media. *Journal of General Microbiology* **3**, 410-417

19. Baddiley, J., Buchanan, J., Rajbhandary, U., and Sanderson, A. (1962) Teichoic acid from the walls of Staphylococcus aureus H. Structure of the N-acetylglucosaminylribitol residues. *Biochem J* **82**, 439

20. Doyle, R. J., McDannel, M. L., Streips, U. N., Birdsell, D. C., and Young, F. E. (1974) Polyelectrolyte Nature of Bacterial Teichoic Acids. *Journal of Bacteriology* **118**, 606-615

21. Danchin, A., and Guèron, M. (1970) Cooperative Binding of Manganese (II) to Transfer RNA. *European Journal of Biochemistry* **16**, 532-536

22. Leroy, J. L., and Guéron, M. (1977) Electrostatic effects in divalent ion binding to tRNA. *Biopolymers* **16**, 2429-2446

23. Neuhaus, F. C., and Baddiley, J. (2003) A Continuum of Anionic Charge: Structures and Functions of d-Alanyl-Teichoic Acids in Gram-Positive Bacteria. *Microbiology and Molecular Biology Reviews* **67**, 686-723

24. Rose, R., Shellis, R., and Lee, A. (1996) The role of cation bridging in microbial fluoride binding. *Caries research* **30**, 458-464

25. Kern, T., Giffard, M., Hediger, S., Amoroso, A., Giustini, C. c., Bui, N. K., Joris, B., Bougault, C., Vollmer, W., and Simorre, J.-P. (2010) Dynamics Characterization of Fully Hydrated Bacterial Cell Walls by Solid-State NMR: Evidence for Cooperative Binding of Metal Ions. *Journal of the American Chemical Society* **132**, 10911-10919

26. Bina-Stein, M., and Stein, A. (1976) Allosteric interpretation of Mg2+ ion binding to the denaturable Escherichia coli tRNAGlu2. *Biochemistry* **15**, 3912-3917

27. Halye, J. L., and Rice, C. V. (2010) Cadmium Chelation by Bacterial Teichoic Acid from Solid-State Nuclear Magnetic Resonance Spectroscopy. *Biomacromolecules* **11**, 333-340

28. Hancock, I., and Baddiley, J. (1985) Biosynthesis of the Bacterial Envelope Polymers Teichoic Acid and Teichuronic Acid. in *The Enzymes of Biological Membranes* (Martonosi, A. ed.), Springer US. pp 279-307

29. Misra, V. K., and Draper, D. E. (1998) On the role of magnesium ions in RNA stability. *Biopolymers* **48**, 113-135

30. Rialdi, G., Levy, J., and Biltonen, R. (1972) Thermodynamic studies of transfer ribonucleic acids. I. Magnesium binding to yeast phenylalanine transfer ribonucleic acid. *Biochemistry* **11**, 2472-2479

31. RÖMer, R., and Hach, R. (1975) tRNA Conformation and Magnesium Binding. *European Journal of Biochemistry* **55**, 271-284

32. Stein, A., and Crothers, D. M. (1976) Equilibrium binding of magnesium(II) by Escherichia coli tRNAfMet. *Biochemistry* **15**, 157-160

33. Koprivnjak, T., Weidenmaier, C., Peschel, A., and Weiss, J. P. (2008) Wall Teichoic Acid Deficiency in Staphylococcus aureus Confers Selective Resistance to Mammalian Group IIA Phospholipase A2 and Human β-Defensin 3. *Infection and Immunity* **76**, 2169-2176

34. Senyürek, I., Paulmann, M., Sinnberg, T., Kalbacher, H., Deeg, M., Gutsmann, T., Hermes, M., Kohler, T., Götz, F., Wolz, C., Peschel, A., and Schittek, B. (2009) Dermcidin-Derived Peptides Show a Different Mode of Action than the Cathelicidin LL-37 against Staphylococcus aureus. *Antimicrobial Agents and Chemotherapy* **53**, 2499-2509

35. Chen, C. Z., and Cooper, S. L. (2000) Recent Advances in Antimicrobial Dendrimers. *Advanced Materials* **12**, 843-846

36. Friedrich, C. L., Moyles, D., Beveridge, T. J., and Hancock, R. E. W. (2000) Antibacterial Action of Structurally Diverse Cationic Peptides on Gram-Positive Bacteria. *Antimicrobial Agents and Chemotherapy* **44**, 2086-2092

37. Gelman, M. A., Weisblum, B., Lynn, D. M., and Gellman, S. H. (2004) Biocidal Activity of Polystyrenes That Are Cationic by Virtue of Protonation. *Organic Letters* **6**, 557-560

38. Milović, N. M., Wang, J., Lewis, K., and Klibanov, A. M. (2005) Immobilized N-alkylated polyethylenimine avidly kills bacteria by rupturing cell membranes with no resistance developed. *Biotechnology and Bioengineering* **90**, 715-722

39. Heckels, J. E., Lambert, P. A., and Baddiley, J. (1977) Binding of Magnesium-Ions to Cell-Walls of Bacillus-Subtilis-W23 Containing Teichoic-Acid or Teichuronic Acid. *Biochem J* **162**, 359-365

Chapter 5: Antimicrobial Branched Polyethyleneimine Functions by Blocking Chelation of Essential Mg^{2+} Ions

1. Delcour, A. H. (2009) Outer membrane permeability and antibiotic resistance. *Biochimica et Biophysica Acta (BBA) - Proteins and Proteomics* **1794**, 808-816

2. Hancock, R. E. W., and Rozek, A. (2002) Role of membranes in the activities of antimicrobial cationic peptides. *Fems Microbiology Letters* **206**, 143-149

3. Gelman, M. A., Weisblum, B., Lynn, D. M., and Gellman, S. H. (2004) Biocidal Activity of Polystyrenes That Are Cationic by Virtue of Protonation. *Organic Letters* **6**, 557-560

4. Milović, N. M., Wang, J., Lewis, K., and Klibanov, A. M. (2005) Immobilized N-alkylated polyethylenimine avidly kills bacteria by rupturing cell membranes with no resistance developed. *Biotechnology and Bioengineering* **90**, 715-722

5. Friedrich, C. L., Moyles, D., Beveridge, T. J., and Hancock, R. E. W. (2000) Antibacterial Action of Structurally Diverse Cationic Peptides on Gram-Positive Bacteria. *Antimicrobial Agents and Chemotherapy* **44**, 2086-2092

6. Kügler, R., Bouloussa, O., and Rondelez, F. (2005) Evidence of a charge-density threshold for optimum efficiency of biocidal cationic surfaces. *Microbiology* **151**, 1341-1348

7. Lambert, P. A., Hancock, I. C., and Baddiley, J. (1975) Interaction of Magnesium-Ions with Teichoic-Acid. *Biochem J* **149**, 519-524

8. Lambert, P. A., Hancock, I. C., and Baddiley, J. (1975) Influence of Alanyl Ester Residues on Binding of Magnesium-Ions to Teichoic-Acids. *Biochem J* **151**, 671-676

9. Heckels, J. E., Lambert, P. A., and Baddiley, J. (1977) Binding of Magnesium-Ions to Cell-Walls of Bacillus-Subtilis-W23 Containing Teichoic-Acid or Teichuronic Acid. *Biochem J* **162**, 359-365

10. Heptinstall, S., Archibald, A. R., and Baddiley, J. (1970) Teichoic Acids and Membrane Function in Bacteria. *Nature* **225**, 519

11. Peschel, A. (2002) How do bacteria resist human antimicrobial peptides? *Trends in Microbiology* **10**, 179-186

12. Bernal, P., Zloh, M., and Taylor, P. W. (2009) Disruption of d-alanyl esterification of Staphylococcus aureus cell wall teichoic acid by the β-lactam resistance modifier (−)-epicatechin gallate. *Journal of Antimicrobial Chemotherapy* **63**, 1156-1162

13. Garimella, R., Halye, J. L., Harrison, W., Klebba, P. E., and Rice, C. V. (2009) Conformation of the Phosphate d-Alanine Zwitterion in Bacterial Teichoic Acid from Nuclear Magnetic Resonance Spectroscopy. *Biochemistry* **48**, 9242-9249

14. Edet Uwem, O., Gihan, H., Poussy Abu El, W., Opetiti, A., Nicole, C., and Elecia, H. (2014) In-vitro cytotoxicity of Polyethyleneimine on HeLa and Vero Cells. *International Journal of Innovation and Applied Studies* **5**, 192-199

15. Demadis, K. D., Paspalaki, M., and Theodorou, J. (2011) Controlled Release of Bis(phosphonate) Pharmaceuticals from Cationic Biodegradable Polymeric Matrices. *Industrial & Engineering Chemistry Research* **50**, 5873-5876

16. Perrine, T. D., and Landis, W. R. (1967) Analysis of polyethylenimine by spectrophotometry of its copper chelate. *Journal of Polymer Science Part A-1: Polymer Chemistry* **5**, 1993-2003

17. Wen, T., Qu, F., Li, N. B., and Luo, H. Q. A facile, sensitive, and rapid spectrophotometric method for copper(II) ion detection in aqueous media using polyethyleneimine. *Arabian Journal of Chemistry*

18. Kobayashi, S., Hiroishi, K., Tokunoh, M., and Saegusa, T. (1987) Chelating properties of linear and branched poly(ethylenimines). *Macromolecules* **20**, 1496-1500

19. Umeda, A., Yokoyama, S., Arizono, T., and Amako, K. (1992) Location of Peptidoglycan and Teichoic Acid on the Cell Wall Surface of Staphylococcus aureus as Determined by Immunoelectron Microscopy. *Journal of Electron Microscopy* **41**, 46-52

20. Majcherczyk, P. A., Langen, H., Heumann, D., Fountoulakis, M., Glauser, M. P., and Moreillon, P. (1999) Digestion of Streptococcus pneumoniae Cell Walls with Its Major Peptidoglycan Hydrolase Releases Branched Stem Peptides Carrying Proinflammatory Activity. *Journal of Biological Chemistry* **274**, 12537-12543

21. Schleifer, K. H. (1985) Analysis of the chemical composition and primary structure of murein. *Methods Microbiol* **18**, 123-156

22. Groisman, E. A., Hollands, K., Kriner, M. A., Lee, E.-J., Park, S.-Y., and Pontes, M. H. (2013) Bacterial Mg2+ Homeostasis, Transport, and Virulence. *Annual Review of Genetics* **47**, 625-646

23. Webb, M. (1949) The Influence of Magnesium on Cell Division: The Effect of Magnesium on the Growth and Cell Division of Various Bacterial Species in Complex Media. *Journal of General Microbiology* **3**, 410-417

24. Takeichi, M., and Okada, T. S. (1972) Roles of magnesium and calcium ions in cell-to-substrate adhesion. *Experimental Cell Research* **74**, 51-60

25. Naik, M. T., Suree, N., Ilangovan, U., Liew, C. K., Thieu, W., Campbell, D. O., Clemens, J. J., Jung, M. E., and Clubb, R. T. (2006) Staphylococcus aureus Sortase A Transpeptidase: Calcium Promotes Sorting Signal Binding by Altering the Mobility and Structure of an Active Site Loop. *Journal of Biological Chemistry* **281**, 1817-1826

26. Khalil, H., Chen, T., Riffon, R., Wang, R., and Wang, Z. (2008) Synergy between Polyethylenimine and Different Families of Antibiotics against a Resistant Clinical Isolate of Pseudomonas aeruginosa. *Antimicrobial Agents and Chemotherapy* **52**, 1635-1641

27. Thomas, K., III, and Rice, C. (2014) Revised model of calcium and magnesium binding to the bacterial cell wall. *Biometals*, 1-10

28. Campanhã, M. T. N., Mamizuka, E. M., and Carmona-Ribeiro, A. M. (1999) Interactions between cationic liposomes and bacteria: the physical-chemistry of the bactericidal action. *Journal of Lipid Research* **40**, 1495-1500

29. Ikeda, T., Tazuke, S., and Suzuki, Y. (1984) Biologically active polycations, 4. Synthesis and antimicrobial activity of poly(trialkylvinylbenzylammonium chloride)s. *Die Makromolekulare Chemie* **185**, 869-876

30. Ilker, M. F., Nüsslein, K., Tew, G. N., and Coughlin, E. B. (2004) Tuning the Hemolytic and Antibacterial Activities of Amphiphilic Polynorbornene Derivatives. *Journal of the American Chemical Society* **126**, 15870-15875

31. Nadeem, M., Baig, S., Qurat-ul-Ain, S., and Qazi, J. (2006) Microbial production of alkaline proteases by locally isolated Bacillus subtilis PCSIR-5. *Pakistan Journal of Zoology* **38**

32. Nagaya, J., Homma, M., Tanioka, A., and Minakata, A. (1996) Relationship between protonation and ion condensation for branched poly(ethylenimine). *Biophysical Chemistry* **60**, 45-51

33. Suh, J., Paik, H. J., and Hwang, B. K. (1994) Ionization of Poly(ethylenimine) and Poly(allylamine) at Various pH′s. *Bioorganic Chemistry* **22**, 318-327

34. Kunath, K., von Harpe, A., Fischer, D., Petersen, H., Bickel, U., Voigt, K., and Kissel, T. (2003) Low-molecular-weight polyethylenimine as a non-viral vector for DNA delivery: comparison of physicochemical properties, transfection efficiency and in vivo distribution with high-molecular-weight polyethylenimine. *Journal of Controlled Release* **89**, 113-125

35. von Harpe, A., Petersen, H., Li, Y., and Kissel, T. (2000) Characterization of commercially available and synthesized polyethylenimines for gene delivery. *Journal of Controlled Release* **69**, 309-322

36. Martínez, D., Vermeulen, M., Trevani, A., Ceballos, A., Sabatté, J., Gamberale, R., Álvarez, M. E., Salamone, G., Tanos, T., Coso, O. A., and Geffner, J. (2006) Extracellular Acidosis Induces Neutrophil Activation by a Mechanism Dependent on Activation of Phosphatidylinositol 3-Kinase/Akt and ERK Pathways. *The Journal of Immunology* **176**, 1163-1171

37. Pankey, G. A., and Sabath, L. D. (2004) Clinical Relevance of Bacteriostatic versus Bactericidal Mechanisms of Action in the Treatment of Gram-Positive Bacterial Infections. *Clinical Infectious Diseases* **38**, 864-870

38. Wu, G., Ding, J., Li, H., Li, L., Zhao, R., Shen, Z., Fan, X., and Xi, T. (2008) Effects of Cations and PH on Antimicrobial Activity of Thanatin and s-Thanatin Against Escherichia coli ATCC25922 and B. subtilis ATCC 21332. *Current Microbiology* **57**, 552-557

39. WEBB, M. (1968) The Influence of Certain Trace Metals on Bacterial Growth and Magnesium Utilization. *Journal of General Microbiology* **51**, 325-335

40. Fischer, D., Bieber, T., Li, Y., Elsässer, H.-P., and Kissel, T. (1999) A Novel Non-Viral Vector for DNA Delivery Based on Low Molecular Weight, Branched Polyethylenimine: Effect of Molecular Weight on Transfection Efficiency and Cytotoxicity. *Pharm Res* **16**, 1273-1279

41. Luten, J., van Nostrum, C. F., De Smedt, S. C., and Hennink, W. E. (2008) Biodegradable polymers as non-viral carriers for plasmid DNA delivery. *Journal of Controlled Release* **126**, 97-110

Chapter 6: Antimicrobial Synergy of BPEI with Antibiotics and Morphological

Changes Associated with BPEI Exposure

1. Luten, J., van Nostrum, C. F., De Smedt, S. C., and Hennink, W. E. (2008) Biodegradable polymers as non-viral carriers for plasmid DNA delivery. *Journal of Controlled Release* **126**, 97-110

2. Fischer, D., Bieber, T., Li, Y., Elsässer, H.-P., and Kissel, T. (1999) A Novel Non-Viral Vector for DNA Delivery Based on Low Molecular Weight, Branched Polyethylenimine: Effect of Molecular Weight on Transfection Efficiency and Cytotoxicity. *Pharm Res* **16**, 1273-1279

3. Edet Uwem, O., Gihan, H., Poussy Abu El, W., Opetiti, A., Nicole, C., and Elecia, H. (2014) In-vitro cytotoxicity of Polyethyleneimine on HeLa and Vero Cells. *International Journal of Innovation and Applied Studies* **5**, 192-199

4. Khalil, H., Chen, T., Riffon, R., Wang, R., and Wang, Z. (2008) Synergy between Polyethylenimine and Different Families of Antibiotics against a Resistant Clinical Isolate of Pseudomonas aeruginosa. *Antimicrobial Agents and Chemotherapy* **52**, 1635-1641

5. Champlin, F. R., Ellison, M. L., Bullard, J. W., and Conrad, R. S. (2005) Effect of outer membrane permeabilisation on intrinsic resistance to low triclosan levels in Pseudomonas aeruginosa. *International Journal of Antimicrobial Agents* **26**, 159-164

6. Nicas, T. I., and Hancock, R. E. (1983) Pseudomonas aeruginosa outer membrane permeability: isolation of a porin protein F-deficient mutant. *Journal of Bacteriology* **153**, 281-285

7. Kusser, W., Zimmer, K., and Fiedler, F. (1985) Characteristics of the binding of aminoglycoside antibiotics to teichoic acids. *European Journal of Biochemistry* **151**, 601-605

8. Best, G. K., and Durham, N. N. (1965) Vancomycin adsorption to Bacillus subtilis cell walls. *Archives of Biochemistry and Biophysics* **111**, 685-691

9. Levy, S. B., and Marshall, B. (2004) Antibacterial resistance worldwide: causes, challenges and responses. *Nat Med*

10. Helander, I. M., Alakomi, H.-L., Latva-Kala, K., and Koski, P. (1997) Polyethyleneimine is an effective permeabilizer of Gram-negative bacteria. *Microbiology* **143**, 3193-3199

11. Vaara, M. (1992) Agents that increase the permeability of the outer membrane. *Microbiological Reviews* **56**, 395-411

12. Leive, L. (1974) THE BARRIER FUNCTION OF THE GRAM-NEGATIVE ENVELOPE. *Annals of the New York Academy of Sciences* **235**, 109-129

13. Chen, C. Z., and Cooper, S. L. (2000) Recent Advances in Antimicrobial Dendrimers. *Advanced Materials* **12**, 843-846

14. Gelman, M. A., Weisblum, B., Lynn, D. M., and Gellman, S. H. (2004) Biocidal Activity of Polystyrenes That Are Cationic by Virtue of Protonation. *Organic Letters* **6**, 557-560

15. Milović, N. M., Wang, J., Lewis, K., and Klibanov, A. M. (2005) Immobilized N-alkylated polyethylenimine avidly kills bacteria by rupturing cell membranes with no resistance developed. *Biotechnology and Bioengineering* **90**, 715-722

16. Friedrich, C. L., Moyles, D., Beveridge, T. J., and Hancock, R. E. W. (2000) Antibacterial Action of Structurally Diverse Cationic Peptides on Gram-Positive Bacteria. *Antimicrobial Agents and Chemotherapy* **44**, 2086-2092

17. Kügler, R., Bouloussa, O., and Rondelez, F. (2005) Evidence of a charge-density threshold for optimum efficiency of biocidal cationic surfaces. *Microbiology* **151**, 1341-1348

18. Weiser, R., Asscher, A. W., and Wimpenny, J. (1968) In vitro Reversal of Antibiotic Resistance by Ethylenediamine Tetraacetic Acid. *Nature* **219**, 1365-1366

19. Wooley, R. E., and Jones, M. S. (1983) Action of EDTA-Tris and antimicrobial agent combinations on selected pathogenic bacteria. *Veterinary Microbiology* **8**, 271-280

20. VOSS, J. G. (1967) Effects of Organic Cations on the Gram-negative Cell Wall and Their Bactericidal Activity with Ethylenediaminetetra-acetate and Surface Active Agents. *Journal of General Microbiology* **48**, 391-400

21. Farca, A. M., Nebbia, P., and Re, G. (1994) Potentiation of antibiotic activity by EDTA-tromethamine against three clinically isolated Gram-positive resistant bacteria. Anin vitro investigation. *Vet Res Commun* **18**, 1-6

22. Anderson, L. M., Henkin, T. M., Chambliss, G. H., and Bott, K. F. (1984) New chloramphenicol resistance locus in Bacillus subtilis. *Journal of Bacteriology* **158**, 386-388

23. Andrews, J. M. (2001) Determination of minimum inhibitory concentrations. *Journal of Antimicrobial Chemotherapy* **48**, 5-16

24. Webb, M. (1949) The Influence of Magnesium on Cell Division: The Effect of Magnesium on the Growth and Cell Division of Various Bacterial Species in Complex Media. *Journal of General Microbiology* **3**, 410-417

25. Paulton, R. J. L. (1970) Analysis of the Multiseptate Potential of Bacillus subtilis. *Journal of Bacteriology* **104**, 762-767

26. Hawkey, P. M. (1998) The origins and molecular basis of antibiotic resistance. *BMJ* **317**, 657-660

27. Moazed, D., and Noller, H. F. (1987) Chloramphenicol, erythromycin, carbomycin and vernamycin B protect overlapping sites in the peptidyl transferase region of 23S ribosomal RNA. *Biochimie* **69**, 879-884

28. Shaw, W. V., Bentley, D. W., and Sands, L. (1970) Mechanism of Chloramphenicol Resistance in Staphylococcus epidermidis. *Journal of Bacteriology* **104**, 1095-1105

29. Montero, C. I., Johnson, M. R., Chou, C.-J., Conners, S. B., Geouge, S. G., Tachdjian, S., Nichols, J. D., and Kelly, R. M. (2007) Responses of Wild-Type and Resistant Strains of the Hyperthermophilic Bacterium Thermotoga maritima to Chloramphenicol Challenge. *Applied and Environmental Microbiology* **73**, 5058-5065

30. Paulsen, I. T., Brown, M. H., and Skurray, R. A. (1996) Proton-dependent multidrug efflux systems. *Microbiological Reviews* **60**, 575-608

31. Burns, J. L., Hedin, L. A., and Lien, D. M. (1989) Chloramphenicol resistance in Pseudomonas cepacia because of decreased permeability. *Antimicrobial Agents and Chemotherapy* **33**, 136-141

32. Montville, T. J., and Bruno, M. E. C. (1994) Evidence that dissipation of proton motive force is a common mechanism of action for bacteriocins and other antimicrobial proteins. *International Journal of Food Microbiology* **24**, 53-74

33. Pankey, G. A., and Sabath, L. D. (2004) Clinical Relevance of Bacteriostatic versus Bactericidal Mechanisms of Action in the Treatment of Gram-Positive Bacterial Infections. *Clinical Infectious Diseases* **38**, 864-870

34. WEBB, M. (1968) The Influence of Certain Trace Metals on Bacterial Growth and Magnesium Utilization. *Journal of General Microbiology* **51**, 325-335

35. Rolfe, M. D., Rice, C. J., Lucchini, S., Pin, C., Thompson, A., Cameron, A. D. S., Alston, M., Stringer, M. F., Betts, R. P., Baranyi, J., Peck, M. W., and Hinton, J. C. D. (2012) Lag Phase Is a Distinct Growth Phase That Prepares Bacteria for Exponential Growth and Involves Transient Metal Accumulation. *Journal of Bacteriology* **194**, 686-701

36. Martin, D. S. (1932) THE OXYGEN CONSUMPTION OF ESCHERICHIA COLI DURING THE LAG AND LOGARITHMIC PHASES OF GROWTH. *The Journal of General Physiology* **15**, 691-708

37. Maier, S. K., Scherer, S., and Loessner, M. J. (1999) Long-Chain Polyphosphate Causes Cell Lysis and Inhibits Bacillus cereus Septum Formation, Which Is Dependent on Divalent Cations. *Applied and Environmental Microbiology* **65**, 3942-3949